ESD-TR-72-365

UIAL-73-1
November 1972

Final Report

AN INVESTIGATION OF SOME SLOW-WAVE CONICAL LOG-SPIRAL AND HELICAL ANTENNAS

John D. Dyson
Electromagnetics Laboratory
(Formerly Antenna Laboratory)
University of Illinois

Prepared for

Massachusetts Institute of Technology

Lincoln Laboratory

This Report Covers the Period

1 September 1971 - 31 August 1972

Approved for public release; distribution unlimited.

UILU-ENG-73-2542

Final Report

AN INVESTIGATION OF SOME SLOW-WAVE CONICAL LOG-SPIRAL AND HELICAL ANTENNAS

John D. Dyson
Electromagnetics Laboratory
(Formerly Antenna Laboratory)
University of Illinois

Prepared for

Massachusetts Institute of Technology

Lincoln Laboratory

Under

Purchase Order No. CC-401

Prime Contract No. F19628-70-C-0230

This Report Covers the Period

1 September 1971 - 31 August 1972

ABSTRACT

This is a two part report.

The first part is concerned with the characteristics of conical spiral antennas constructed with zigzag, i.e., slow-wave geometry, arms. This construction permits a reduction in size of approximately 15 percent below that required for the conventional antenna. It also increases the pattern beamwidth and lowers the characteristic impedance.

In part 2, a 2 1/4-turn monofilar conical helix, fed at the base of the cone against an inner metal core, was investigated. This small circumference (approximately 1/4 wavelength) antenna can be made to be an axial radiating structure, while the conventional helix of this size radiates a maximum of energy broadside to the antenna axis.

Accepted for the Air Force
Joseph J. Whelan, USAF
Acting Chief, Lincoln Laboratory Liaison Office

ACKNOWLEDGEMENT

The measured near field, impedance and VSWR data on the slow-wave conical log-spiral antennas were extracted from a thesis submitted by S. L. Mathews in partial fulfillment of the requirements for the Master of Science Degree at the University of Illinois (reference 3 to this report). In addition, Appendices A, B, and C have been taken directly from that source.

TABLE OF CONTENTS

TABLE OF CONTENTS (Continued)

LIST OF FIGURES

Figure Page

Figure Page

Figure Page

Figure Page

Figure Page

Figure Page

INTRODUCTION

The logarithmic spiral antennas have found extensive use because of their very wide bandwidth and excellent circular polarization properties. These structures are not small in wavelengths, however, and for many practical applications an attempt at size reduction seems justified. This problem could be attacked by loading the antenna with dielectric or ferrite material and there have been several extensive studies of loading carried out. Possibly the best known, in the unclassified literature,is the work at the University of Michigan.[1]

For the past year we have been concerned with a second attack, namely constructing the antennas in a slow-wave geometry. This problem was briefly looked at here at the University of Illinois a number of years ago and at other places, but with the exception of a paper on the flat spiral antenna[2] there is little quantitative information available in the open literature.

The investigation thus far has been limited to the use of a zigzag geometry on conical logarithmic spiral antennas.[3] Several families of conical spiral antennas with a suitable range of parameters have been constructed and investigated, by measuring the amplitude and phase of the near fields along the surface of the antenna, and relating this information to far field radiation pattern measurements. This information has been supplemented by VSWR and impedance measurements.

We have constructed these antennas with the arms following a zigzag path within the envelope formed by the edges of a conventional wide arm conical log-spiral antenna. The "geometric slowing factor" has been defined to be the ratio of the path length along the zigzag path, between two

radius vectors on the antenna, to the path length along the center line of the conventional spiral geometry between the given radius vectors. This slowing factor can be varied by varying the angular width of the envelope which bounds the undulating geometry, or by changing the period of the path.

In this investigation we have defined an "electrical slowing factor" to be the ratio of the measured propagation constant along the modified (i.e., zigzag) antenna to that measured along the unmodified antenna. We have observed a large difference between the geometric and electric slowing factors.

Based upon this information we have used this slow-wave geometry to design one version of a slow wave conical helix antenna fed against an inner metal cone. This report is divided into two parts. The first deals with the conical spiral antennas. The second with the preliminary investigation of the slow-wave conical helix.

PART I - THE SLOW-WAVE CONICAL SPIRAL

1.1 The Conical Log-Spiral Parameters

The radiating characteristics of the conical log-spiral antenna are dependent upon the physical parameters indicated in Figure 1. The principle parameters are the base diameter in wavelengths, the included cone angle $2\theta_o$; the angular arm width δ ; and the rate of wrap α. The angular arm width δ is defined as the projection of the angle δ' (see Figure 1) on a plane perpendicular to the axis of the cone. The angle of wrap α is the angle between the spiral and a radius vector extending from the tip to the base along the surface of the cone, the angle being measured clockwise from the radius vector.

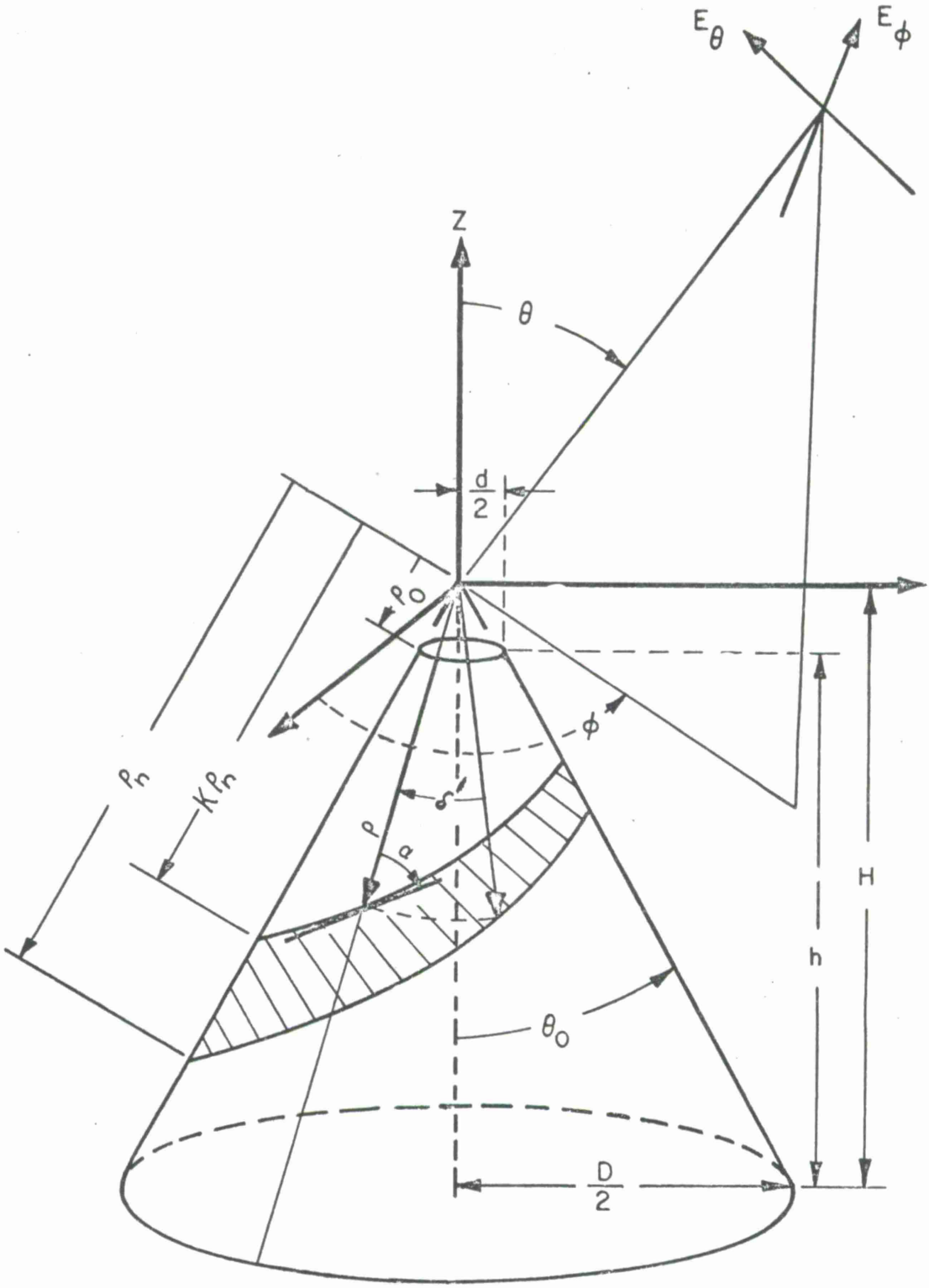

Figure 1. Conical antenna with associated parameters.

The antennas referred to in this report are identified in the following manner:

2C - 10 - 70 - 90 - 15/30 - 2.0

1 2 3 4 5 6

1 - Two arm conical

2 - Included cone angle of 10°

3 - Angle of wrap, α

4 - Angular width of spiral arm for the conventional antennas.

For the zigzag structures:

4 - Represents the angular width of the spiral envelope of the undulating arm (see Figure A1 of Appendix A).

5 - The first number, i.e., 15 in this case represents the actual angular arm width of the undulating arm, the second number, i.e., 30 represents the angular width of one cycle of undulation. In this study we have used two arm widths, 7.5 and 15°).

6 - The geometric slowing factor as calculated (see Appendix C).

Variation in the angle of wrap, α, was limited to the angles 65° and 70°. An included cone angle of 10° and a base diameter of 7 in. were chosen.

This is obviously a limited range of parameters. Their choice was dictated with an ultimate application in mind.

1.2 The Slow-Wave Geometry

Four slowing factors were chosen for each family of antennas (α = 65° and 70°) to determine how these factors would affect the required size of the antenna. The geometry to give these slowing factors is discussed in detail in Appendix A. Two arm widths were chosen for each slowing factor to determine the effect of this parameter. Each slow-wave antenna was compared

to the appropriate normal complementary conical spiral arm antenna ($\delta' = 90°$) since this antenna can conveniently be taken as an optimum design for any rate of wrap, α. The slow-wave antennas were also compared to spiral antennas with arm widths equal to the two slow-wave arm widths (the determination of these widths is discussed in Appendix B). Figure 2 shows a family of slow-wave antennas and Figure 3 shows one slow-wave antenna between an antenna with spiral arm width equal to the envelope of the slow-wave geometry and an antenna with spiral arm width equal to the arm width of the slow-wave structure.

1.3 Near Field Measurements

1.3.1 Amplitude Measurements

It is known that the current flowing from the point of excitation (the apex) of the conical antenna, passes through a transmission line type region to a region where there is rapid radiation of energy into space. This latter, the active region, is fairly well defined and for normal operation of the antenna, a constant distance from the true apex of the cone in wavelengths.[4] Measurements were made to provide a comparison of the near fields of the slow-wave structure to those on the corresponding conventional conical antennas.

The fields near the surface of the antenna were measured with an electric field, or charge, probe as shown in Figure 4. The variable choke was adjusted to a quarter-wave length, and absorbing material was placed on the probe line to supress induced currents. The probe was positioned to be perpendicular to the surface and moved on a path parallel to the surface of the cone, at a spacing of 0.045 λ from the surface, by a carriage mechanism that was synchronized to the X-axis of an X-Y plotter. The entire arrangement of the test equipment system for measuring amplitude and phase is shown in Figure 5.

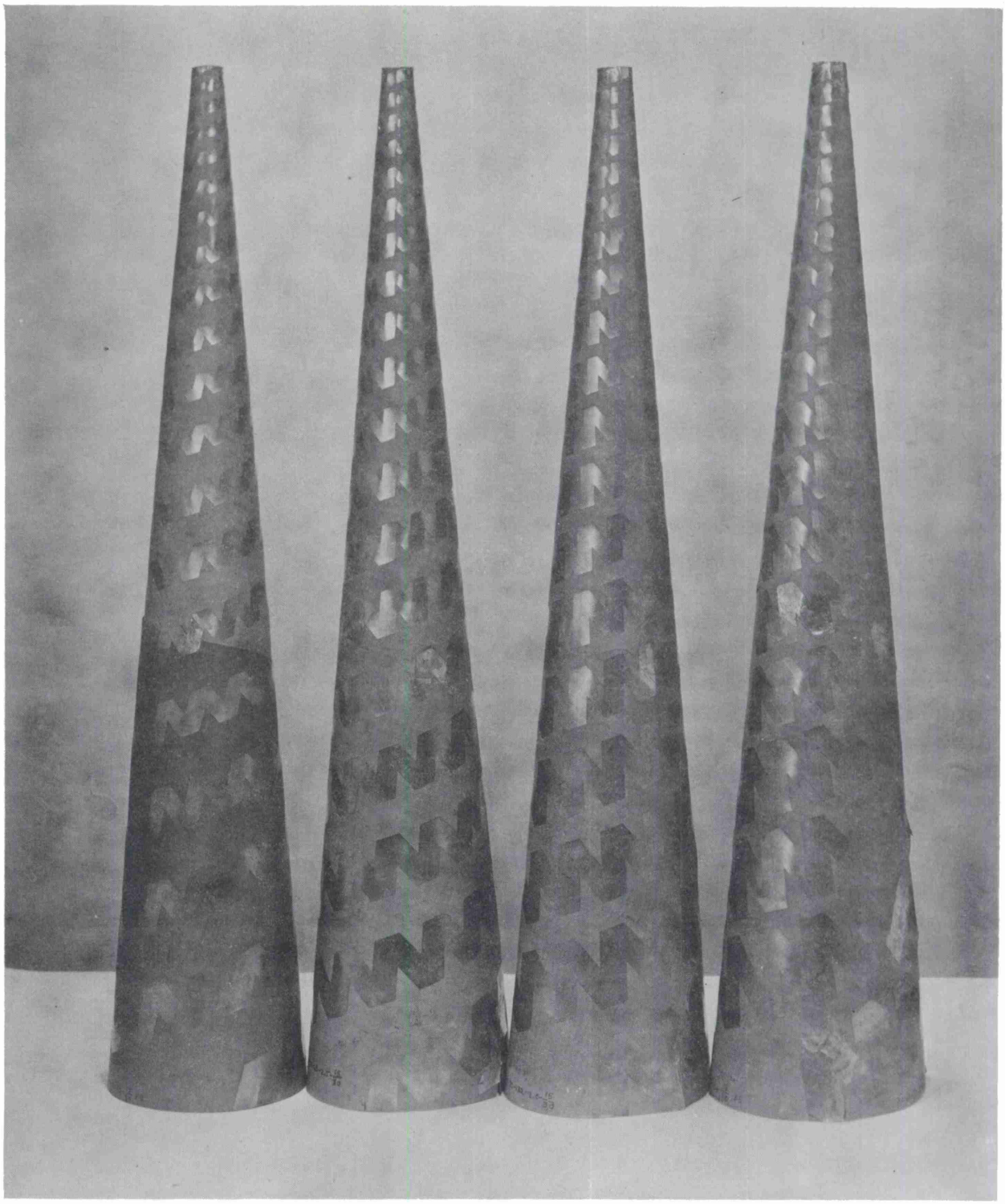

Figure 2. Family of zigzag antennas, $\alpha = 70°$, with slowing factors of 2.0, 2.5, 3.0, and 3.5 (from left to right).

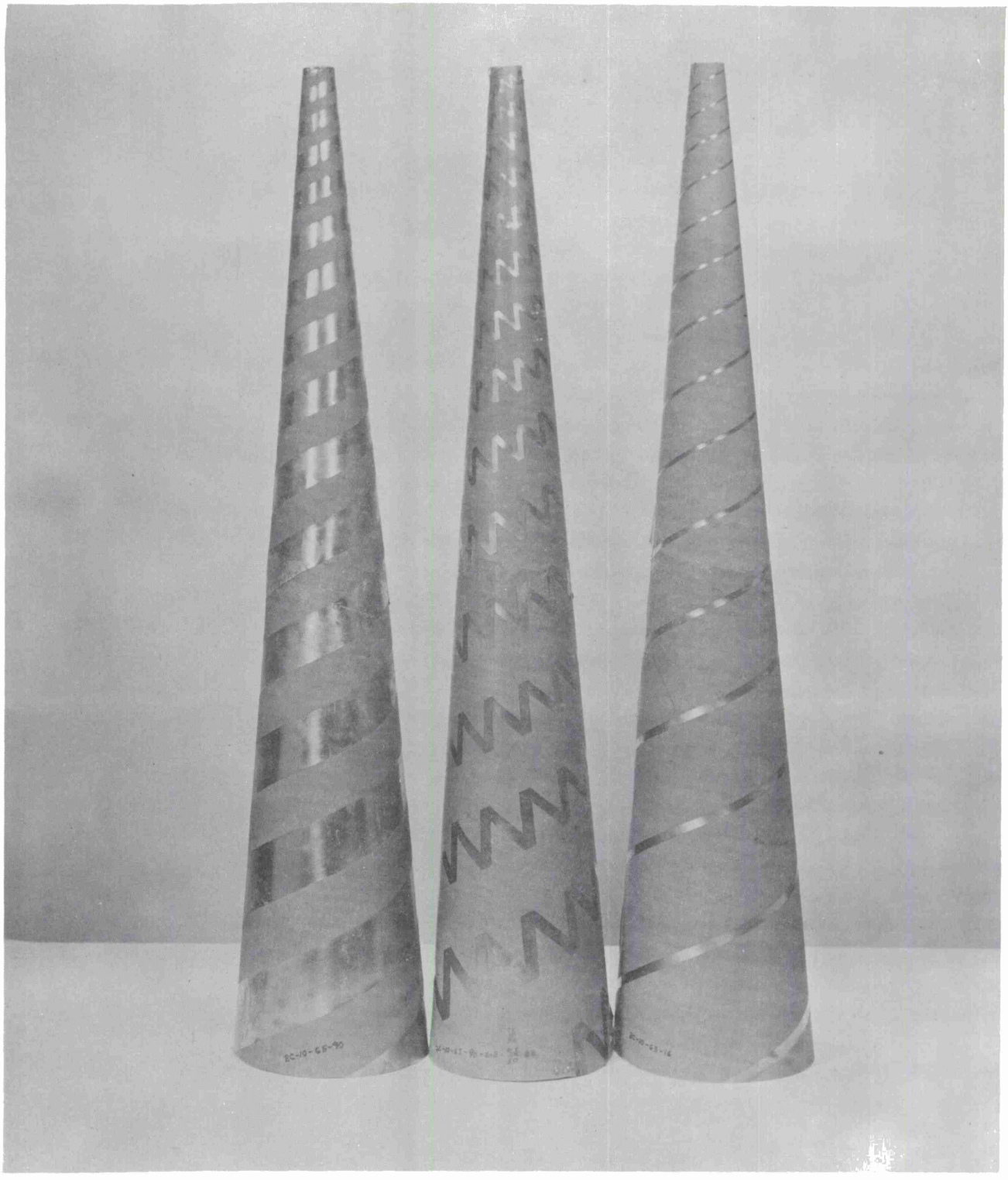

Figure 3. Complementary ($\delta' = 90°$), thin zigzag, and "equivalent" ($\delta' = 16°$) spiral antennas for $\alpha = 65°$.

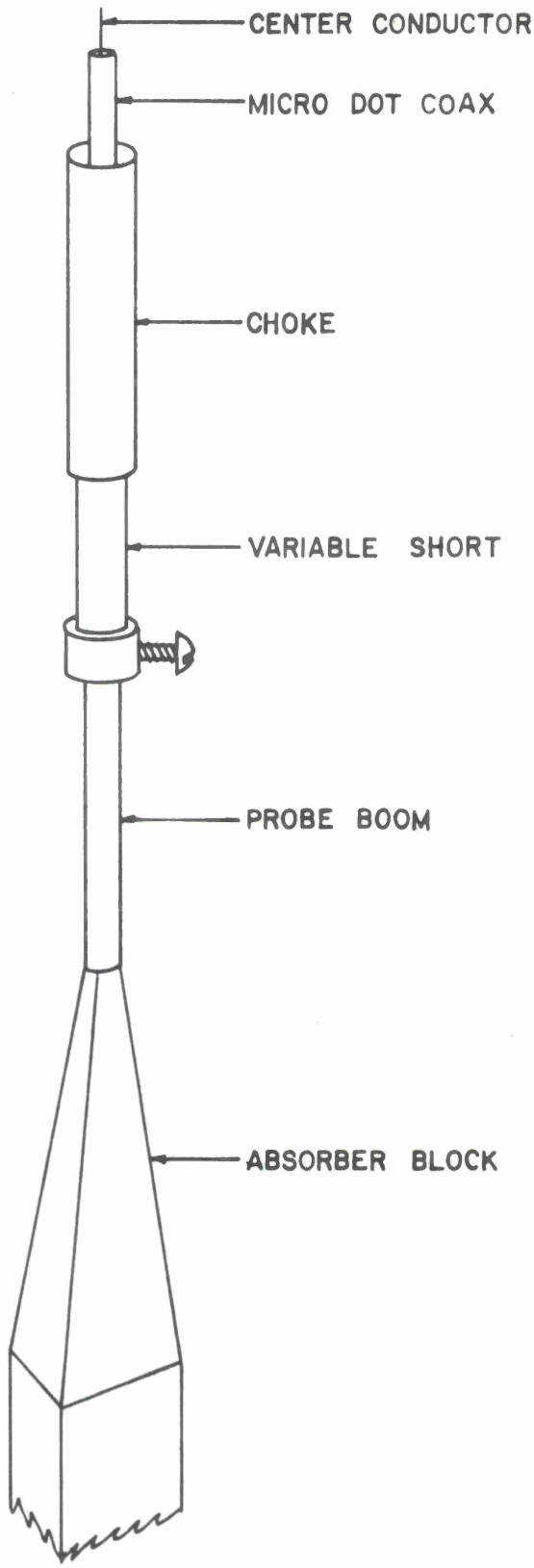

Figure 4. Near-field measurement probe.

Near Field Measurements For Amplitude And Phase

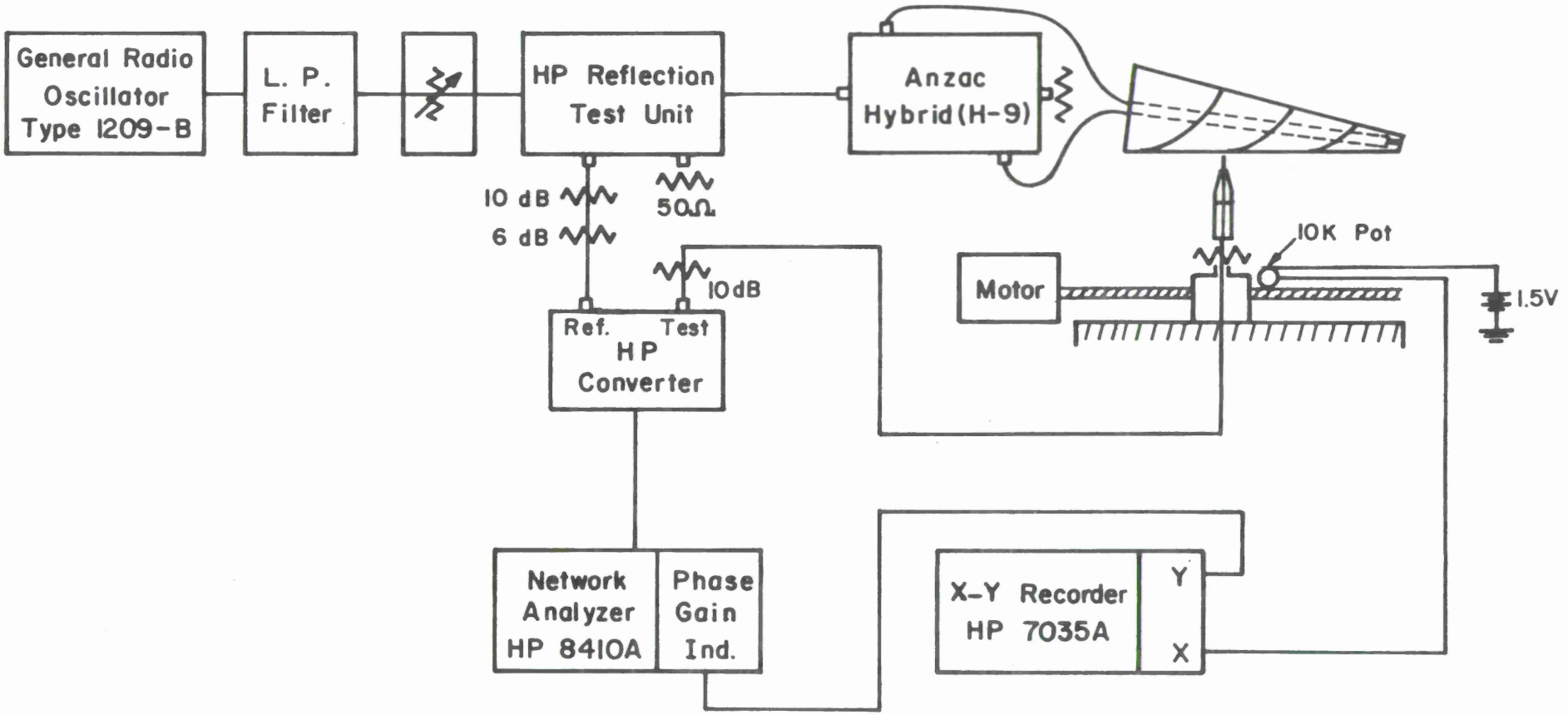

Figure 5. Near-field amplitude and phase measurement system.

Figures 6 and 7 show the relative amplitudes of the normal component of the electric field near the surface of the cones of two normal spiral arm antennas with an angle of wrap $\alpha = 65°$, $\delta' = 90°$ and 16° compared to the amplitude of these fields on a wide and thin arm slow-wave antenna (widths of 15/30 and 7.5/30), both with the same geometric slowing factor.

The first portion of these curves is characteristic of the transmission line region on the log-spiral antennas. The fields are tightly bound to the structure and little energy is coupled to the probe. Farther from the apex of the antenna,the fields become more loosely bound and energy is more efficiently radiated. Considering as an example the curve for the 2C - 10 - 65 - 90 antenna in this figure, the region from approximately .63 to 1.4 wavelengths from the apex could be defined to be the active radiating region. This would be in agreement with previous studies.[4] This definition is based upon the approximate points where the near fields, as measured here, are 3 dB below the maximum recorded level on the apex side of the maximum, and 15 dB below this maximum on the base side. The antenna current in this region determines, to a first order, the radiating characteristics of the antenna. It is obvious that the active regions of the slow-wave antennas are displaced toward the apex, and since the antennas can be truncated at a size such that near fields have decayed approximately 15 db below the recorded maximum, a smaller size structure should be possible for any frequency of normal operation.

The curve for the narrower arm antenna (7.5/30) shows the greatest shift. Figures 8 and 9 represent similar plots of the measured charge distribution for antennas with a slightly tighter wrap ($\alpha = 70°$). In these and all other near field amplitude and phase plots, the curves start at the truncated tip of the antenna cone and end at the base of the cone.

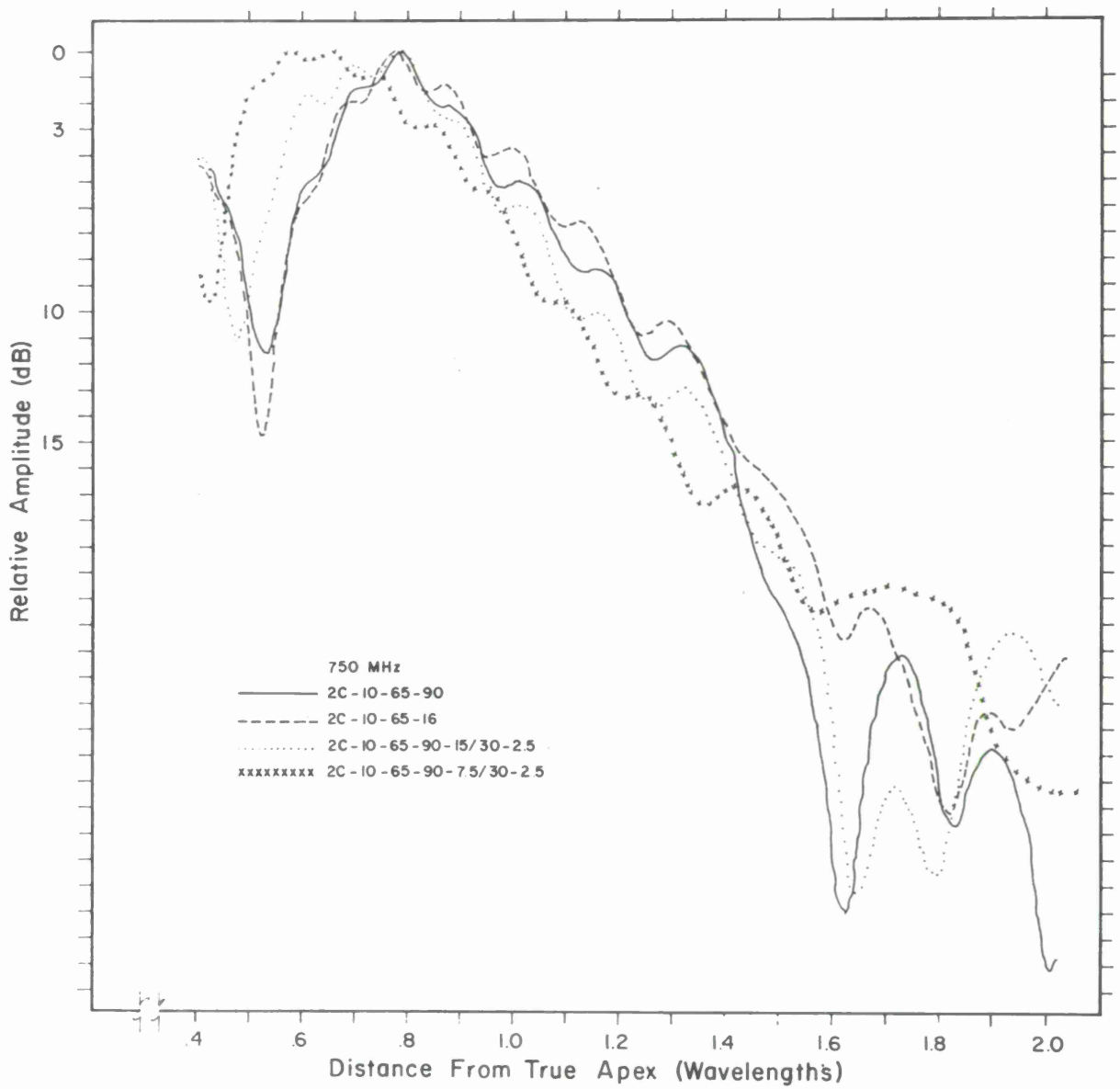

Figure 6. Measured relative amplitude of near fields on wide and thin zigzag antennas (α = 65°, slowing factor = 2.5).

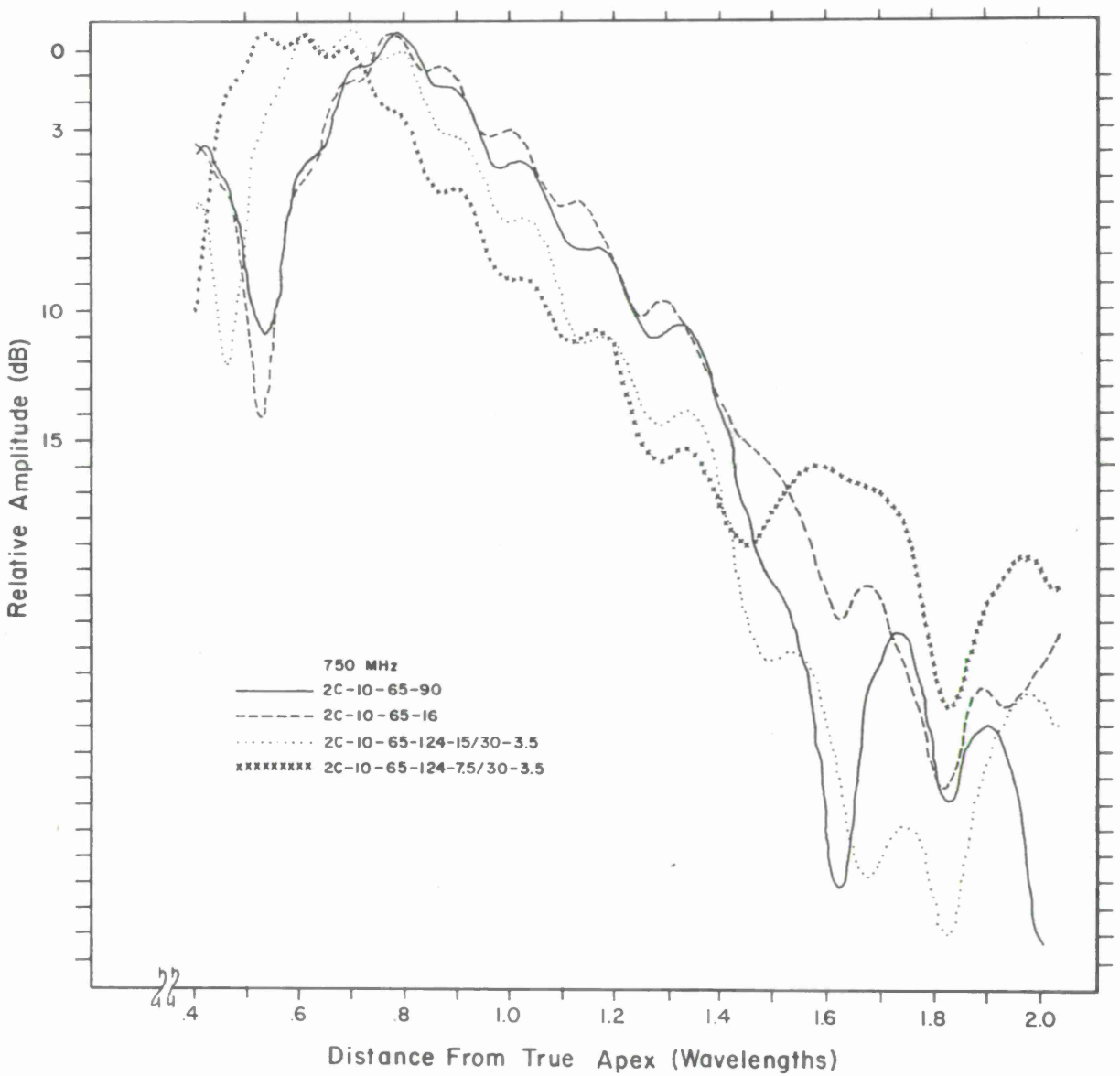

Figure 7. Measured relative amplitude of near fields on wide and thin zigzag antennas ($\alpha = 65°$, slowing factor = 3.5).

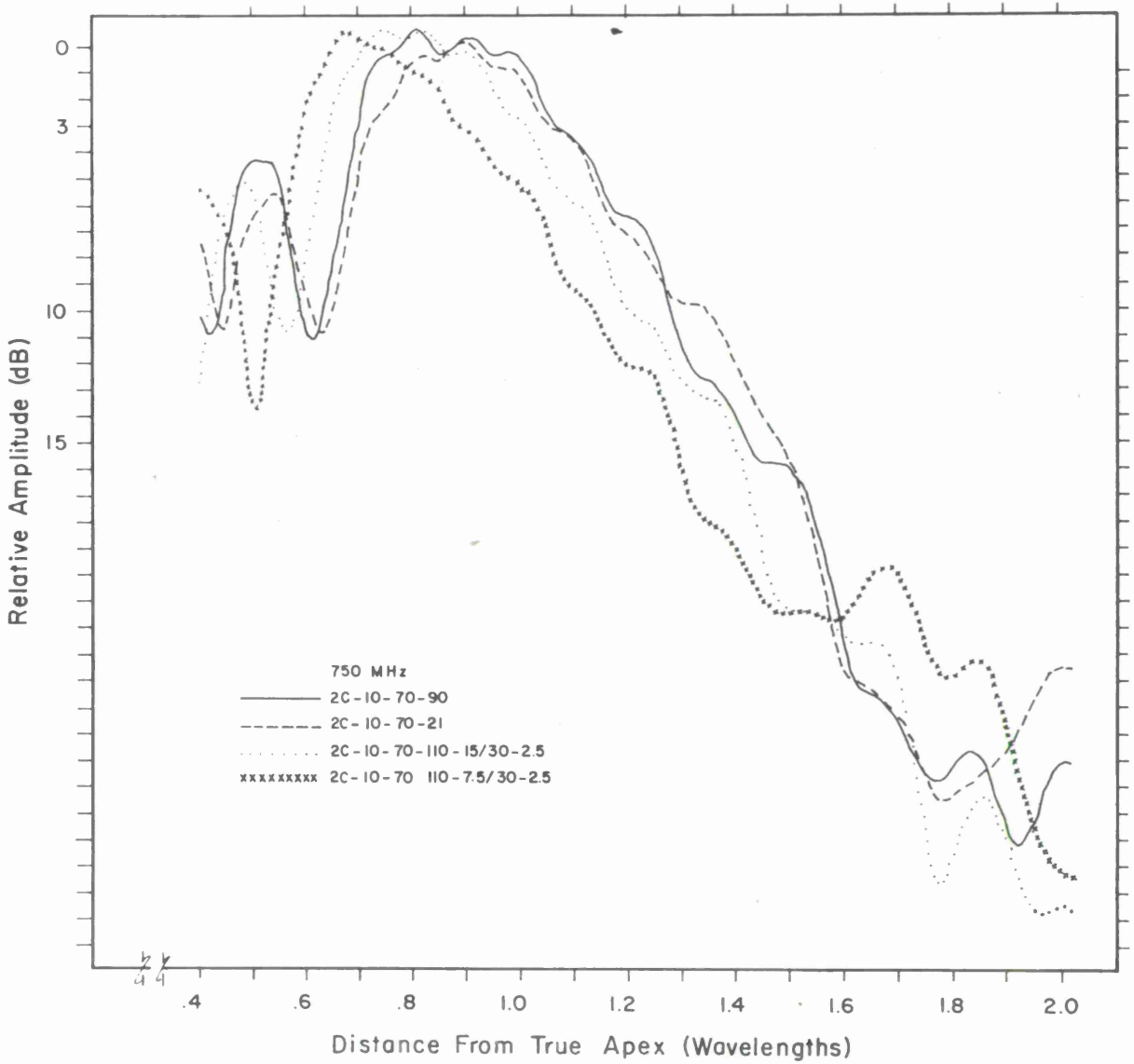

Figure 8. Measured relative amplitude of near fields on wide and thin zigzag antennas (α = 70°, slowing factor = 2.5).

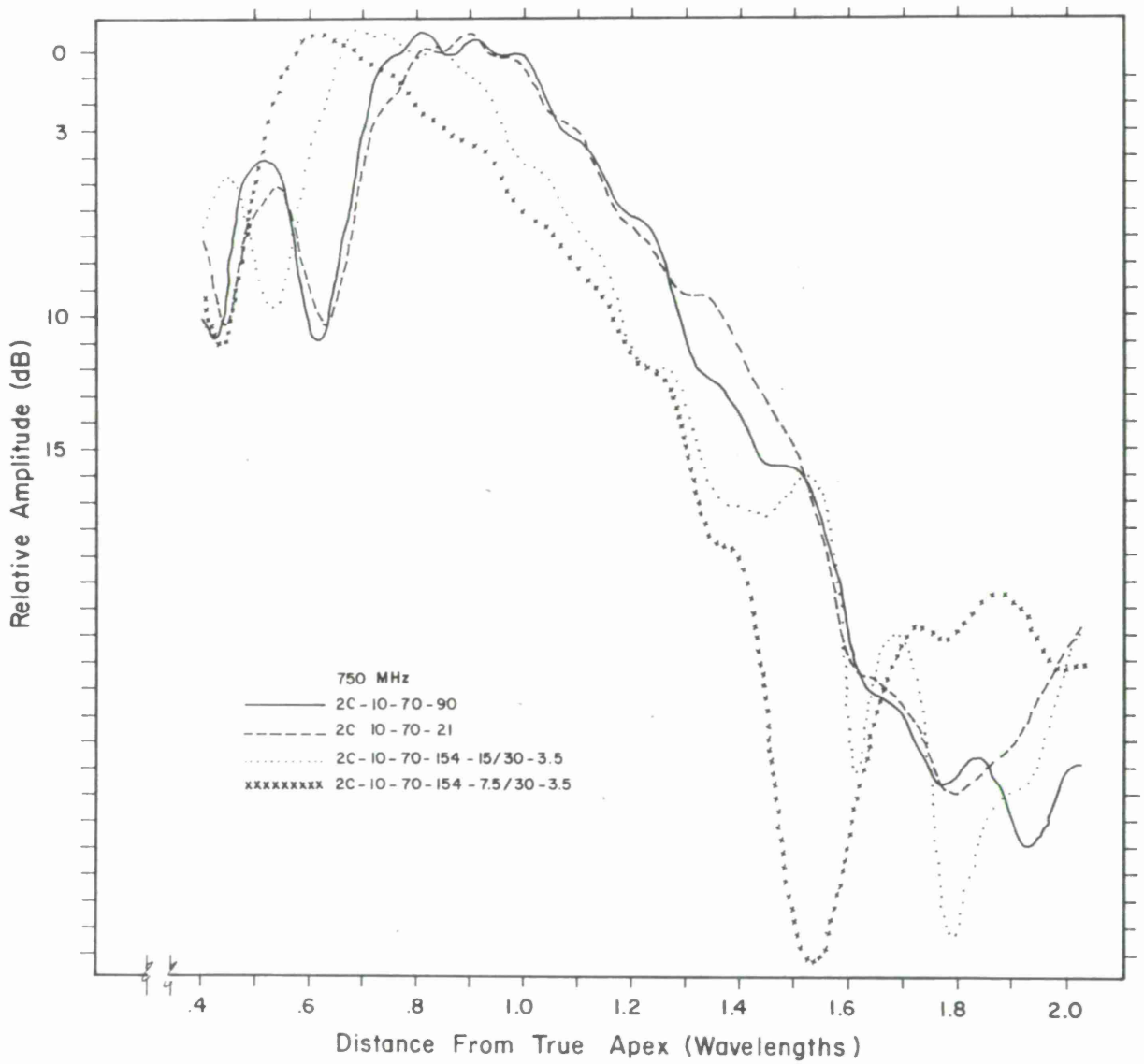

Figure 9. Measured relative amplitude of near fields on wide and thin zigzag antennas (α = 70°, slowing factor = 3.5).

Also noticable, and this characteristic is present when these antennas are "loaded" by any means, the active region is slightly wider on the slow-wave antennas than it is for the conventional antenna. This will tend to broaden the radiation pattern[4] and mean that the bandwidth will be reduced for any fixed size structure.

Figures 10 and 11 show the calculated electric slowing factor versus the geometrically designed slowing factor for the two angles of wrap, as compared to the complementary ($\delta' = 90°$) spiral arm antenna and the antennas of angular spiral arm widths equal to the two zigzag arm widths. (See Appendix C for calculation method). It is apparent that the narrower arm geometry (7.5/30) is a slower wave structure than the wider arm geometry. However, there is a wide discrepancy between the electric and geometric slowing factors.*

1.3.2 Phase Measurements

The relative phase of the normal component of the electric field along a radial line near the surface of the cones was measured. As a reference, the relative phase measured on the conventional spiral antennas is plotted in Figures 12 and 13. The small arrows on these curves indicate the distance from the apex where the measured amplitude of these fields were 3 dB down on the apex side, and 10 and 15 dB down from the recorded maximum on the base side, of this maximum. There is an essentially linear change in phase over the active region, with little dependence upon the three arm widths which were investigated.

Figures 14 thru 17 show the measured phase along the slow-wave spiral antennas. Figures 18 and 19 show a direct comparison between the conventional antennas and antennas with a slowing factor of 2.5.

*For each angle of wrap α, there was one antenna corresponding to a particular geometric slowing factor where the data were not in accord with the trend of the curve. These points were plotted in Figures 10 and 11 but were omitted from consideration. The top point refers to the top curve, etc.

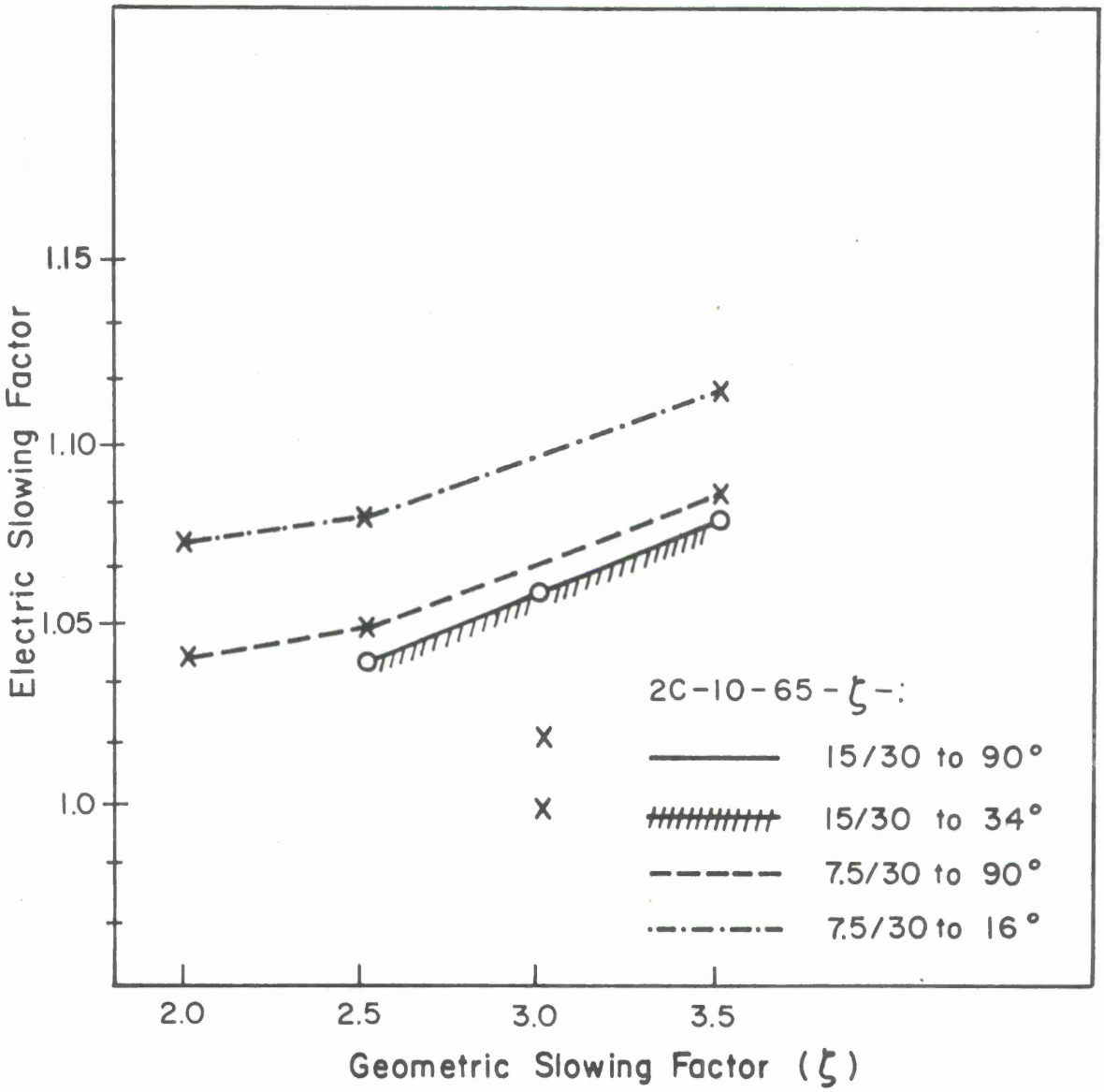

Figure 10. Calculated electric slowing factor compared to the geometrical slowing (ζ) for wide and thin zigzag antennas, relative to the respective complementary and "equivalent" arm width spiral antennas ($\alpha = 65°$).

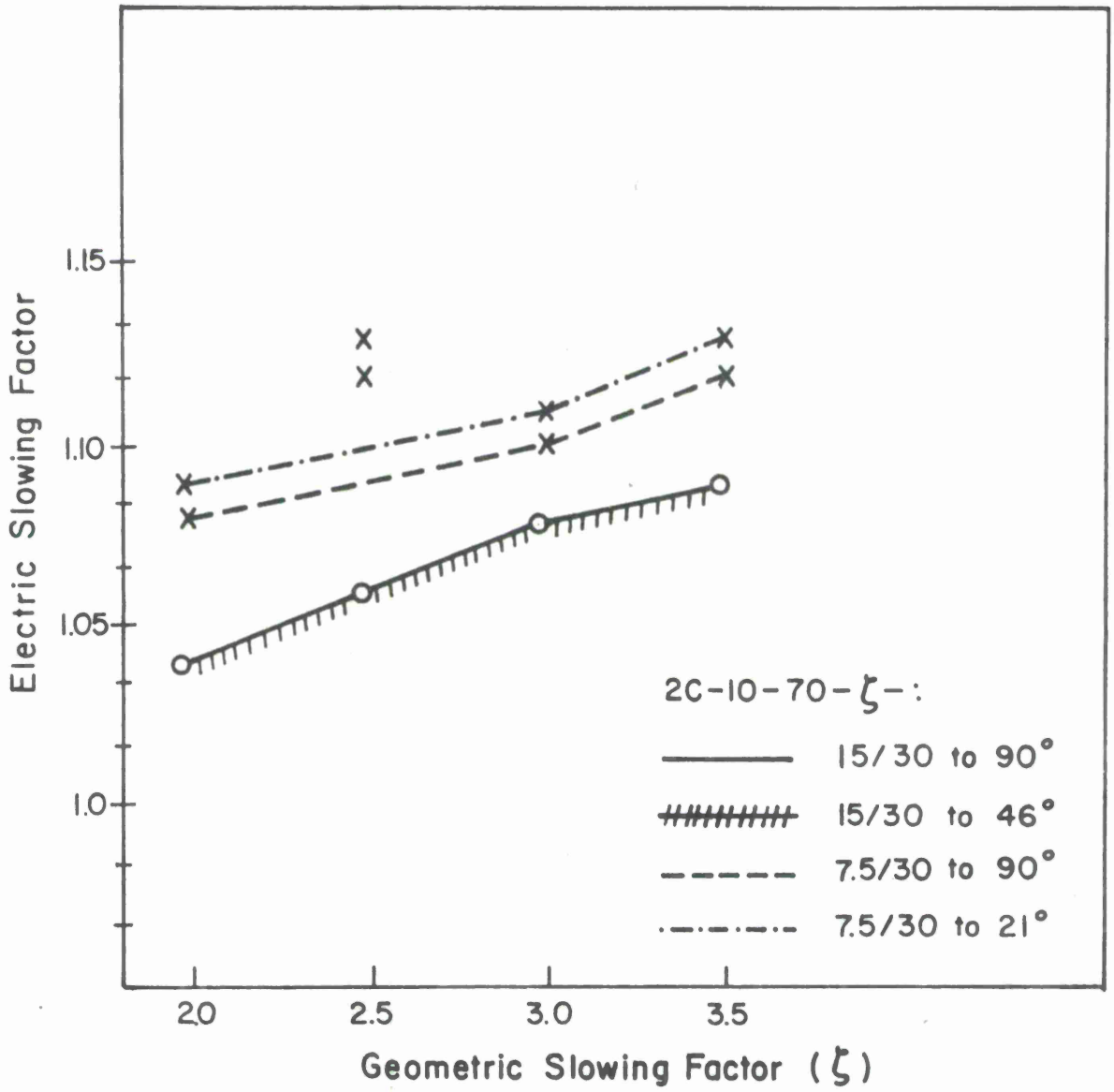

Figure 11. Calculated electric slowing factor compared to the geometrical slowing factor (ζ) for wide and thin zigzag antennas, relative to the respective complementary and "equivalent" arm width spiral antennas ($\alpha = 70°$).

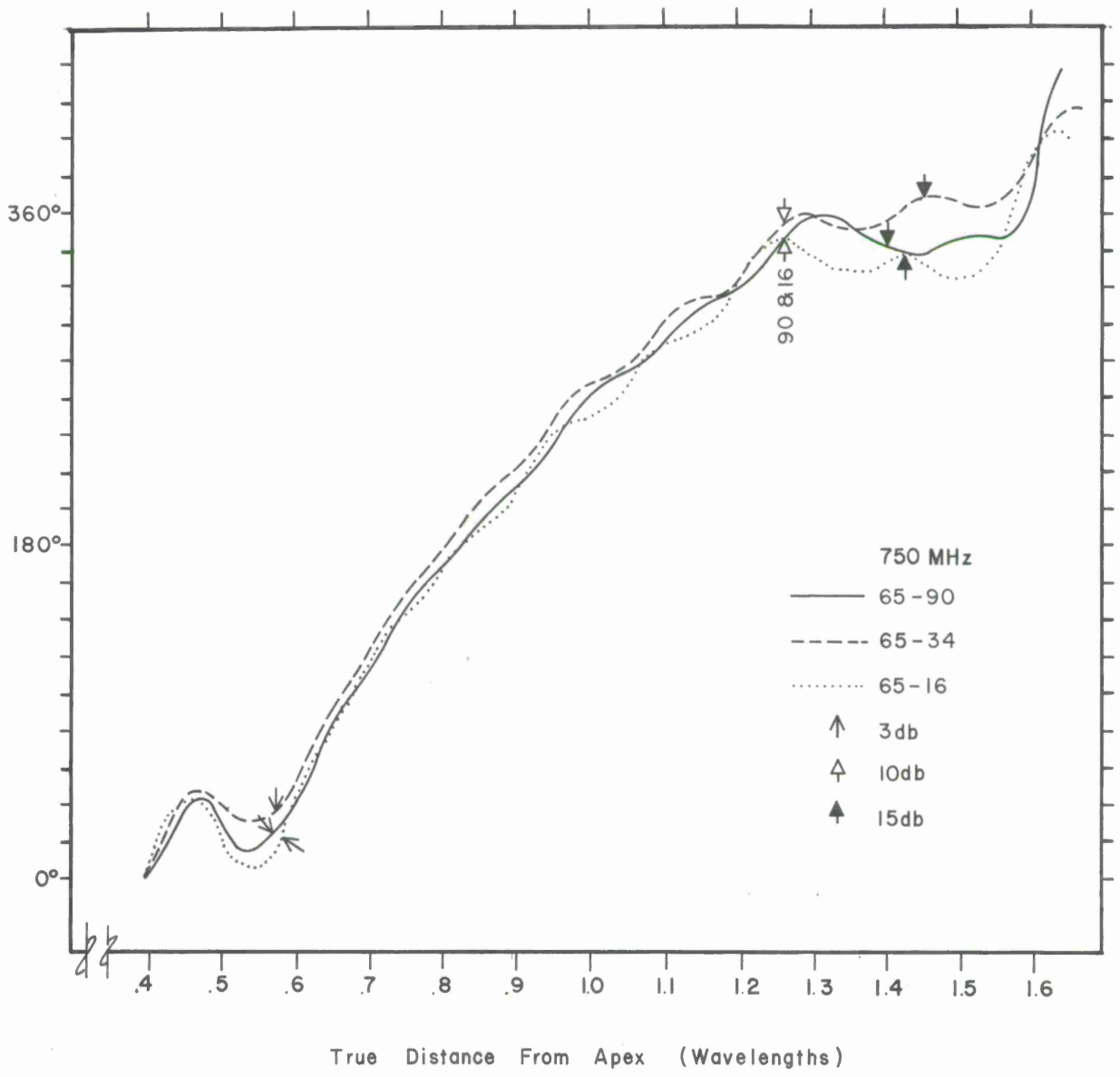

Figure 12. Relative phase of the near fields measured on the normal spiral antennas ($\alpha = 65°$).

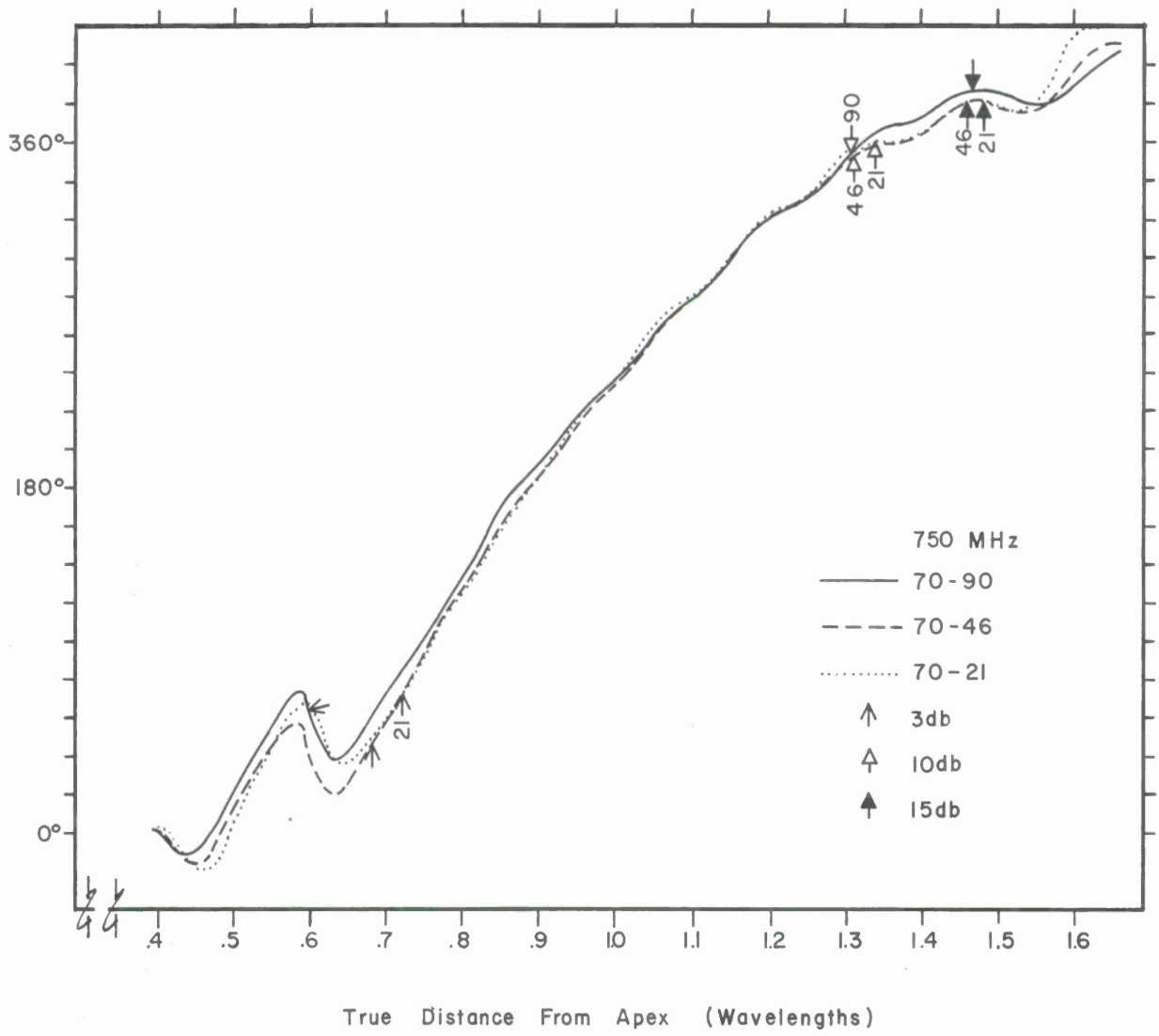

Figure 13. Relative phase of the near fields measured on the normal spiral antennas ($\alpha = 70°$).

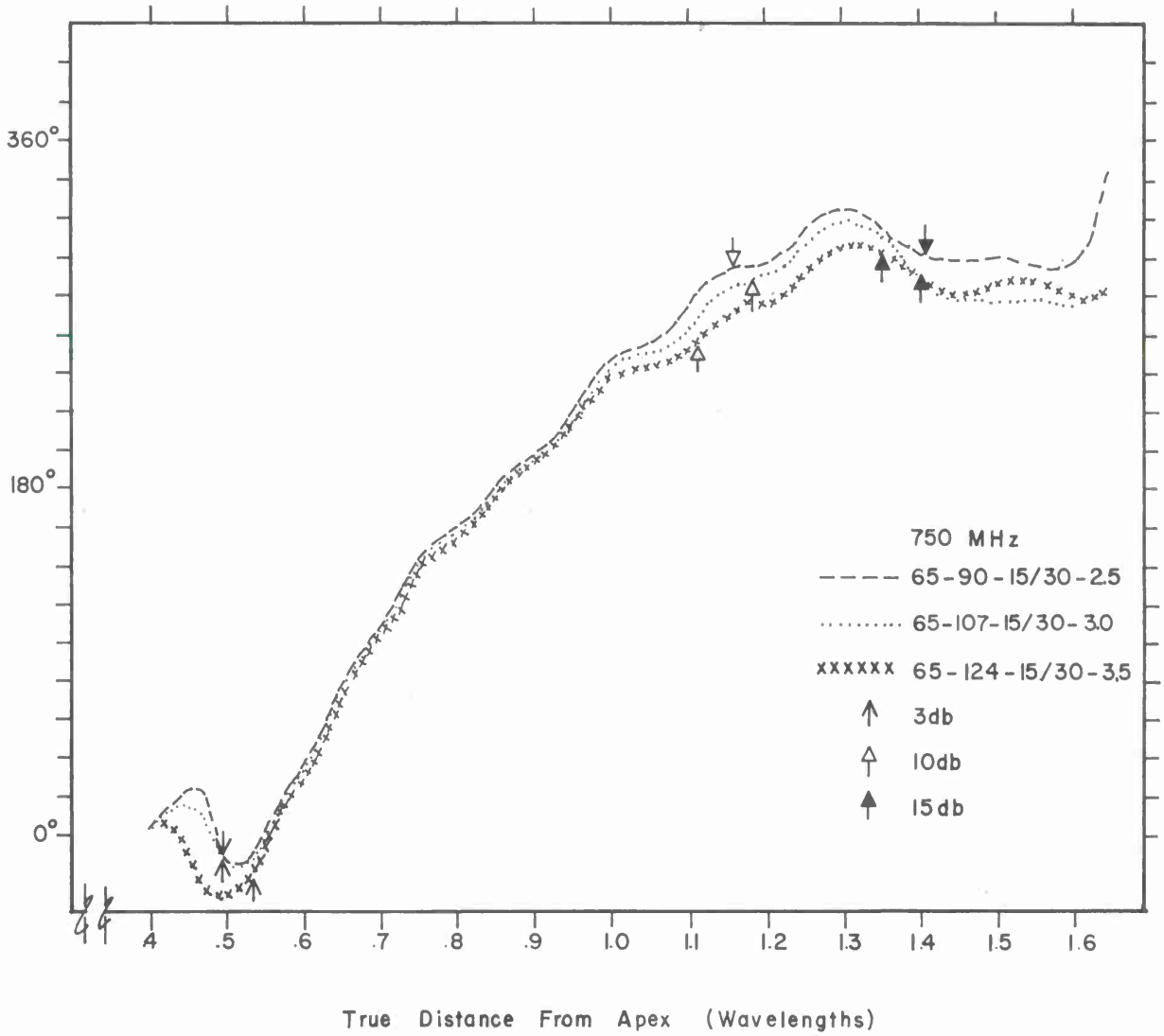

Figure 14. Relative phase of the near fields measured on the wide zigzag antennas for all geometrical slowing factors (ζ) ($\alpha = 65°$).

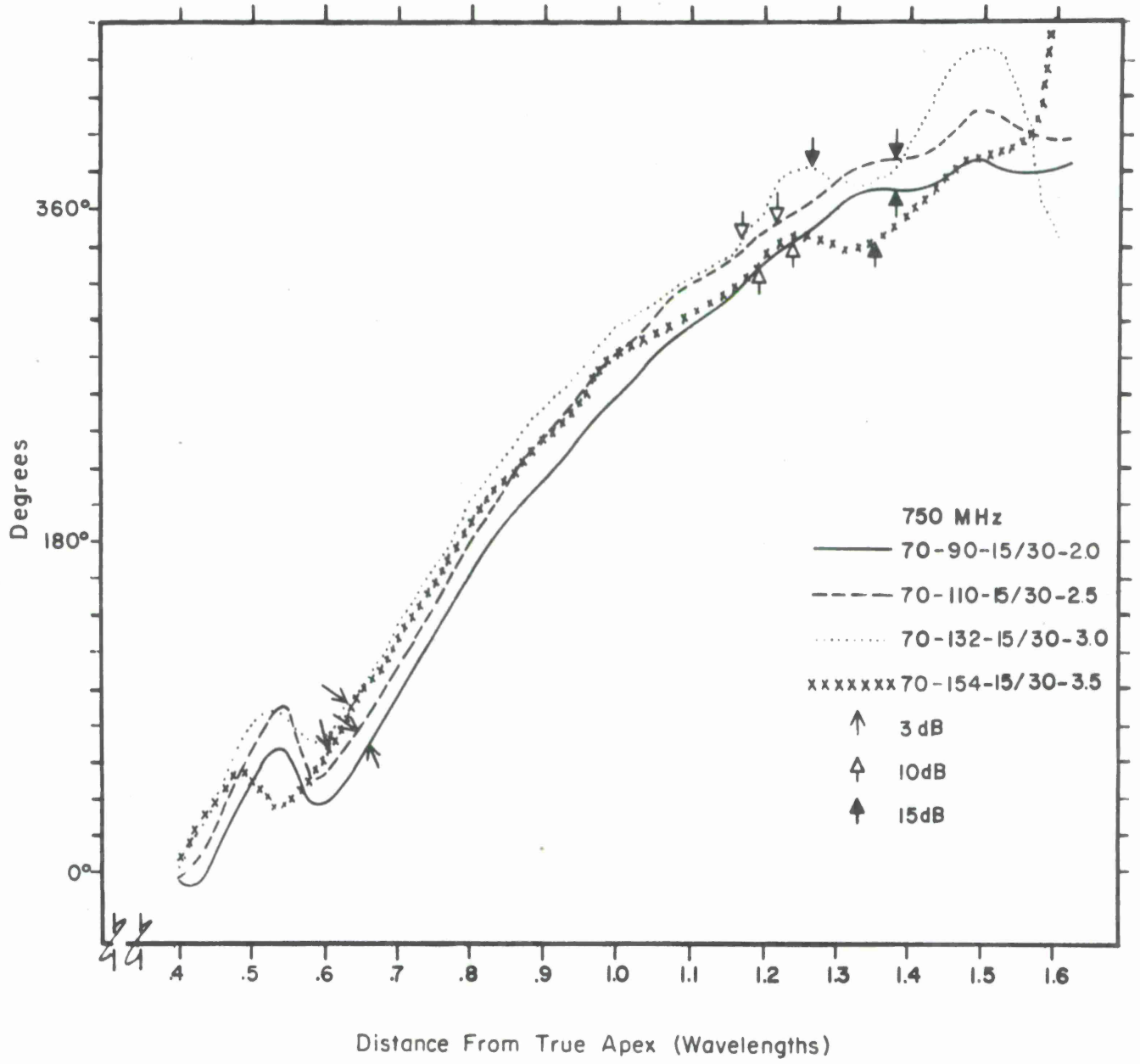

Figure 15. Relative phase of the near fields measured on the wide zigzag antennas for all geometrical slowing factors (ζ) (α = 70°).

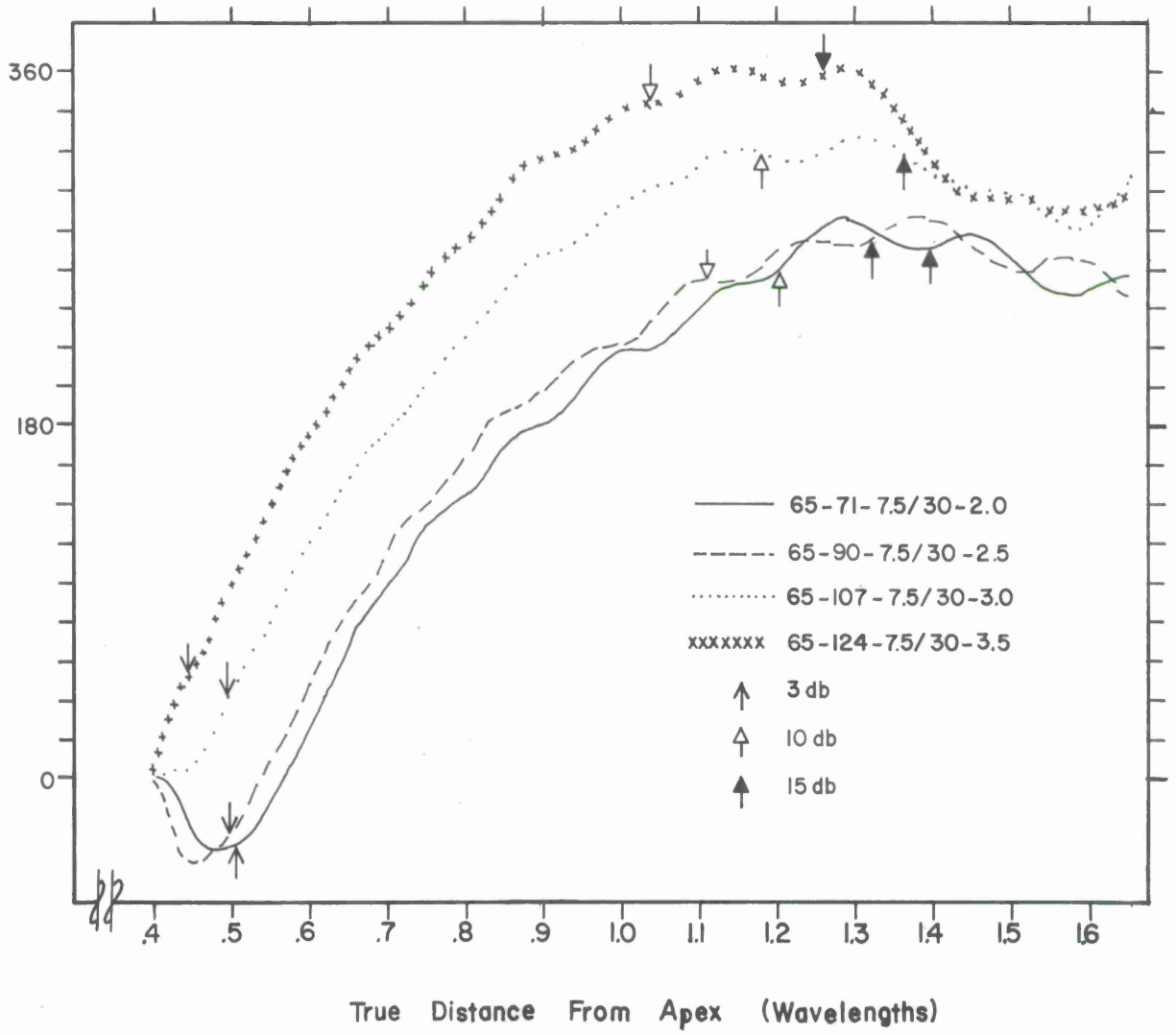

Figure 16. Relative phase of the near fields measured on the thin zigzag antennas for all geometrical slowing factors (ζ) (α = 65°).

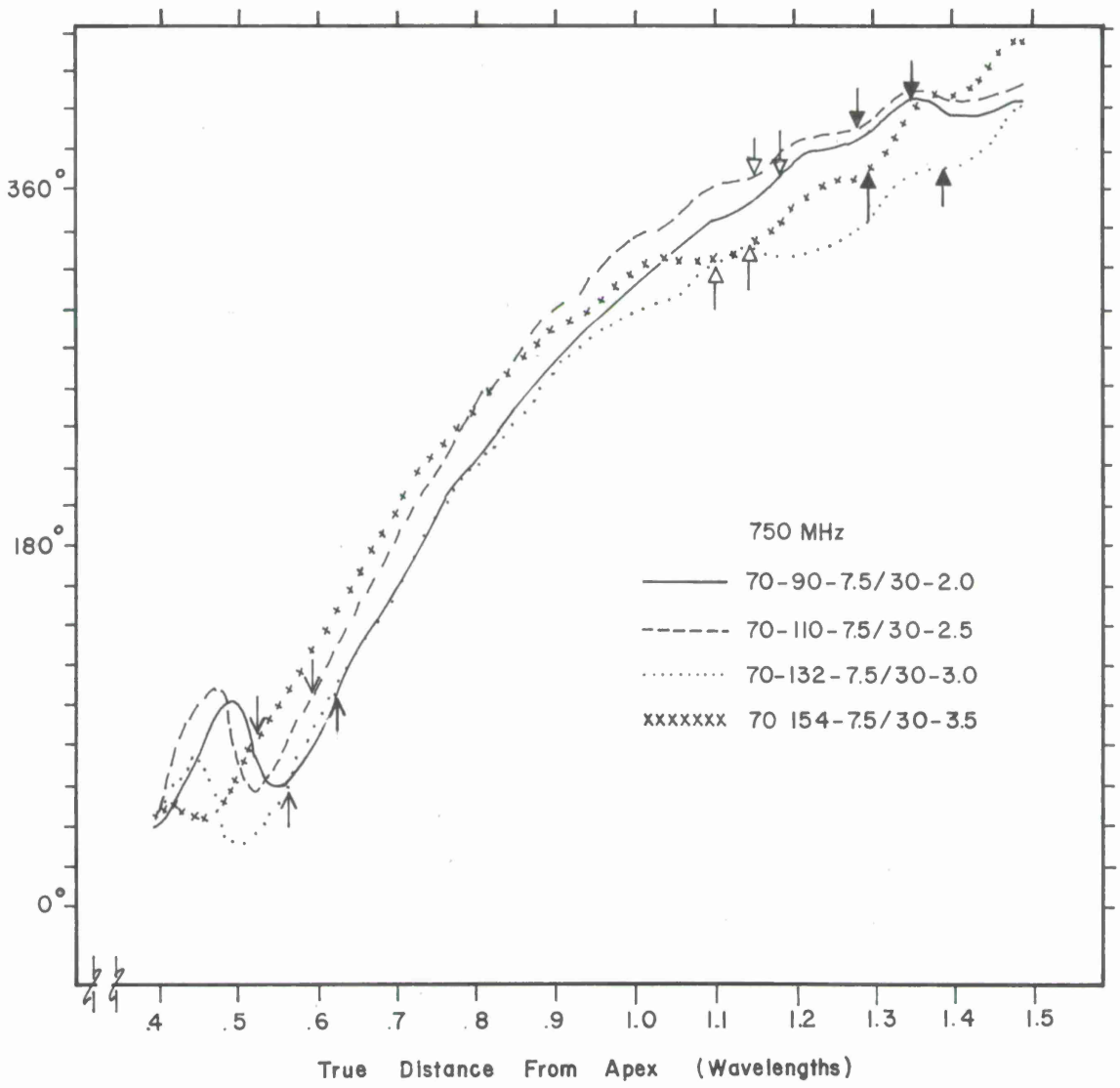

Figure 17. Relative phase of the near fields measured on the thin zigzag antennas for all geometrical slowing factors (ζ) (α = 70°).

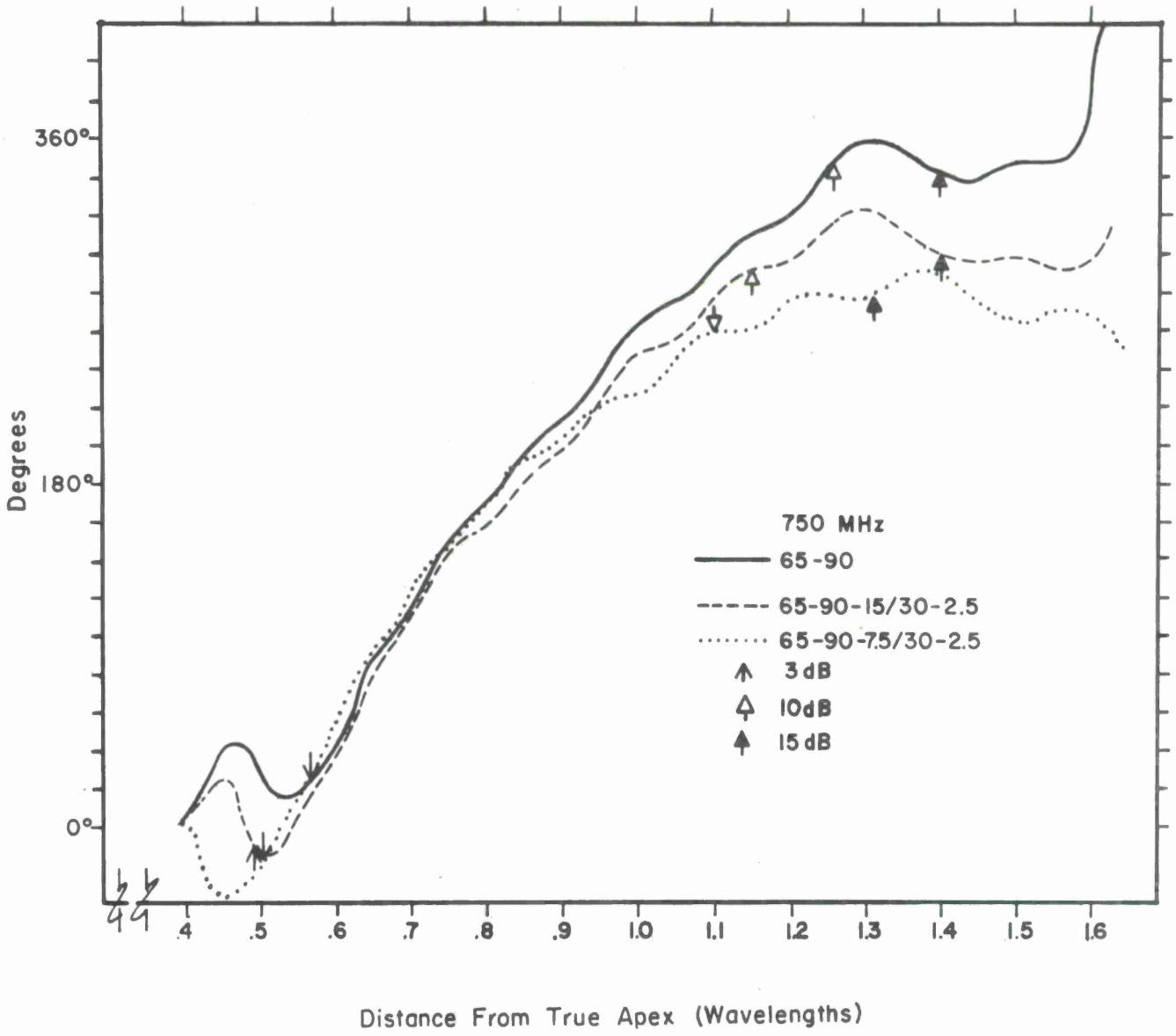

Figure 18. Comparing the relative phase of the near fields for wide and thin zigzag antennas to complementary antenna (α = 65°, geometrical slowing factor (ζ) = 2.5).

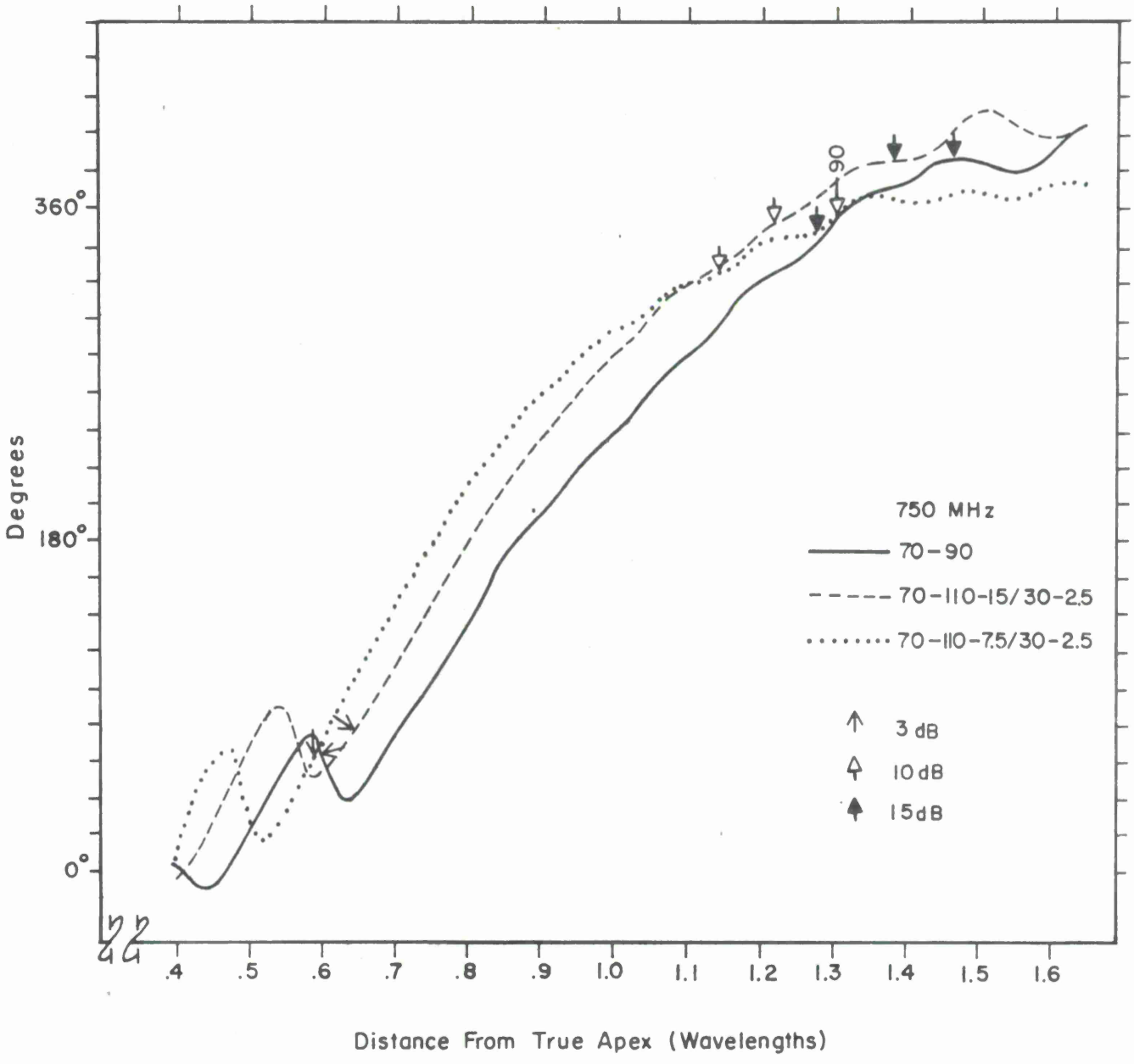

Figure 19. Comparing the relative phase of the near fields for wide and thin zigzag antennas to complementary antennas (α = 70°, geometrical slowing factor (ζ) = 2.5).

We note that there is a displacement in some of the curves indicating that the guide wavelength along the surface has been reduced, causing the shift of the active region towards the apex. Thus the active region begins and ends at smaller radii, yielding a smaller antenna. This corroborates the near-field amplitude data.

1.4 Far-Field Measurements

1.4.1 Radiation Patterns

Radiation patterns were recorded for the conventional, or "control" antennas, and the slow-wave antennas at 800 MHz. At this frequency the base diameter was approximately 0.47 wavelengths and all of these antennas should be operating in a normal "frequency independent mode", i.e., with a very minimum of tip or base truncation effects. Patterns were recorded for two planes of constant angle ϕ. The antennas were illuminated by a linearly polarized field with constantly rotating plane of polarization. The patterns are plotted in decibels and hence the width of envelope of the excursions of the pattern, at any angle θ, is the axial ratio in dB of the antenna at that angle of incidence.

Patterns for a conventional antenna with spiral angle $\alpha = 65°$, and a slow-wave antenna with $\alpha = 65°$ and a slowing factor of 3.5, are shown in Figures 20 and 21. Similar patterns for $\alpha = 70°$ antennas are shown in Figures 22 and 23.

The increase in beamwidth, as the arms are constructed in a slow-wave geometry, is obvious. The wider beam width and "rougher" patterns result from the broadening of the active region.[4] A fairly complete set of radiation patterns for the range of parameters which was investigated is included as Appendix D.

The measured maximum 3 dB and 10 dB beamwidths of the $\alpha = 70°$ antennas are plotted in Figure 24. The conventional antennas (no slowing) with $\delta' = 90°$, are plotted along the left axis (a slowing factor of 1.0). The slow-wave structures with the wider arms (15/30) showed less change with increased slowing than the thin arm (7.5/30). This effect was noted

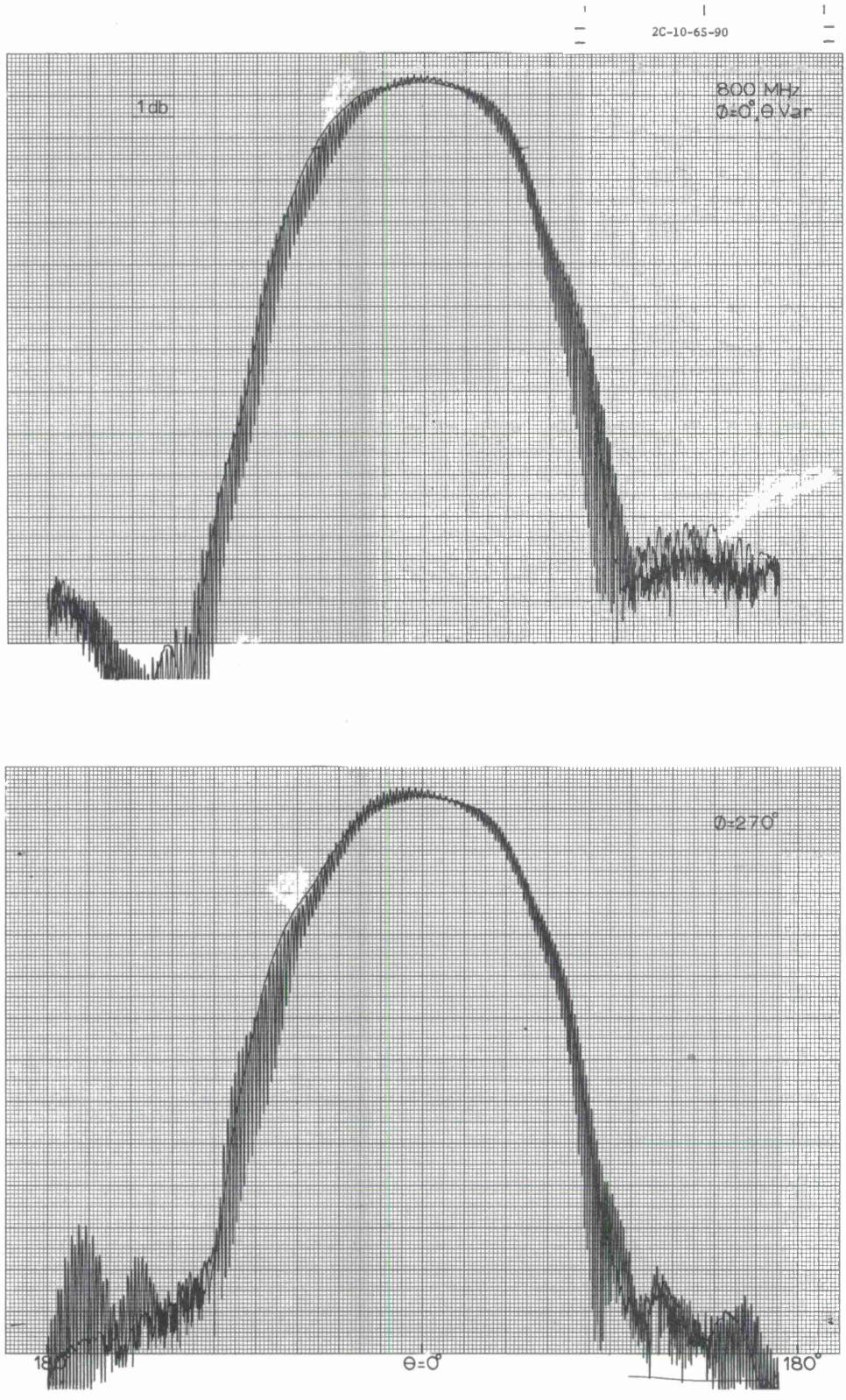

Figure 20. Radiation patterns of conventional conical spiral antenna, $\alpha = 65°$, $\delta' = 90°$. Recorded with continually rotating linearly polarized receiving antenna.

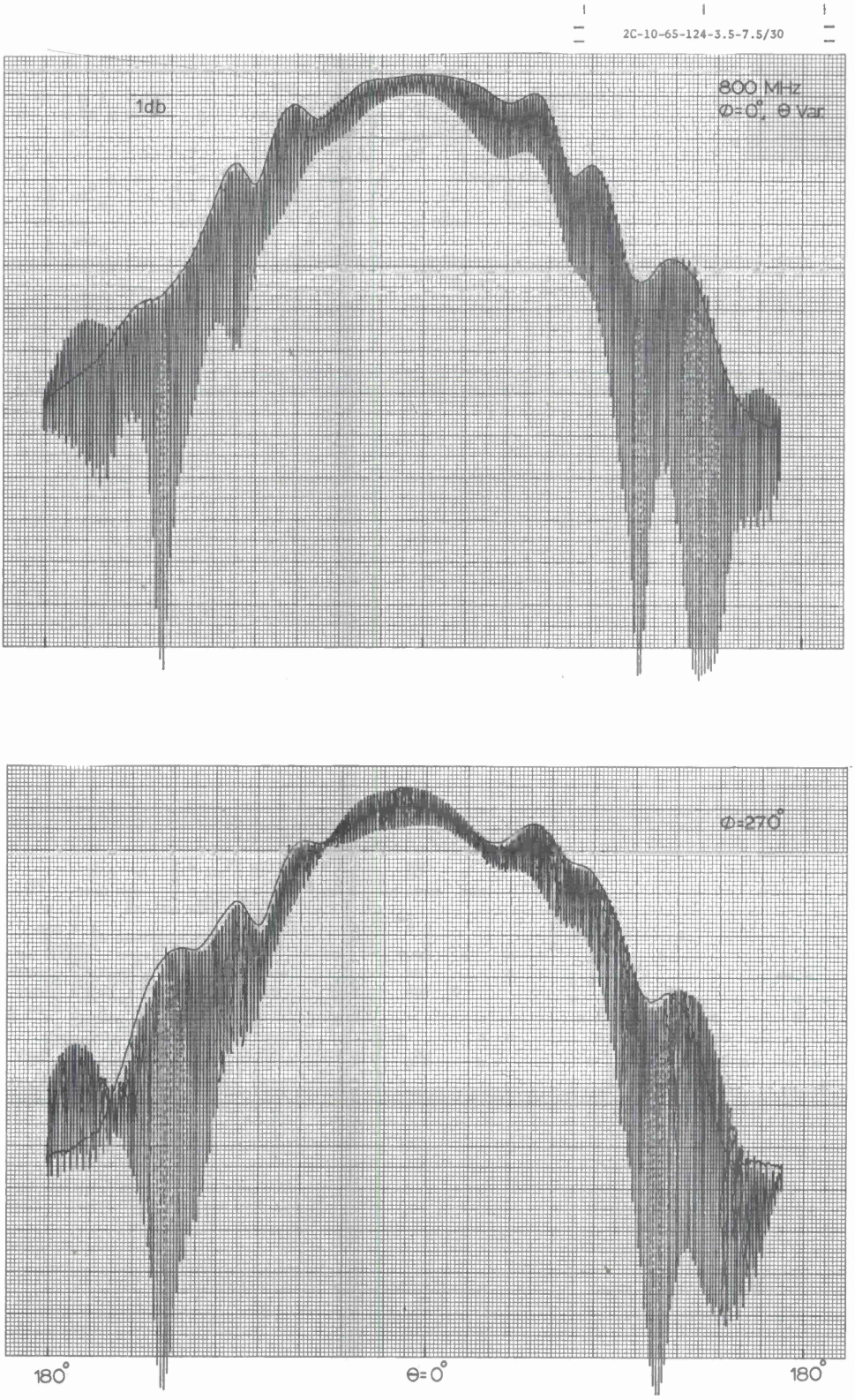

Figure 21. Radiation patterns of slow-wave conical spiral antenna, $\alpha = 65°$, narrow arm width (7.5/30), slowing factor 3.5.

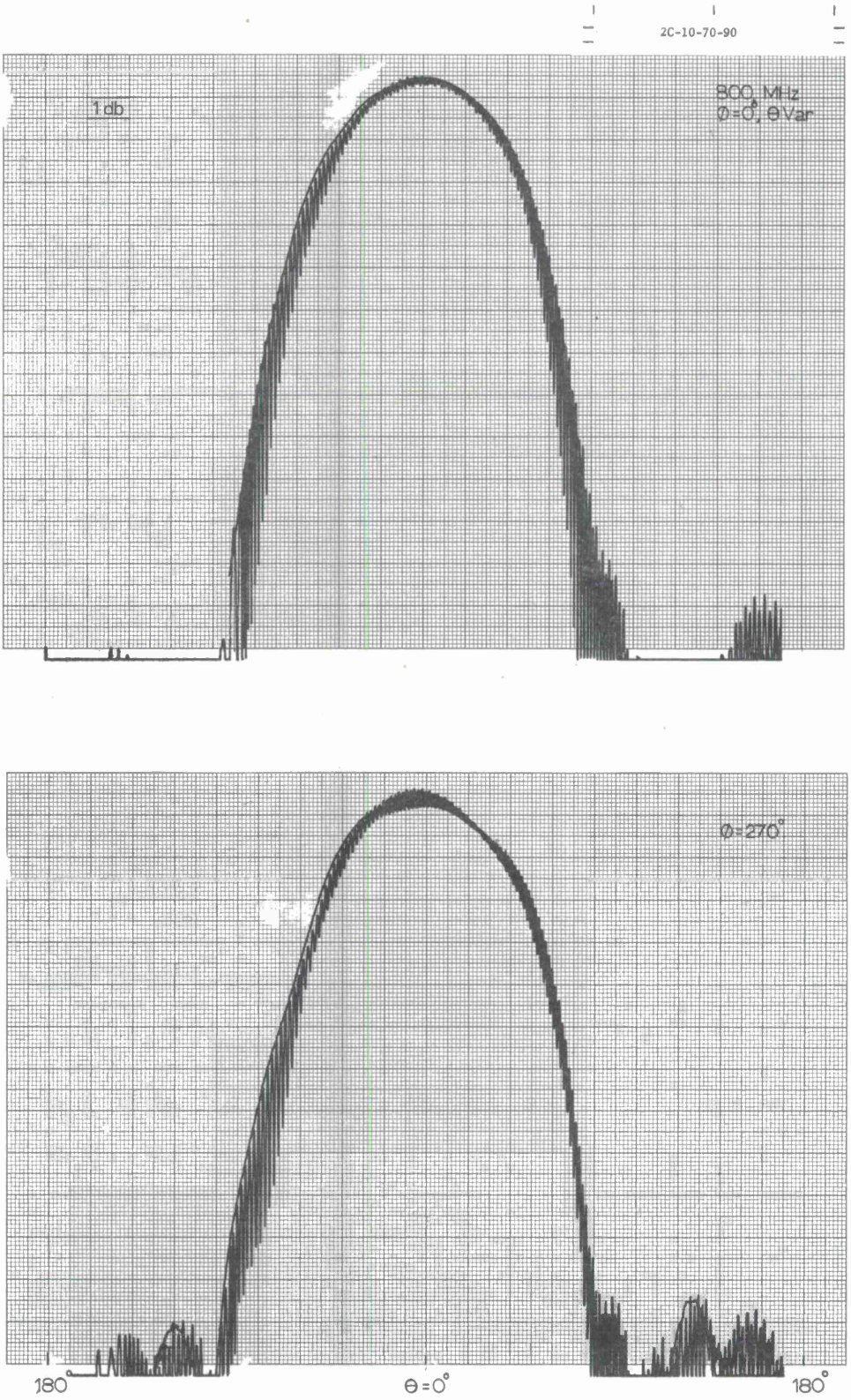

Figure 22. Radiation patterns of conventional conical spiral antenna, $\alpha = 70°$, $\delta' = 90°$.

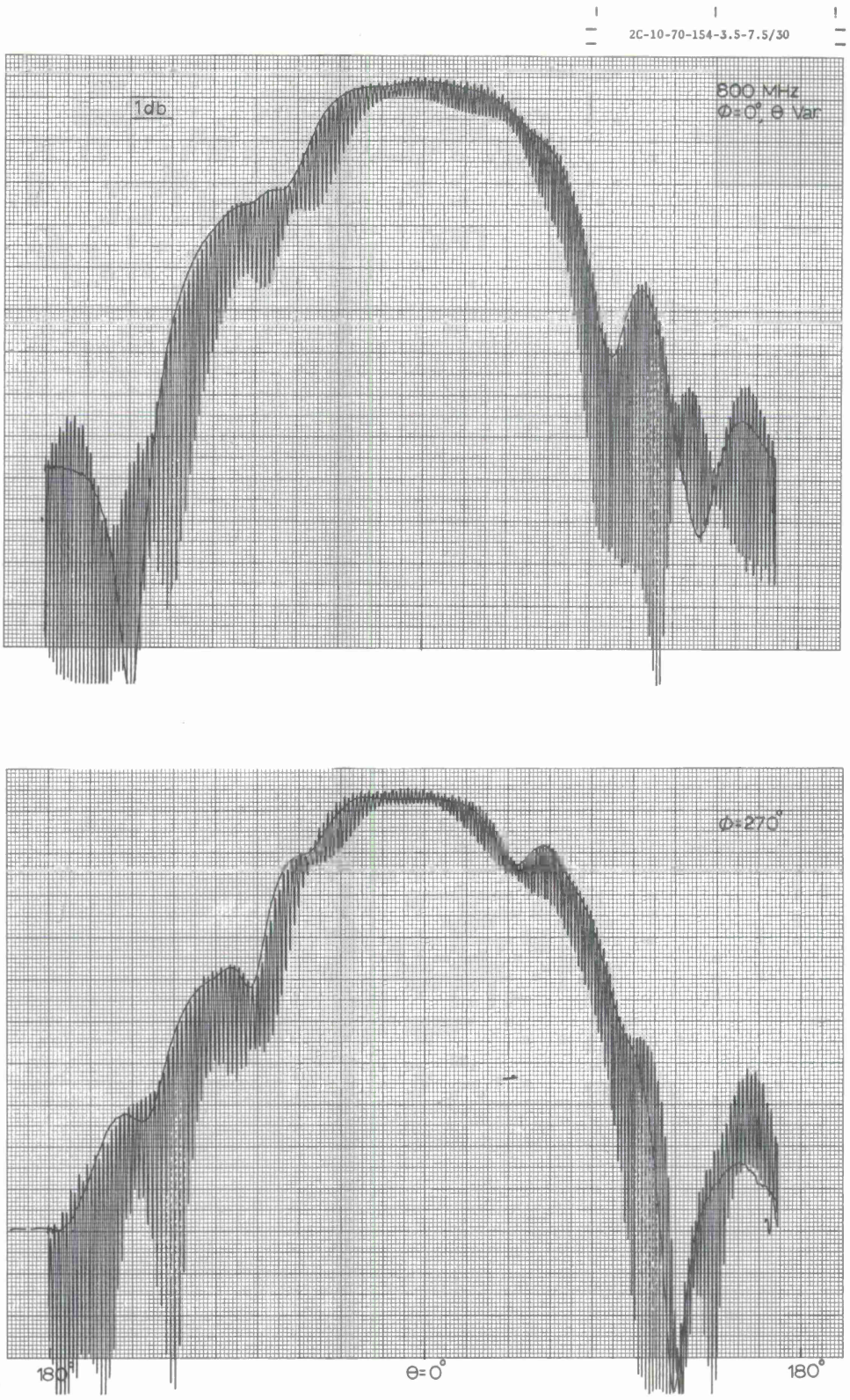

Figure 23. Radiation patterns of slow-wave conical spiral antenna, $\alpha = 70°$, narrow arm width (7.5/30), slowing factor 3.5.

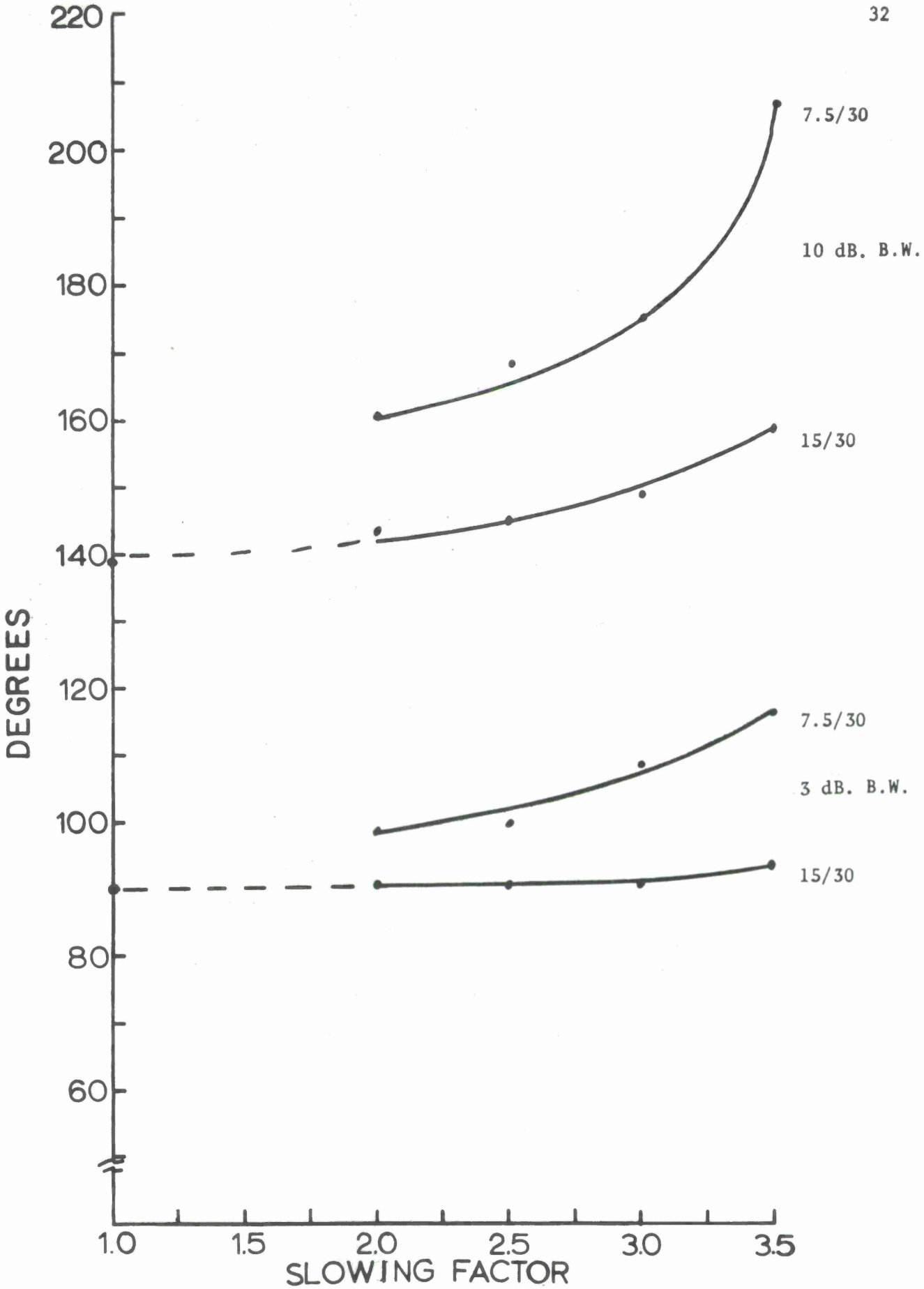

Figure 24. The 3 dB and 10 dB beamwidths of the $\alpha = 70^{\circ}$ antennas as a function of arm width and slowing factor.

in the near field measurements. This effect can possibly be due to two things. First, it seems possible that the antenna current follows along the shortest possible path down the antenna. It apparently is concentrated along the inner edge of the undulation, and a thinner arm width (constructed as these antennas were) causes this inner edge to be a longer path. Secondly, the wider arm width causes adjacent segments of arms to be closer and the capacitive coupling from segment to segment is greatly increased.

The patterns of the $\alpha = 65°$ antennas were rougher than those for the $\alpha = 70°$ antennas, and this trend continues for still more loosely wrapped antennas. As a result the trend in beam widths was not as consistent for the $\alpha = 65°$ antennas, and only the data for the $\alpha = 70°$ is condensed on Figure 24.

1.4.2 Relative Gain

For application of these antennas at wavelengths long for the size of the structure, the relative gain on axis becomes important. To obtain information on this gain, sweep frequency measurements were made from 250 to 900 MHz, where the base diameter of these antennas varied from approximately .15 to .54 wavelengths. The antennas were illuminated with a linearly polarized incident field with the plane of polarization constantly rotating. The magnitude of the signal received by the antenna under test was recorded where this field was incident upon the apex of the cone ($\theta = 0°$), and incident upon the base of the cone ($\theta = 180°$). Figure 25 shows a plot of this recorded data for a conventional antenna (2C-10-65-90). Similar plots were made for the slow-wave antennas.

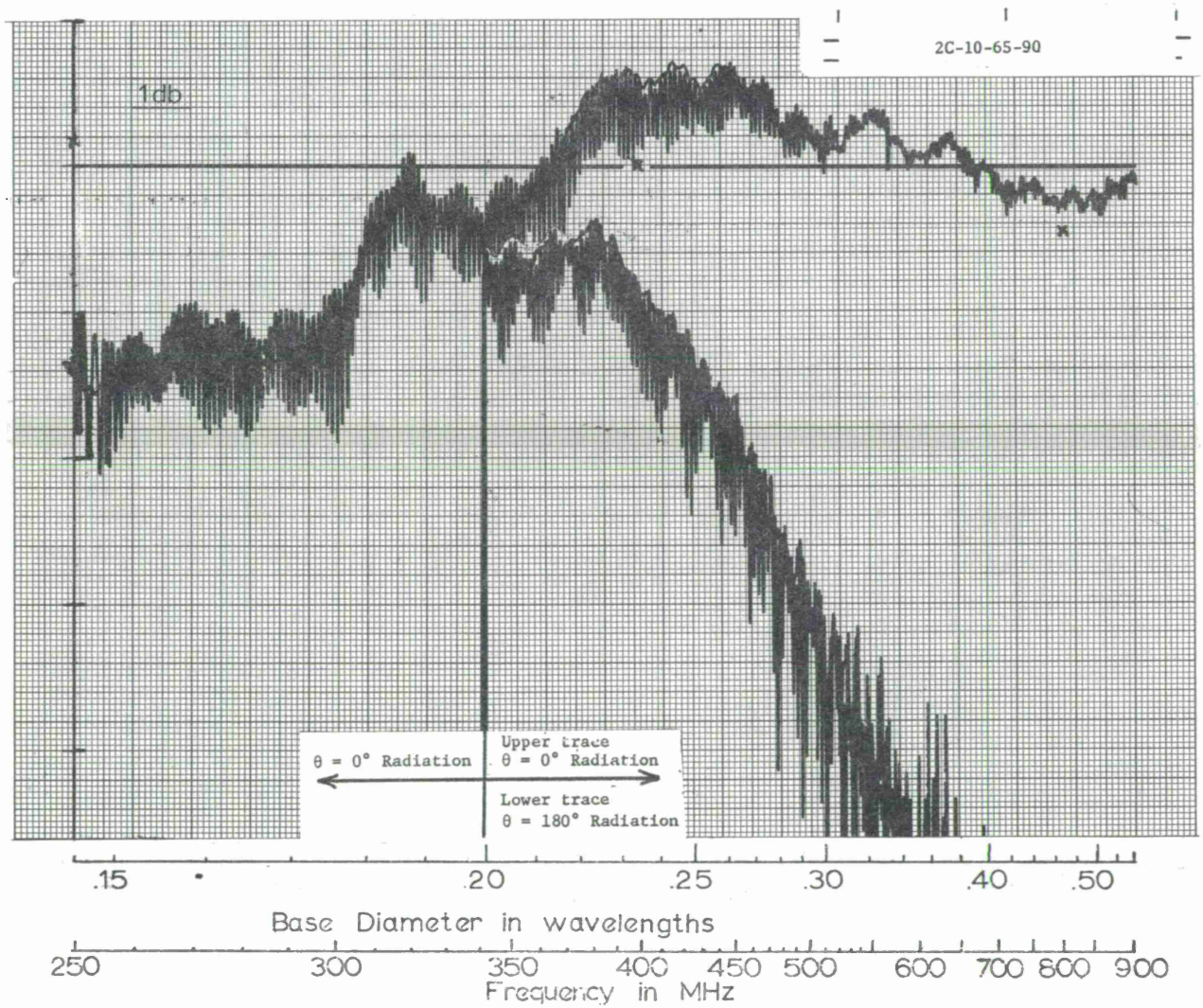

Figure 25 Relative amplitude of axial radiation from conventional conical spiral antenna, $\alpha = 65°$, $\delta' = 90°$. Data recorded with rotating linearly polarized receiving antenna. Data points indicated by x are isotropic levels.

At about 340 MHz the front-to-back ratio had decreased to 2 dB and since at lower frequencies the traces for front ($\theta = 0°$) and back ($\theta = 180°$) radiation merge and become difficult to distinguish, the plot of the back radiation ($\theta = 180°$) is shown only for higher frequencies. The exact cut-off point for this and later plots for other antennas is arbitrary and is only a very rough basis for comparing antennas.

It should be noted that the generator exciting the source antenna was not leveled and the source antenna (an LPDA) did not have a constant gain. Hence the reader must exercise caution in interpreting this type plot. However, since the test conditions were held constant for all antennas, a direct comparison between plots for different antennas is valid. In addition, each plot contains much information.

The width of the envelope of each trace is the axial-ratio in dB. The front to back ratio in dB is readily available. The "broadband power gain" at base diameters of approximately .147, .235, and .475 wavelength (i.e., 250, 400 and 800 MHz) can be readily determined since at these wavelengths the linearly polarized isotropic level is indicated by a small X.

By current IEEE Standards definition, the power gain of an antenna is an inherent property of the antenna and it does not involve system losses arising from mismatch of impedance. We here are interested in the broadband unmatched properties of the antenna, so mismatch loss to a 50 ohm system is included in the data. We thus have defined the "broadband power gain" to be the conventional power gain modified by mismatch loss.

This broadband power gain (BBPG) can be determined at the three mentioned wavelengths by adding the power in the two orthogonal components of the elliptically polarized response and comparing this to the isotropic

level. Table No. 1 has been calculated to make this convenient. The axial ratio in dB, is read from the recorded plot. Table No. 1 is entered at this axial ratio and a correction term (C) indicating the relative power in dB in the smaller of the two orthogonal circularly polarized field components is determined. This correction term is added to the maximum recorded level at that point on the plot, to determine the total power received (or radiated in the transmitting case). The difference between this total power level and the isotropic level is the broadband power gain of the antenna in dB. Thus the BBPG for the antenna of Figure 25 is approximately -4.6, +5.0, and +4.1 dB at 250, 400, and 800 MHz.

A similar plot for a thin arm ($\delta' = 16°$) conventional antenna with the same rate of wrap is shown in Figure 26 and for a slow-wave structure with this same equivalent arm width ($\delta' = 16°$) and a slowing factor of 3.5 is shown in Figure 27.

To evaluate the performance of the slow-wave antenna we can compare it to the $\delta' = 90°$ antenna (the "optimized" antenna) as in Figure 28 and to the $\delta' = 16°$ antenna as in Figure 29.

There is a significant increase in energy radiated on-axis at the very long wavelengths from the slow-wave antenna. As will become evident in the next section, this increase in the BBPG is primarily due to a better impedance match to a 50-ohm system, and hence less energy reflected at the antenna terminals.

Figures 30 through 34 show these on-axis response curves for a conventional $\delta' = 90°$, $\delta' = 21°$ and a slow-wave antenna, all with an angle of wrap, α, of 70°.

Response curves for other antennas in the two families which were tested are included in Appendix E hereto.

Table No. 1. Relationship between a given axial ratio in db (R), and the relative power in dB in the smaller of the two orthogonal circularly polarized field components (C).

R dB	C dB	R dB	C dB	R dB	C dB	R dB	C dB	R dB	C dB	R dB	C dB	R dB	C dB
0.00	3.01	1.00	2.54	2.00	2.12	3.00	1.76	4.10	1.43	6.75	0.83	10.7	0.35
0.02	3.00	1.02	2.53	2.02	2.12	3.02	1.76	4.15	1.41	6.80	0.82	10.8	0.35
0.04	2.99	1.04	2.52	2.04	2.11	3.04	1.75	4.20	1.40	6.85	0.82	10.9	0.34
0.06	2.98	1.06	2.51	2.06	2.10	3.06	1.74	4.25	1.39	6.90	0.81	11.0	0.33
0.08	2.97	1.08	2.50	2.08	2.09	3.08	1.74	4.30	1.37	6.95	0.80	11.1	0.32
0.10	2.96	1.10	2.50	2.10	2.09	3.10	1.73	4.35	1.36	7.00	0.79	11.2	0.32
0.12	2.95	1.12	2.49	2.12	2.08	3.12	1.72	4.40	1.35	7.05	0.78	11.3	0.31
0.14	2.94	1.14	2.48	2.14	2.07	3.14	1.72	4.45	1.33	7.10	0.77	11.4	0.30
0.16	2.93	1.16	2.47	2.16	2.06	3.16	1.71	4.50	1.32	7.15	0.77	11.5	0.30
0.18	2.92	1.18	2.46	2.18	2.06	3.18	1.71	4.55	1.31	7.20	0.76	11.6	0.29
0.20	2.91	1.20	2.45	2.20	2.05	3.20	1.70	4.60	1.29	7.25	0.75	11.7	0.28
0.22	2.90	1.22	2.44	2.22	2.04	3.22	1.69	4.65	1.28	7.30	0.74	11.8	0.28
0.24	2.89	1.24	2.43	2.24	2.03	3.24	1.69	4.70	1.27	7.35	0.73	11.9	0.27
0.26	2.88	1.26	2.43	2.26	2.03	3.26	1.68	4.75	1.25	7.40	0.73	12.0	0.27
0.28	2.87	1.28	2.42	2.28	2.02	3.28	1.67	4.80	1.24	7.45	0.72	12.2	0.25
0.30	2.86	1.30	2.41	2.30	2.01	3.30	1.67	4.85	1.23	7.50	0.71	12.4	0.24
0.32	2.85	1.32	2.40	2.32	2.00	3.32	1.66	4.90	1.22	7.55	0.70	12.6	0.23
0.34	2.84	1.34	2.39	2.34	2.00	3.34	1.65	4.95	1.21	7.60	0.70	12.8	0.22
0.36	2.83	1.36	2.38	2.36	1.99	3.36	1.65	5.00	1.19	7.65	0.69	13.0	0.21
0.38	2.82	1.38	2.37	2.38	1.98	3.38	1.64	5.05	1.18	7.70	0.68	13.2	0.20
0.40	2.81	1.40	2.37	2.40	1.97	3.40	1.63	5.10	1.17	7.75	0.67	13.4	0.19
0.42	2.81	1.42	2.36	2.42	1.97	3.42	1.63	5.15	1.16	7.80	0.67	13.6	0.19
0.44	2.80	1.44	2.35	2.44	1.96	3.44	1.62	5.20	1.15	7.85	0.66	13.8	0.18
0.46	2.79	1.46	2.34	2.46	1.95	3.46	1.62	5.25	1.13	7.90	0.65	14.0	0.17
0.48	2.78	1.48	2.33	2.48	1.94	3.48	1.61	5.30	1.12	7.95	0.65	14.2	0.16
0.50	2.77	1.50	2.32	2.50	1.94	3.50	1.60	5.35	1.11	8.00	0.64	14.4	0.16
0.52	2.76	1.52	2.32	2.52	1.93	3.52	1.60	5.40	1.10	8.10	0.63	14.6	0.15
0.54	2.75	1.54	2.31	2.54	1.92	3.54	1.59	5.45	1.09	8.20	0.61	14.8	0.14
0.56	2.74	1.56	2.30	2.56	1.92	3.56	1.59	5.50	1.08	8.30	0.60	15.0	0.14
0.58	2.73	1.58	2.29	2.58	1.91	3.58	1.58	5.55	1.07	8.40	0.59	15.2	0.13
0.60	2.72	1.60	2.28	2.60	1.90	3.60	1.57	5.60	1.06	8.50	0.57	15.4	0.12
0.62	2.71	1.62	2.28	2.62	1.89	3.62	1.57	5.65	1.05	8.60	0.56	15.6	0.12
0.64	2.70	1.64	2.27	2.64	1.89	3.64	1.56	5.70	1.04	8.70	0.55	15.8	0.11
0.66	2.69	1.66	2.26	2.66	1.88	3.66	1.56	5.75	1.02	8.80	0.54	16.0	0.11
0.68	2.68	1.68	2.25	2.68	1.87	3.68	1.55	5.80	1.01	8.90	0.53	16.5	0.10
0.70	2.67	1.70	2.24	2.70	1.87	3.70	1.54	5.85	1.00	9.00	0.52	17.0	0.09
0.72	2.66	1.72	2.24	2.72	1.86	3.72	1.54	5.90	0.99	9.10	0.50	17.5	0.08
0.74	2.66	1.74	2.23	2.74	1.85	3.74	1.53	5.95	0.98	9.20	0.49	18.0	0.07
0.76	2.65	1.76	2.22	2.76	1.85	3.76	1.53	6.00	0.97	9.30	0.48	18.5	0.06
0.78	2.64	1.78	2.21	2.78	1.84	3.78	1.52	6.05	0.96	9.40	0.47	19.0	0.05
0.80	2.63	1.80	2.20	2.80	1.83	3.80	1.51	6.10	0.95	9.50	0.46	19.5	0.05
0.82	2.62	1.82	2.20	2.82	1.82	3.82	1.51	6.15	0.94	9.60	0.45	20.0	0.04
0.84	2.61	1.84	2.19	2.84	1.82	3.84	1.50	6.20	0.93	9.70	0.44	21.0	0.03
0.86	2.60	1.86	2.18	2.86	1.81	3.86	1.50	6.25	0.92	9.80	0.43	22.0	0.03
0.88	2.59	1.88	2.17	2.88	1.81	3.88	1.49	6.30	0.91	9.90	0.42	23.0	0.02
0.90	2.58	1.90	2.16	2.90	1.80	3.90	1.48	6.35	0.91	10.00	0.41	24.0	0.02
0.92	2.57	1.92	2.16	2.92	1.79	3.92	1.48	6.40	0.90	10.1	0.40	25.0	0.01
0.94	2.57	1.94	2.15	2.94	1.78	3.94	1.47	6.45	0.89	10.2	0.40	26.0	0.01
0.96	2.56	1.96	2.14	2.96	1.78	3.96	1.47	6.50	0.88	10.3	0.39	27.0	0.01
0.98	2.55	1.98	2.13	2.98	1.77	3.98	1.46	6.55	0.87	10.4	0.38	28.0	0.01
						4.00	1.46	6.60	0.86	10.5	0.37	29.0	0.01
						4.05	1.44	6.65	0.85	10.6	0.36	30.0	0.00
								6.70	0.84				

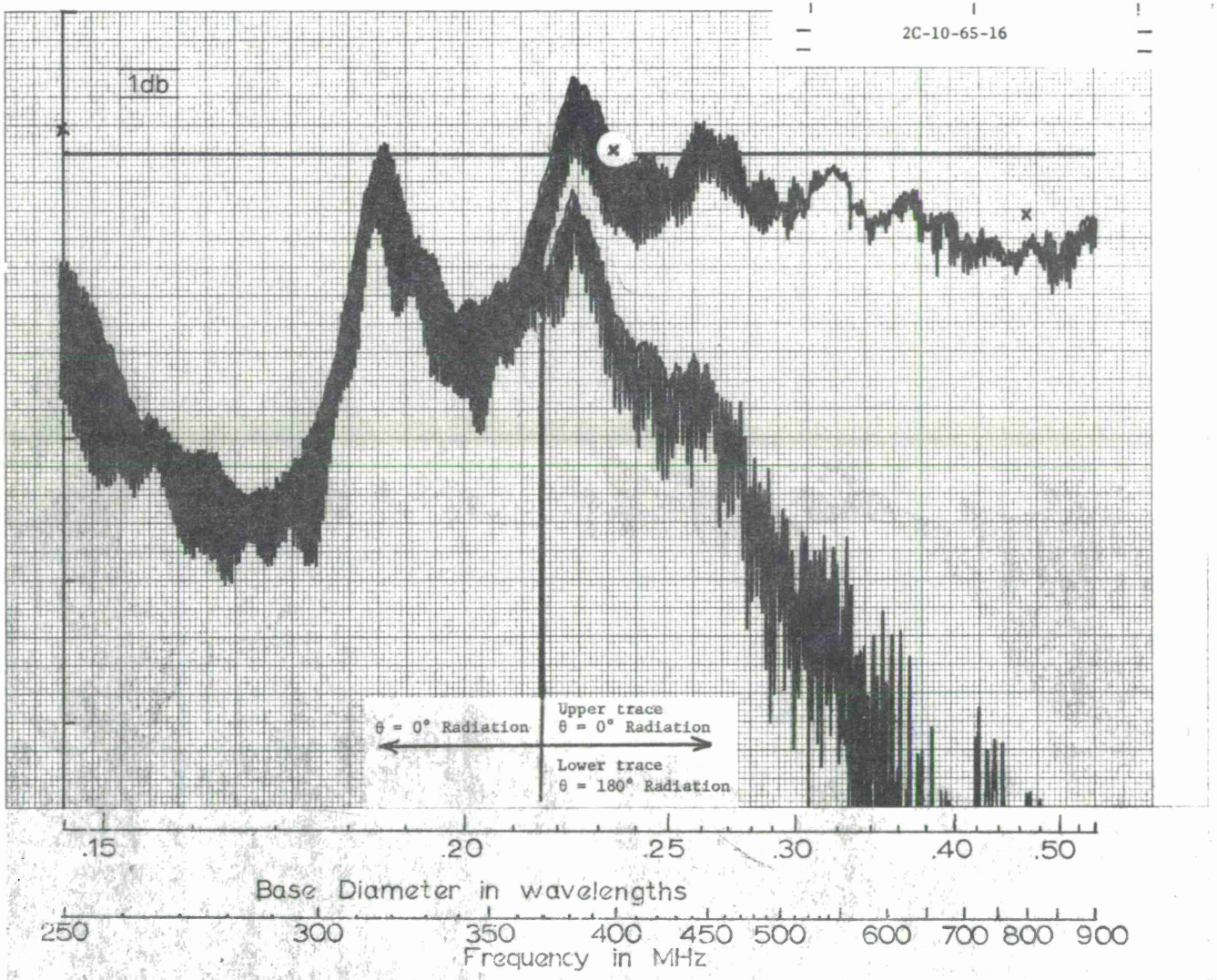

Figure 26 Relative amplitude of axial radiation from conventional conical spiral antenna, $\alpha = 65°$, $\delta' = 16°$. Data recorded with rotating linearly polarized receiving antenna. Data points indicated by x are isotropic levels.

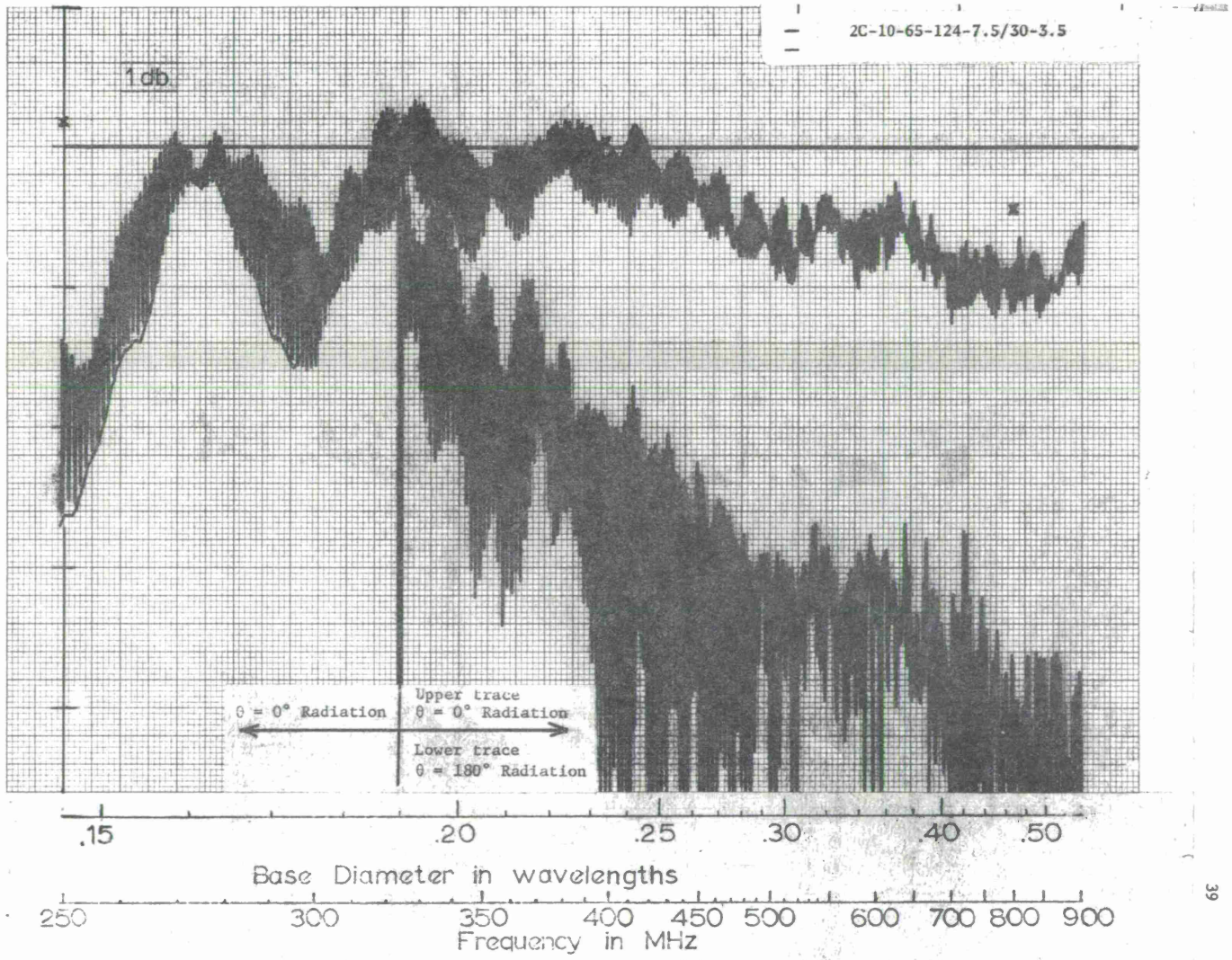

Figure 27 Relative amplitude of axial radiation from slow-wave conical spiral antenna, $\alpha = 65°$, arm width (7.5/30), slowing factor 3.5. Data points (x) are isotropic levels.

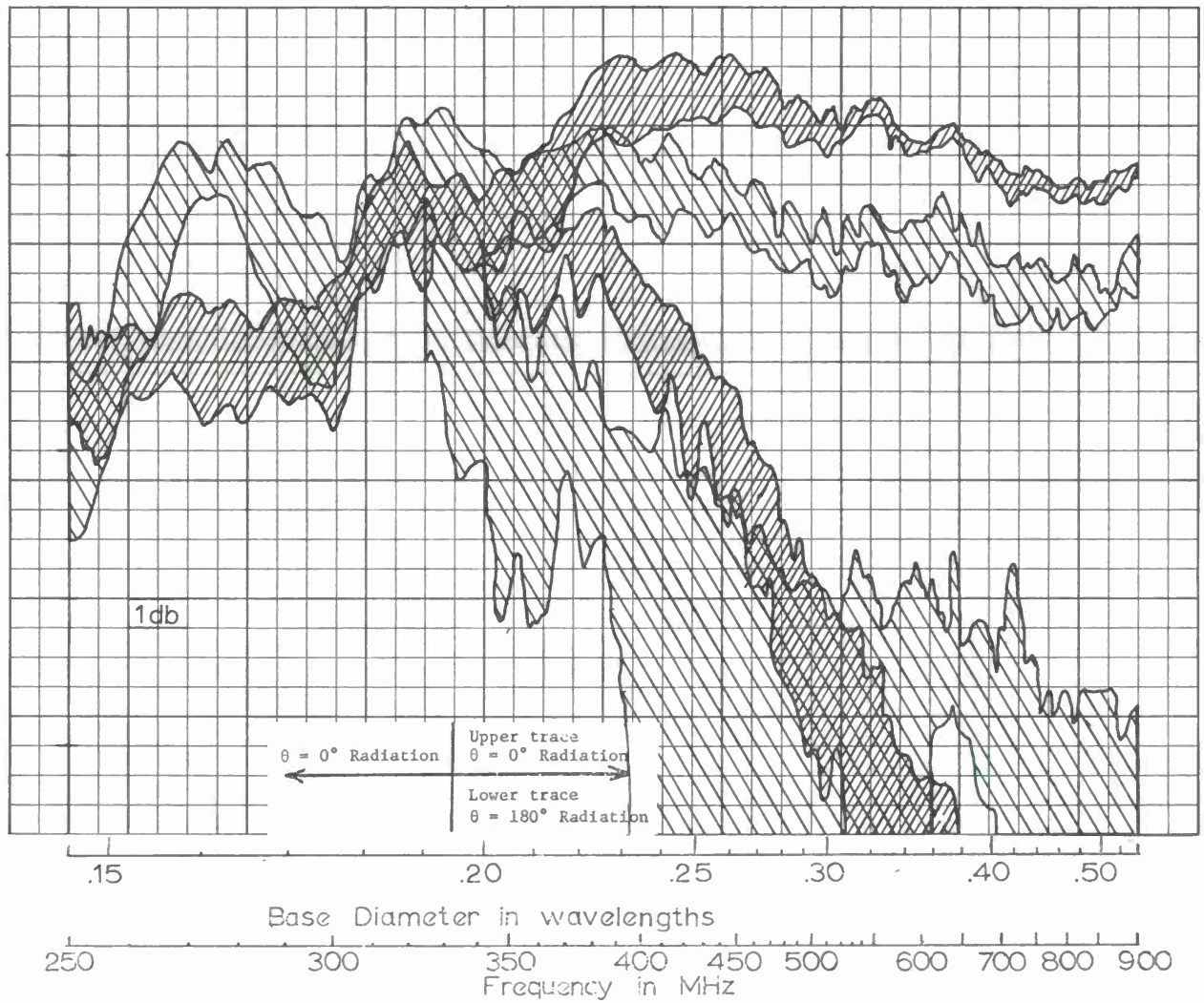

Figure 28 Data from Figures 25 and 27 superimposed to indicate relative amplitude of radiated fields from conventional complementary arm antenna ($\delta' = 90°$) and slow-wave antenna.

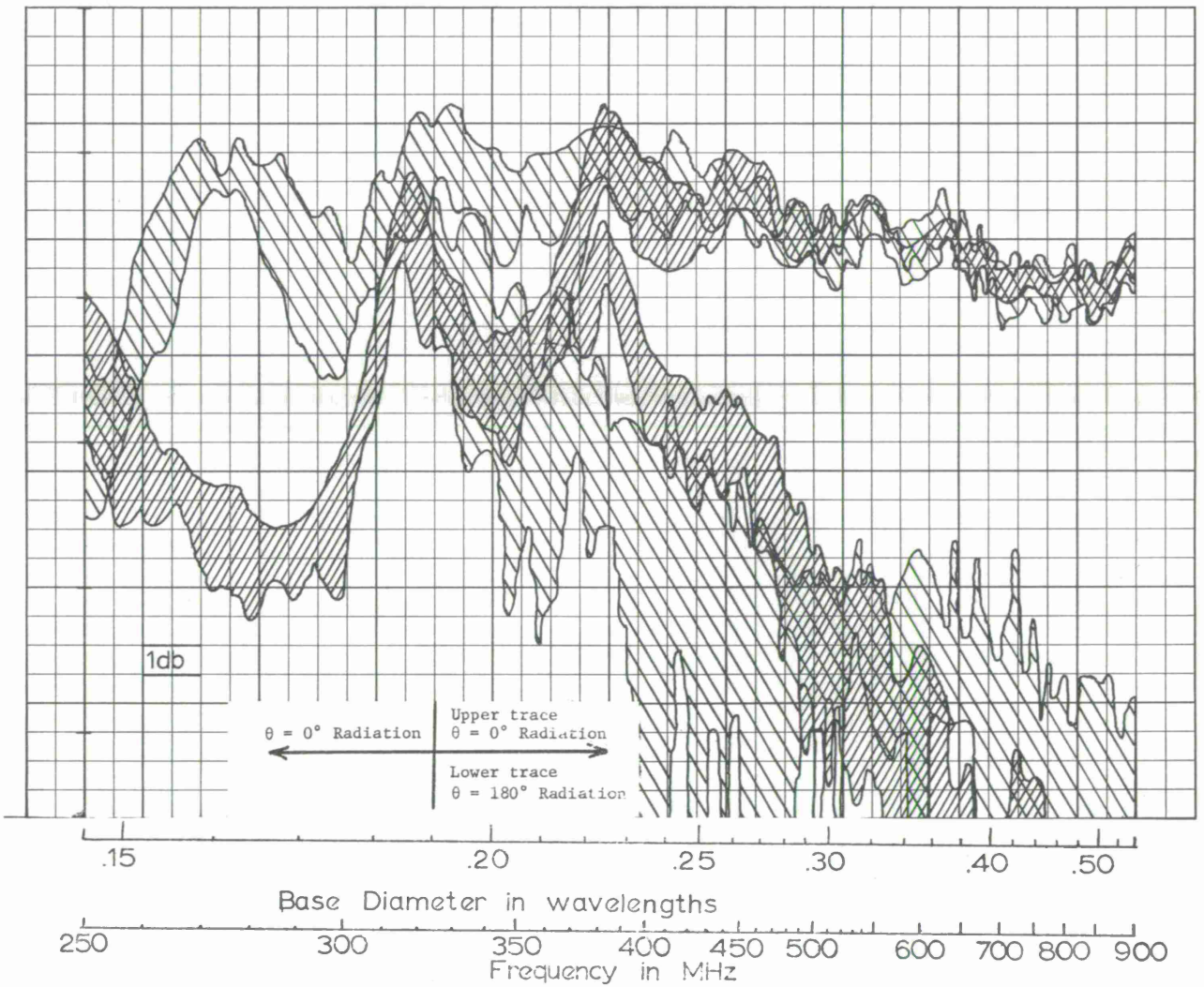

Figure 29 Data from Figures 26 and 27 superimposed to indicate relative amplitude of radiated fields from conventional narrow arm spiral antenna ($\delta' = 16°$) and equivalent arm width slow-wave antenna.

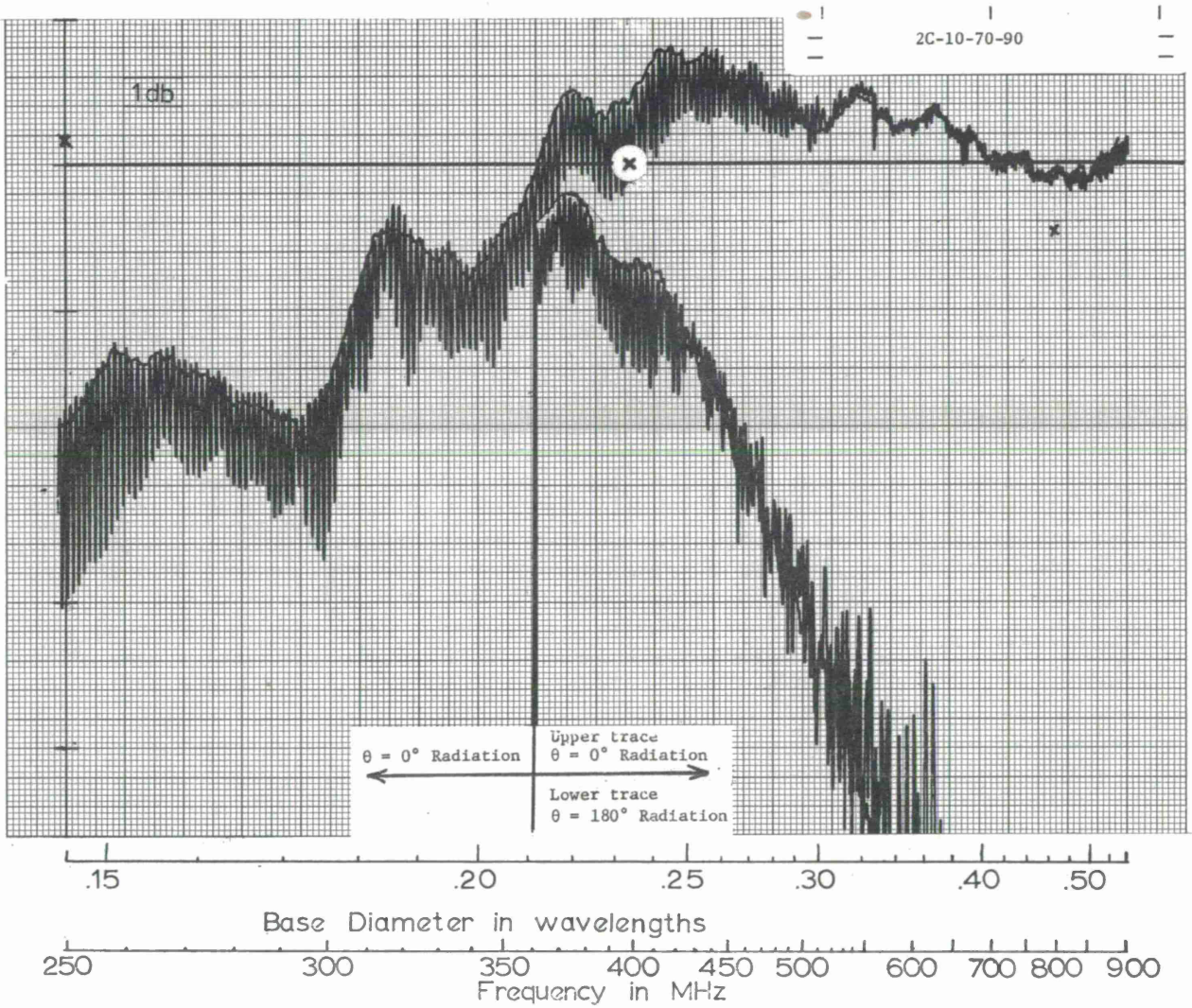

Figure 30 Relative amplitude of axial radiation from conventional conical spiral antenna, $\alpha = 70°$, $\delta' = 90°$. Data recorded with rotating linearly polarized receiving antenna. Data points (x) are isotropic levels.

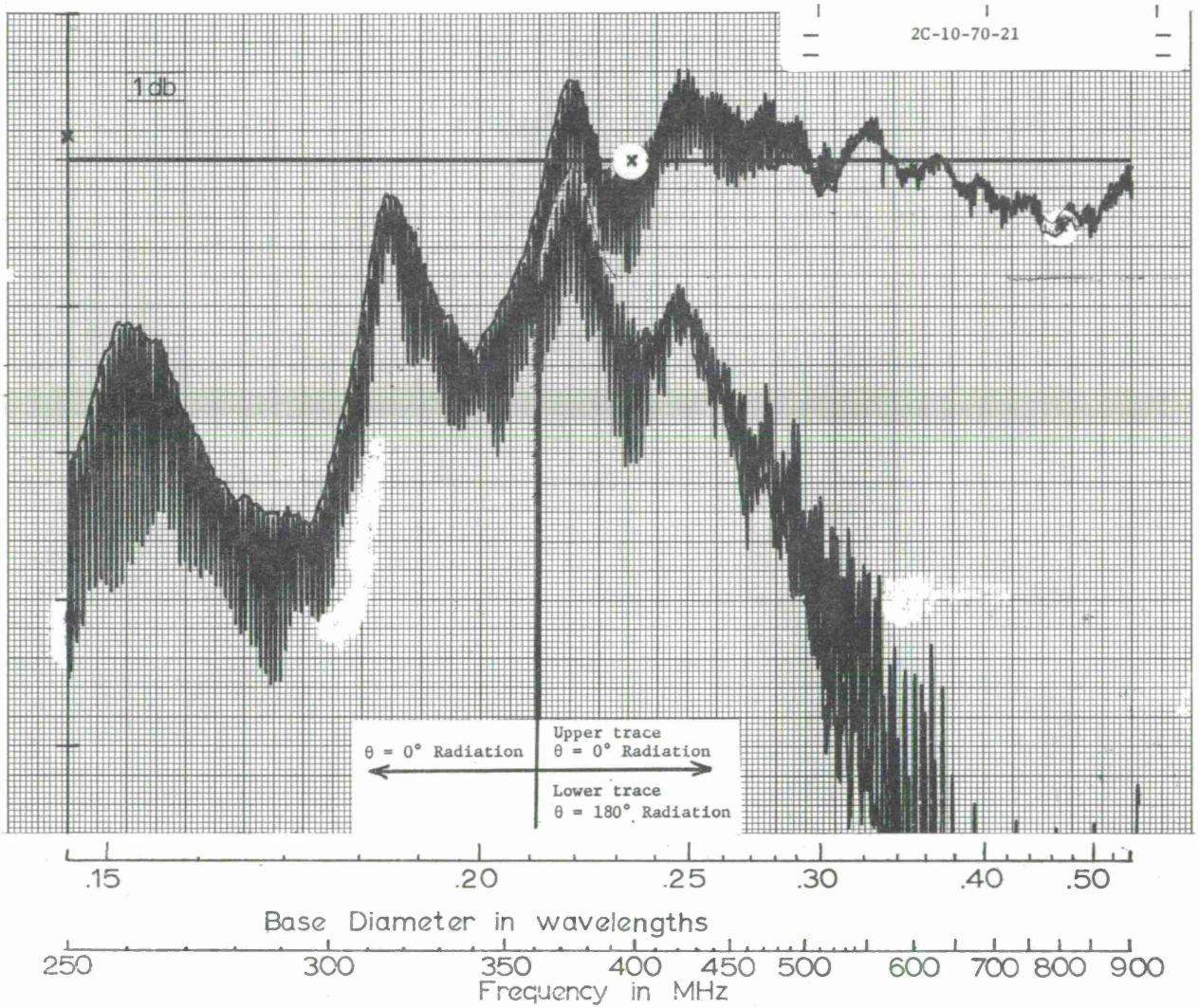

Figure 31 Relative amplitude of axial radiation from conventional conical spiral antenna, $\alpha = 70°$, $\delta' = 21°$. Data recorded with rotating linearly polarized receiving antenna. Data points (x) are isotropic levels.

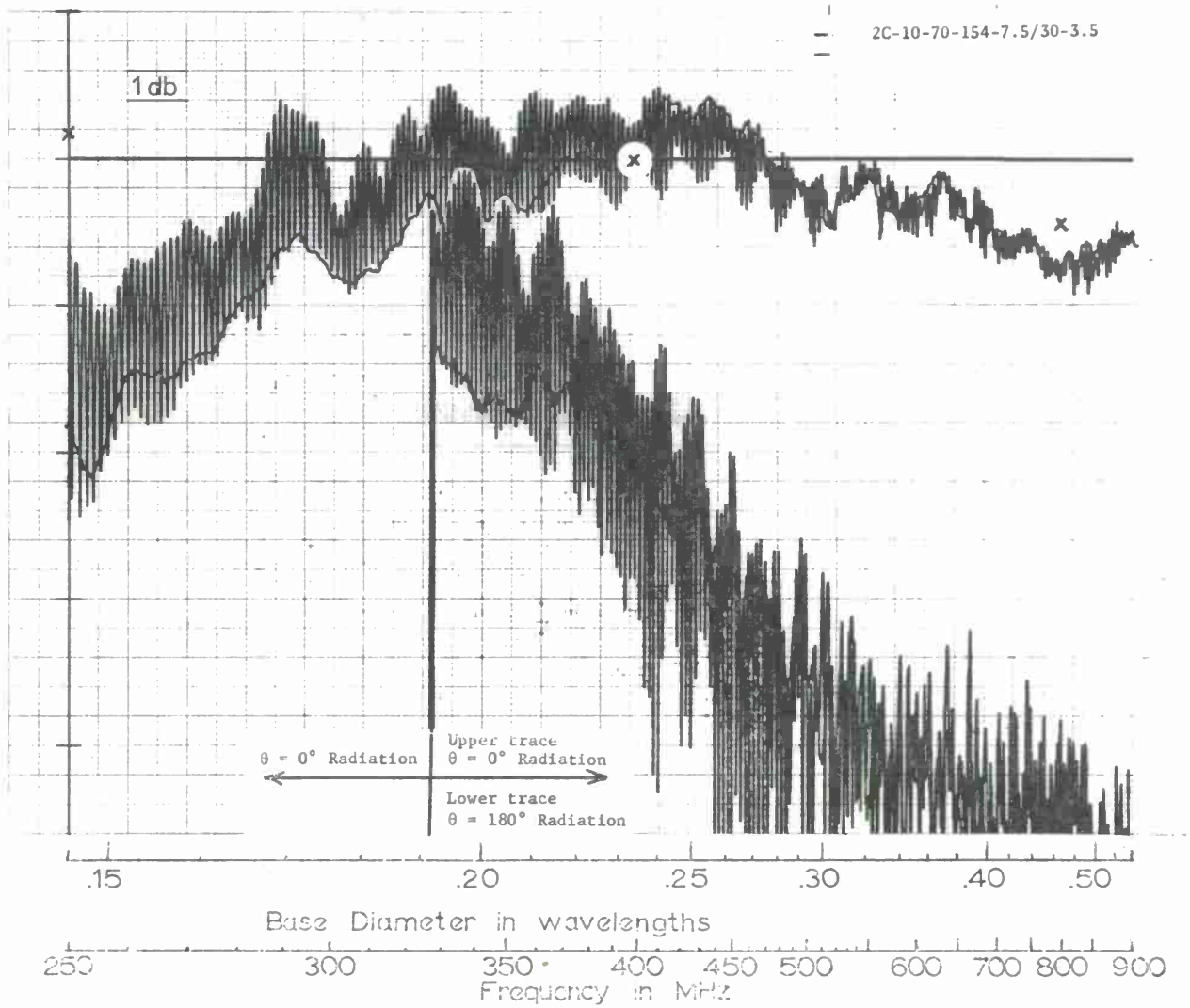

Figure 32 Relative amplitude of axial radiation from slow-wave conical spiral antenna, $\alpha = 70°$, arm width (7.5/30), slowing factor 3.5.

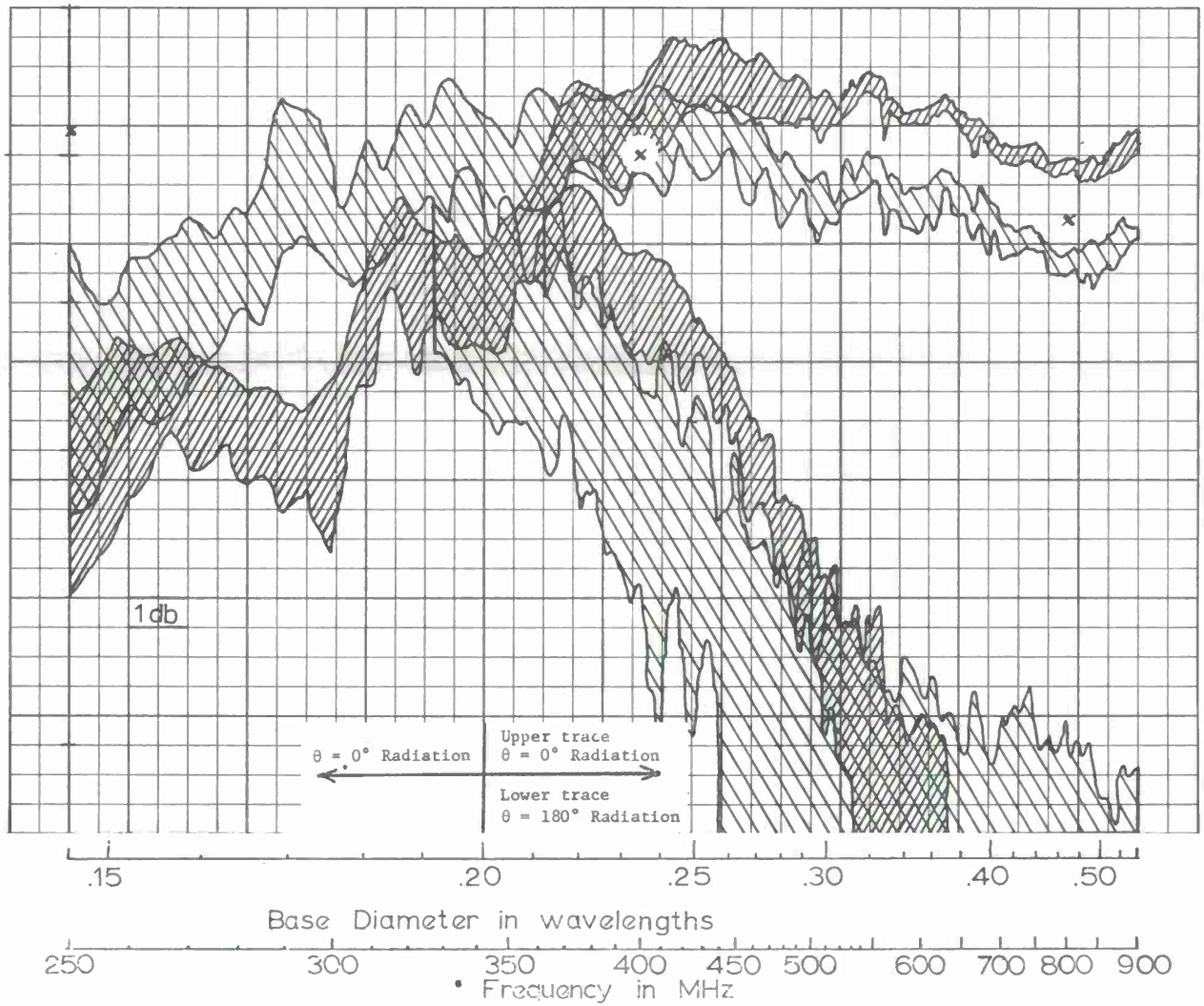

Figure 33 Data from Figures 30 and 32 superimposed to indicate relative amplitude of axial radiation from conventional complementary ($\delta' = 90°$) spiral antenna and slow wave spiral antenna.

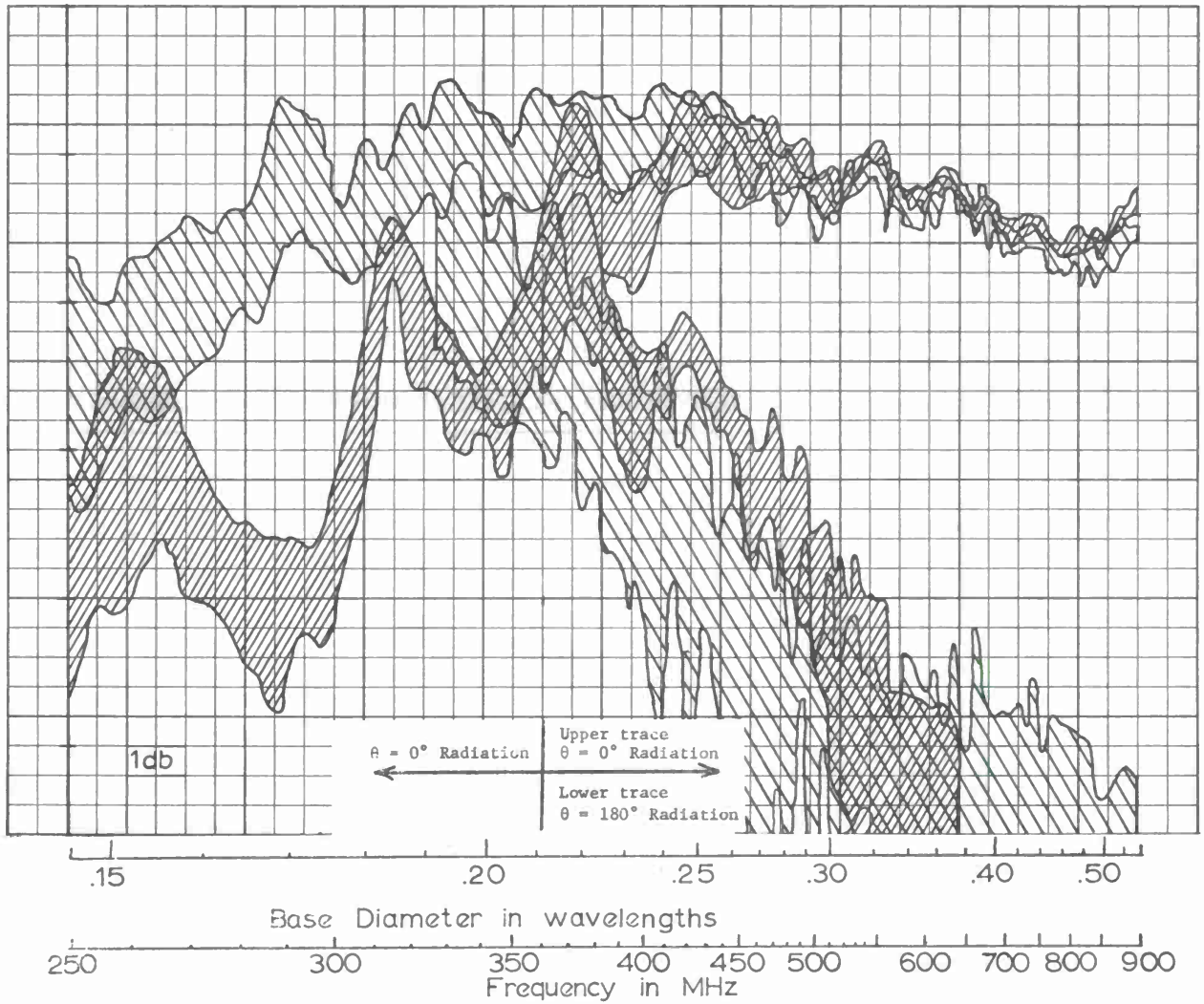

Figure 34 Data from Figures 31 and 32 superimposed to indicate relative amplitude of axial radiation from conventional narrow arm ($\delta' = 21°$) antenna and equivalent arm width slow-wave antenna.

1.5 Impedance and VSWR Measurements

The input impedance of these balanced antennas was measured with a technique that permits the measurements of balanced impedance with unbalanced coaxial equipment.[5] The equipment used for these measurements is shown in Figure 35. On a direct Smith chart plot of these data the input impedance is normalized to 100 ohms. One such plot for a conventional $\alpha = 65°$, $\delta' = 90°$ antenna is shown in Figure 36. The impedance rapidly spirals in and converges into a relatively small area about the characteristic value for this antenna when operated without end effect. A similar plot for a thinner arm antenna ($\alpha = 65°$, $\delta' = 16°$), Figure 37, shows a convergence to a much higher characteristic impedance. This characteristic has been observed before.[4] The impedance has converged to a real characteristic impedance at and beyond 420 MHz (base diameter equal to approximately .245λ), with impedance levels of approximately 1.7 Z_o and 4.0 Z_o for the two antennas δ respectively, where Z_o = 100 ohms. These two plots can be compared with the impedance plot for the $\alpha = 65°$ antenna with a slowing factor of 3.5 shown in Figure 38. This latter antenna is representative of the wider slow-wave arm antennas (width 15/30). The antenna impedance has converged to the neighborhood of a real characteristic value (1.5 Z_o in this case), at a lower frequency than either of the conventional arm antennas. The impedance was recorded above 500 MHz but not plotted on this figure. It remained in the neighborhood of this value.

When we recorded the impedance of the thin-arm version of this antenna (7.5/30) we noted a convergence to a non-real value and then a wandering away from that value, as indicated in Figure 39.

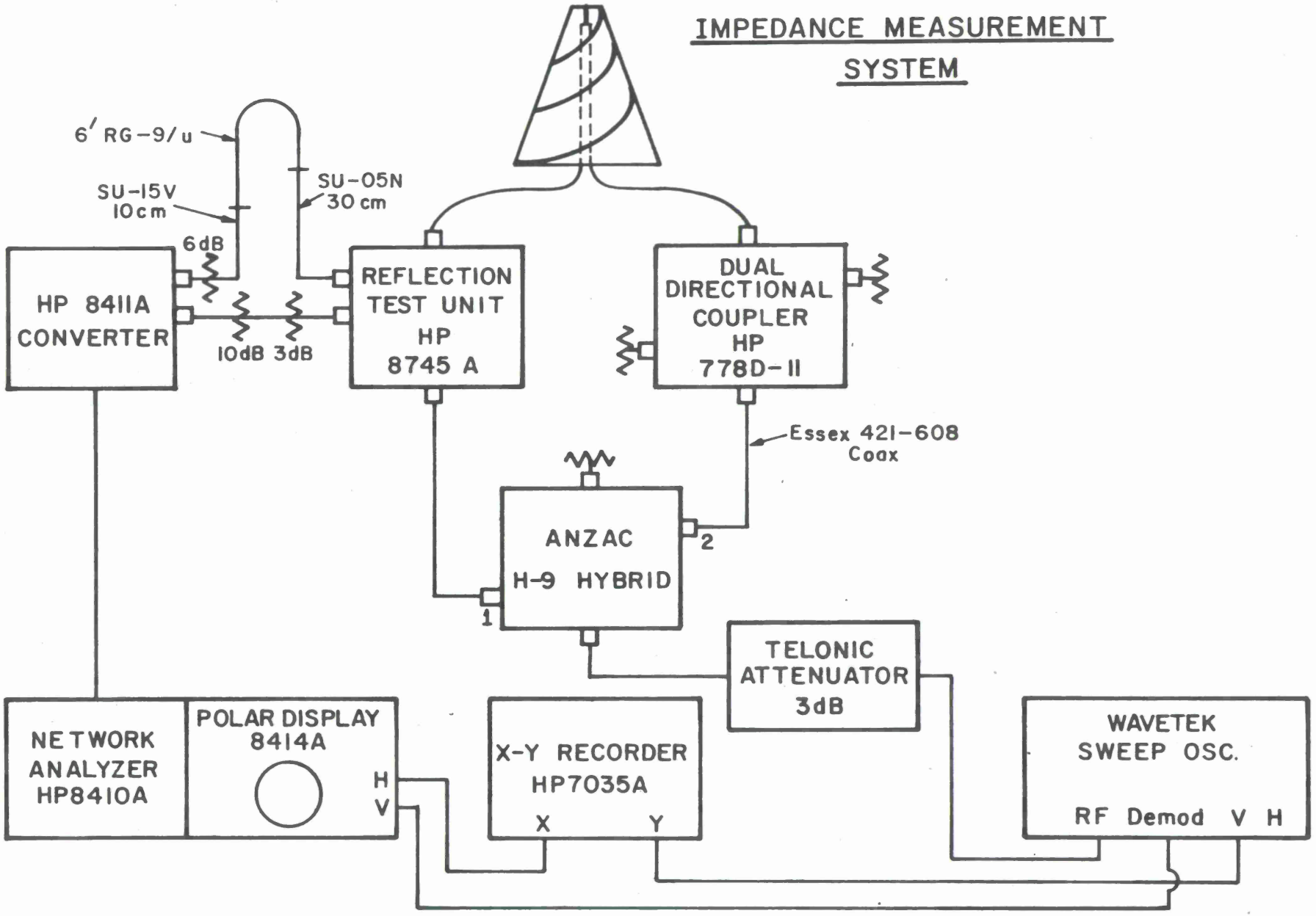

Figure 35. Impedance measuring system for conical antennas.

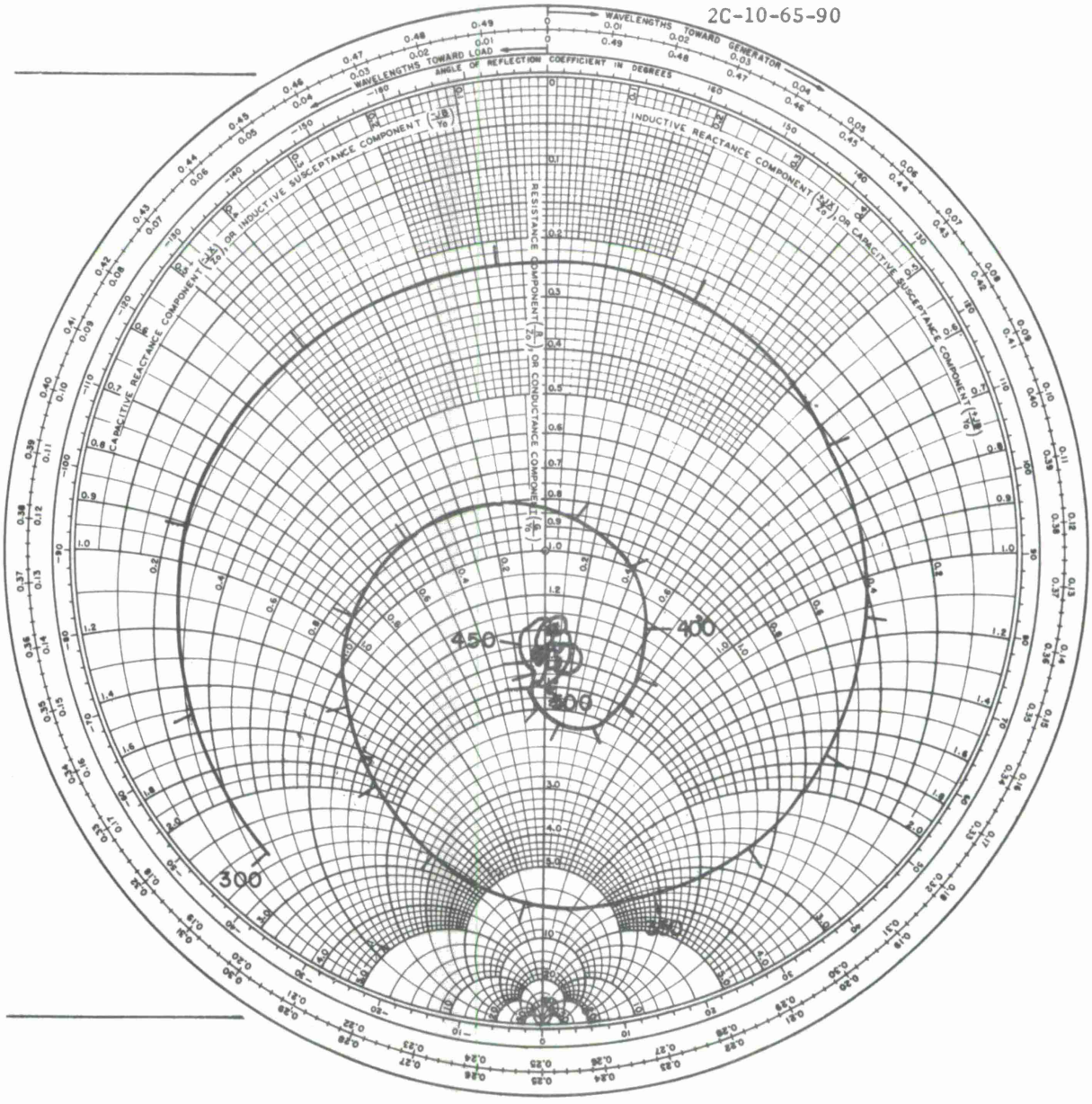

Figure 36. Smith Chart impedance plot for complementary antenna ($\alpha = 65°$ and $\delta' = 90°$). (Z_o = 100 ohms.)

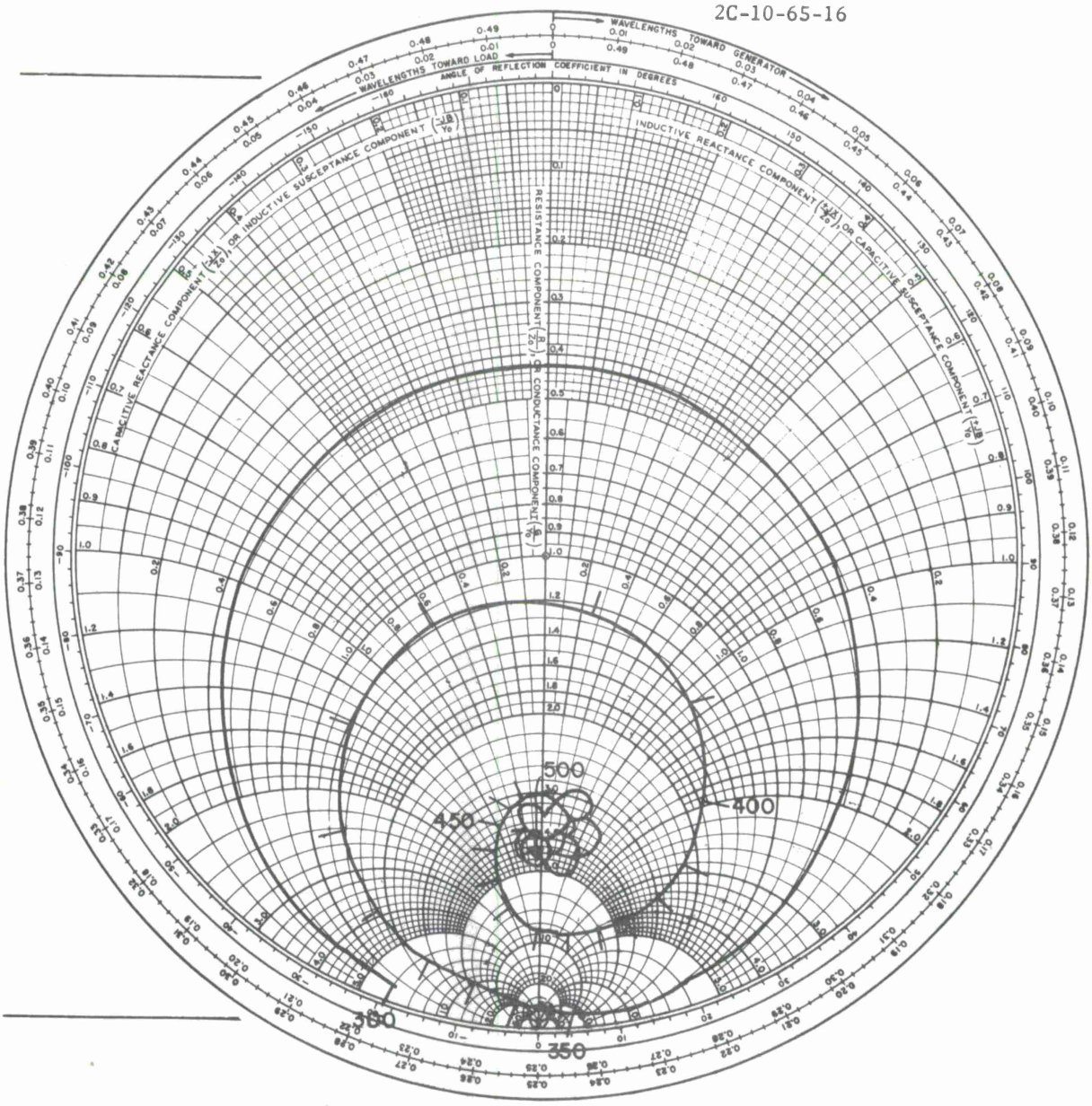

Figure 37. Smith Chart impedance plot for normal spiral antenna with "equivalent" arm width equal to thin zigzag arm width (α = 65° and δ' = 16°). (Z_o = 100 ohms.)

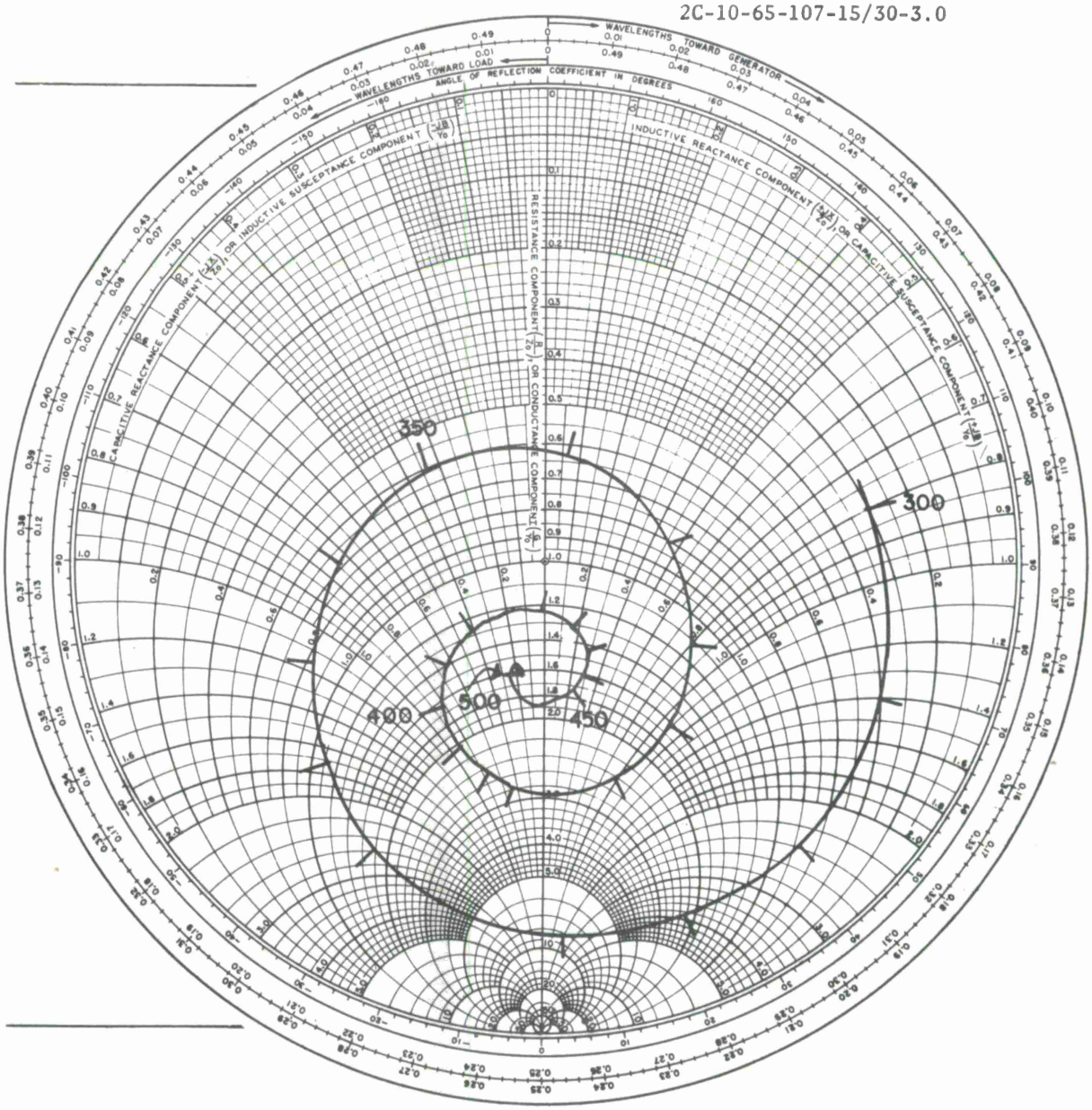

Figure 38. Smith Chart impedance plot for wide zigzag antenna with geometrical slowing factor = 3.5 (α = 65°). (Z_o = 100 ohms.)

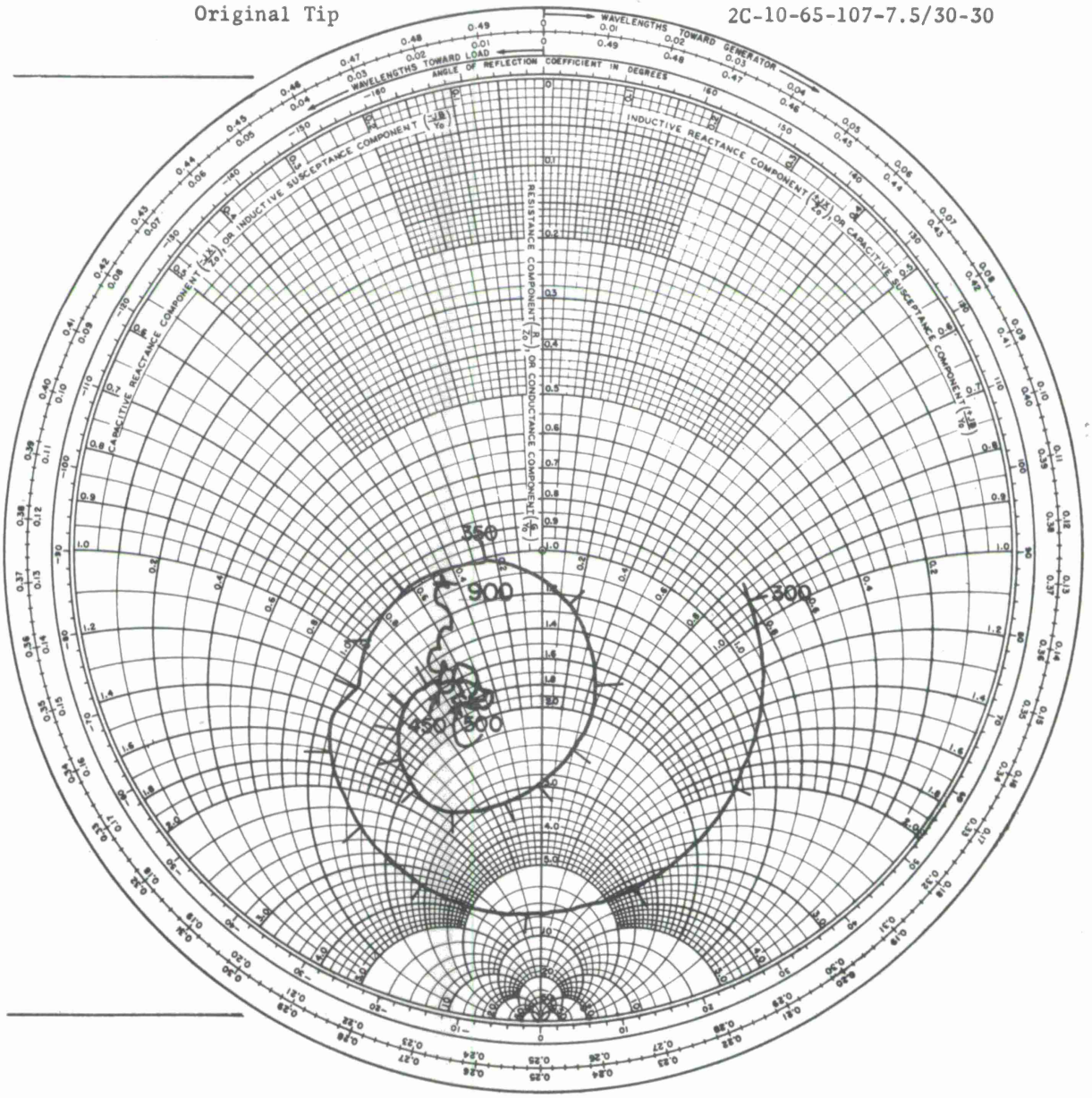

Figure 39. Smith Chart impedance plot for thin zigzag antenna with geometrical slowing factor = 3.5 (α = 65°). (Z_o = 100 ohms.)

The reactive component in the impedance was due to the tip construction, as shown in Figure 40(a). The tip was modified, as shown in Figure 40(b) to form a continuation of the arm width, rather than the arm envelope width. The modification brought the impedance level closer to the real axis, and the impedance remained clustered near this axis with increasing frequency (Figure 41). This latter effect was also accomplished by continuing the zigzag slow-wave pattern right up to the feed tabs, dispensing with the short spiral "feeder" arm shown on the conical surface. It had previously been shown that the tip construction, including the tapered feed tabs on the truncated tip of the cone, are an important factor in controlling and eliminating any reactive component in the characteristic input impedance.[4]

Table II shows the measured "characteristic" impedance (Z_c) of the normal spiral arm antennas and the zigzag antennas which were studied. The arrows in this table indicate the "equivalent" normal arm antenna to which the slow-wave antennas can be compared.* As reflected in Figures 36 through 39, the VSWR of all of these antennas, referred to Z_c, will increase as the wavelength of operation is increased, or the base diameter of the antenna is decreased, below the conventional design size, and the lower portion of the active region becomes distorted by the base truncation.

This increase in VSWR, referred to the characteristic impedance of the particular antenna, Z_c, is shown in Figures 42 and 43 for the $\alpha = 65°$ antennas and in Figures 44 and 45 for the $\alpha = 70°$ antennas.

---

* There is no explanation at this time as to why the trend for the $\alpha = 70°$, thin zigzag antennas appears to be reversed from that of the other antennas. The impedance is increasing instead of decreasing with increasing geometrical slowing factor.

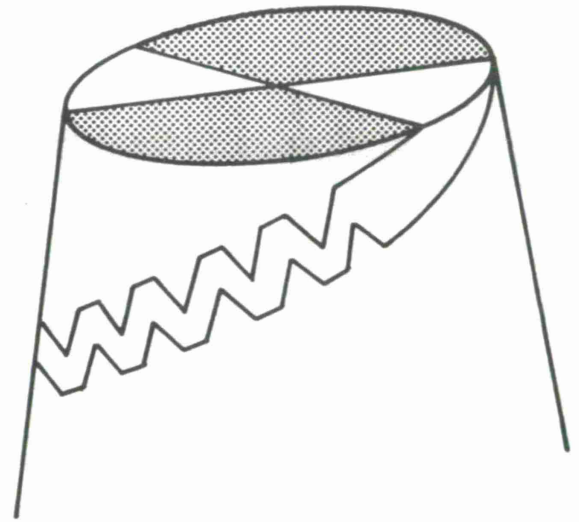

(a)

ORIGINAL TIP

Figure 40a. Original tip construction for thin zigzag antenna with geometrical slowing factor = 3.5 (α = 65°).

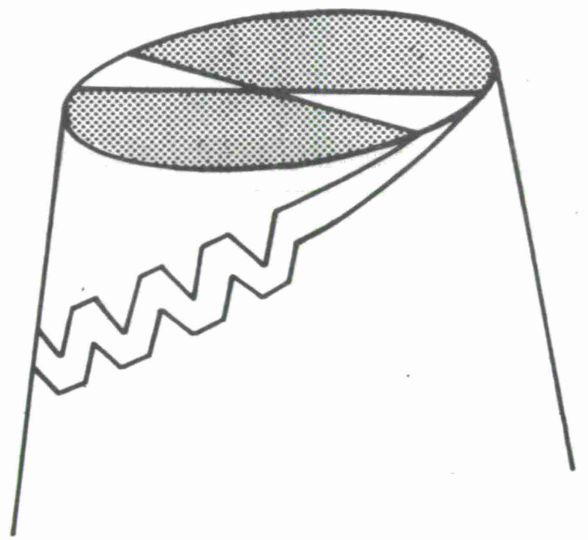

(b)

MODIFIED TIP

Figure 40b. Modified tip construction for thin zigzag antenna with geometrical slowing factor = 3.5 (α = 65°).

Modified Tip 2C-10-65-107-7.5/30-3.0

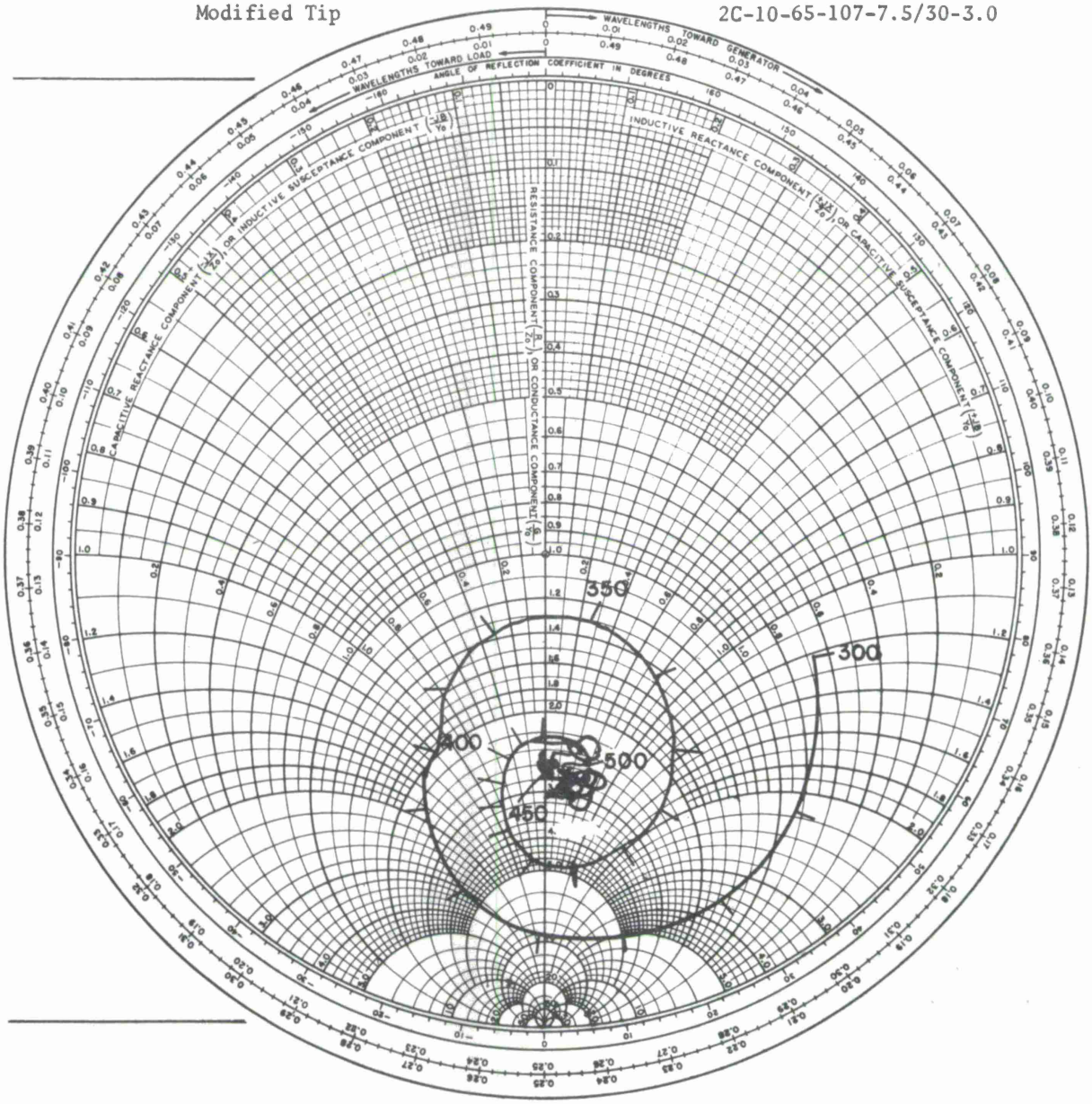

Figure 41. Smith Chart impedance plot for thin zigzag antenna with modified tip construction and geometrical slowing factor = 3.5 (α = 65°). (Z_o = 100 ohms.)

TABLE II

MEASURED "CHARACTERISTIC" IMPEDANCE (Z_c) OF CONICAL SPIRAL ARM AND ZIGZAG ARM ANTENNAS ($2\theta_o = 10°$)

Antenna	Spiral Arm Width (δ') in Degrees					Zigzag Slowing Factor			
	16	21	34	46	90	2.0	2.5	3.0	3.5
$\alpha = 65°$									
Spiral Arm	380		280		155				
Wide ZZ (15/30)			↑		←	205	177	155	153
Thin ZZ (7.5/30)		↑			←	270	260	255	250
$\alpha = 70°$									
Spiral Arm		310		230	162				
Wide ZZ (15/30)				↑	←	160	140	120	77
Thin ZZ (7.5/30)		↑			←	210	245	260	

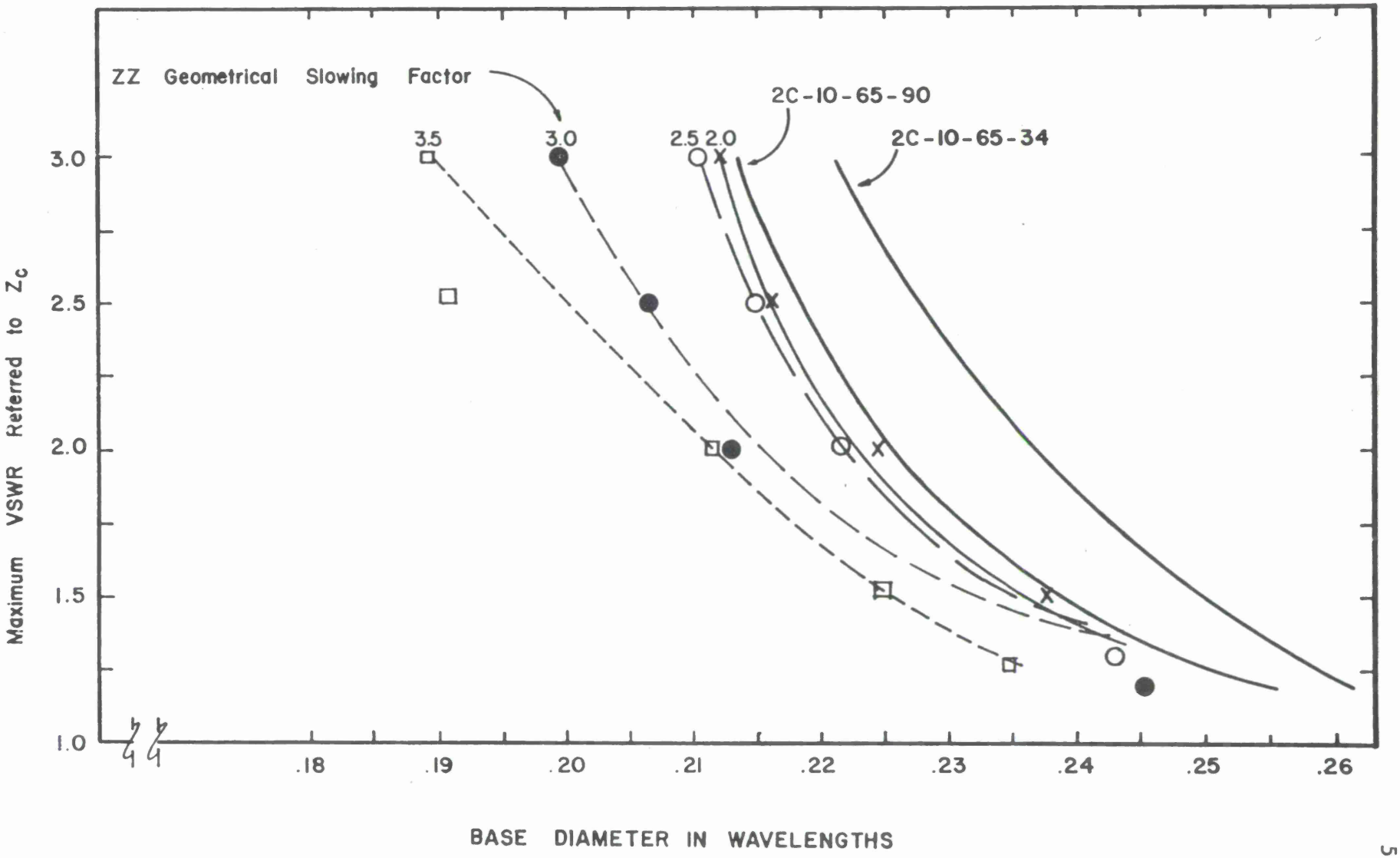

Figure 42. Maximum VSWR of the normal spiral arm and the wide arm (15/30) zigzag antennas referred to the characteristic impedance of these antennas as a function of the base diameter of the cone in wavelengths. $\alpha = 65^{o}$

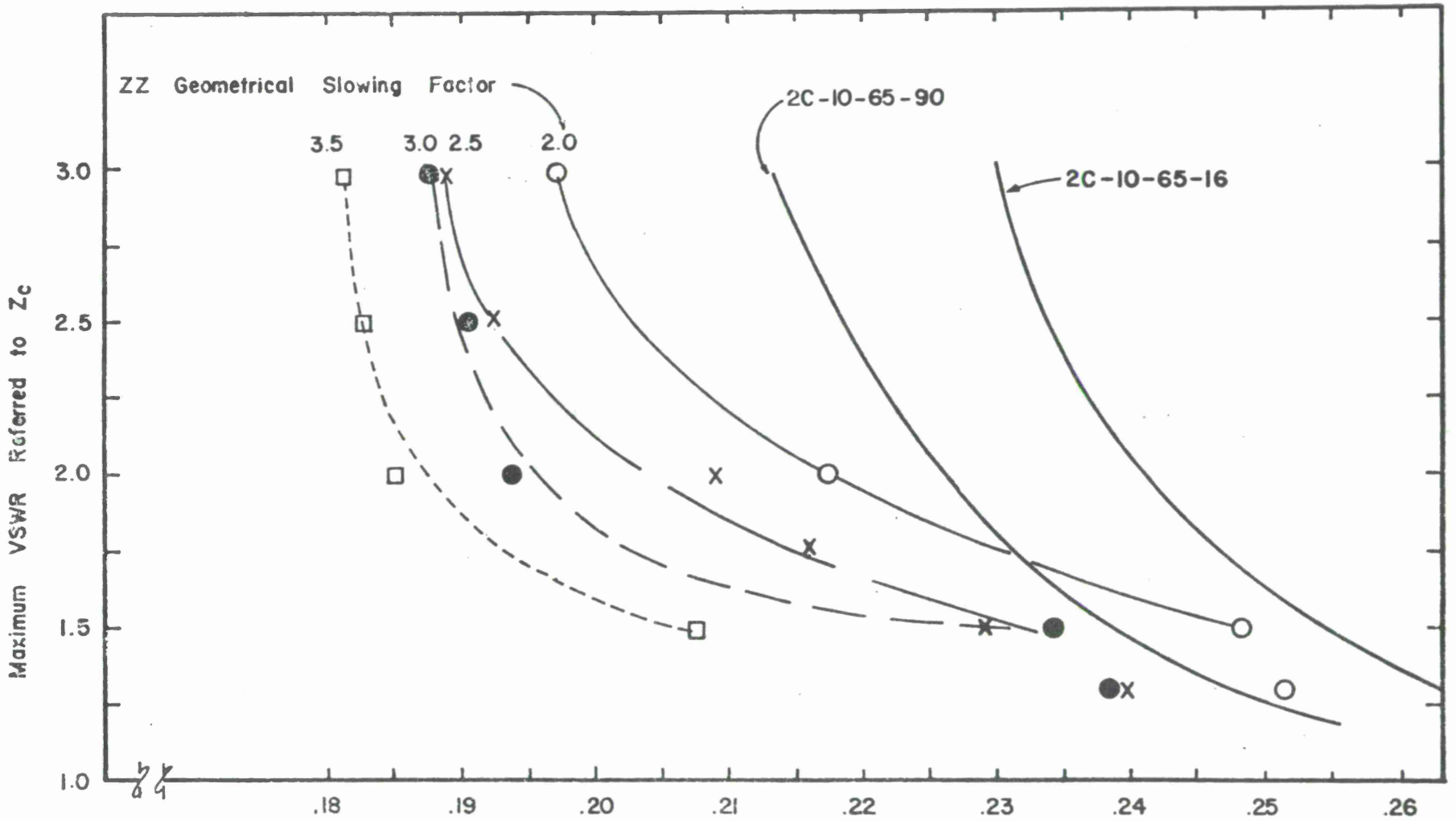

Figure 43. Maximum VSWR of the normal spiral arm and the thin arm (7.5/30) zigzag antennas referred to the characteristic impedance of these antennas as a function of the base diameter of the cone in wavelengths. $\alpha = 65^{\circ}$

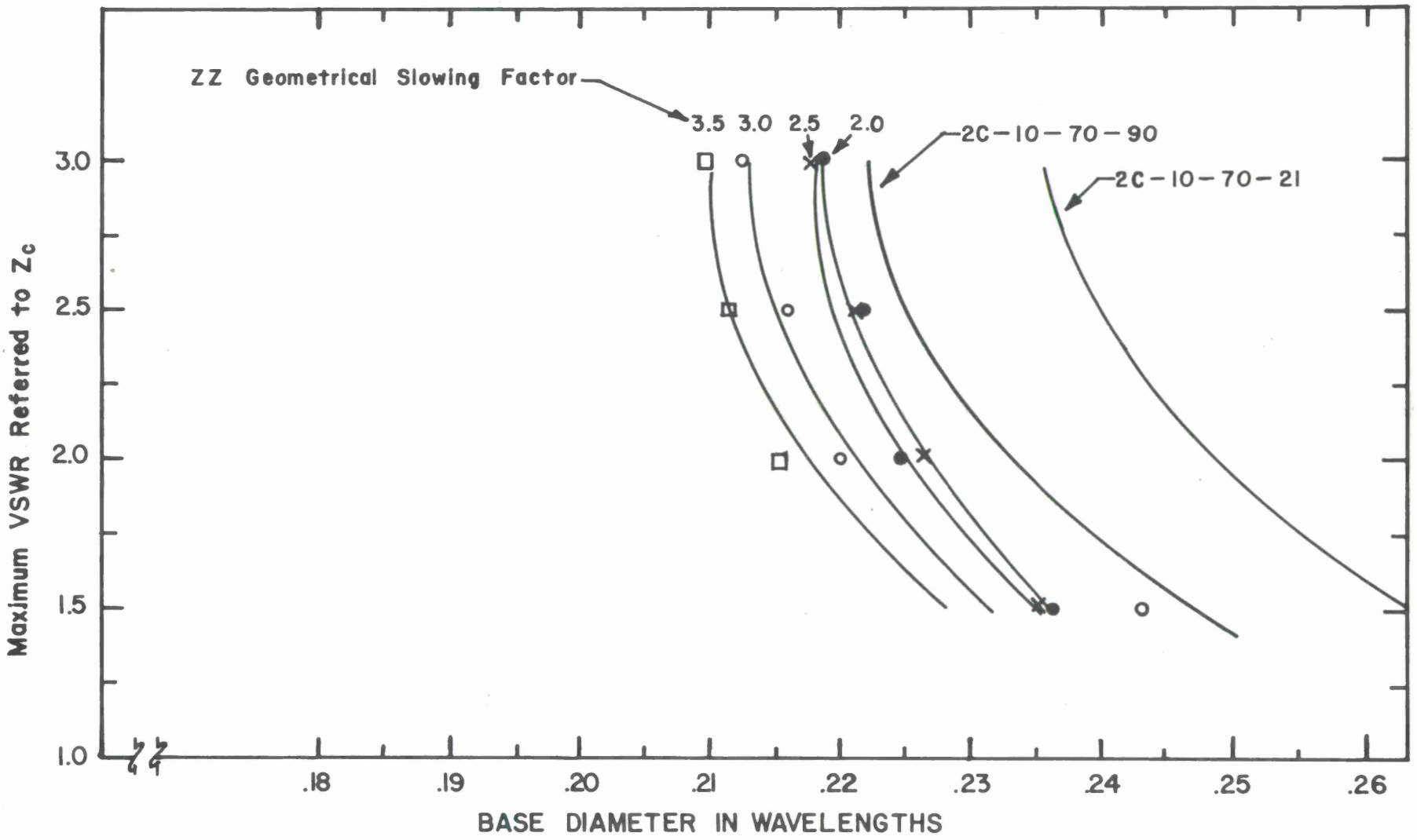

Figure 44. Maximum VSWR of the normal spiral arm and the wide arm (15/30) zigzag antennas referred to the characteristic impedance of these antennas as a function of the base diameter of the cone in wavelengths. $\alpha = 70^{o}$

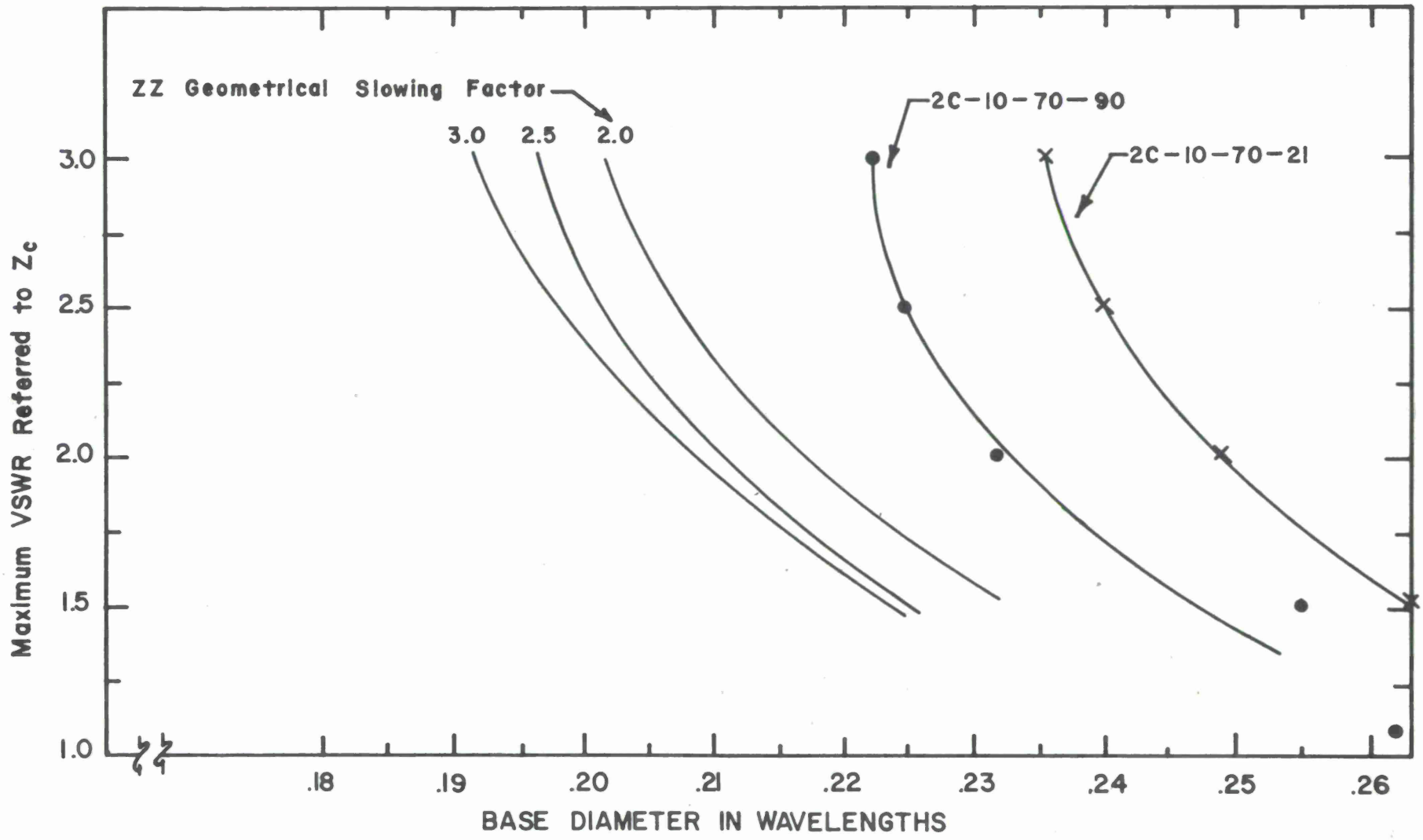

Figure 45. Maximum VSWR of the normal spiral arm and the narrow arm (7.5/30) zigzag antennas referred to the characteristic impedance of these antennas as a function of the base diameter of the cone in wavelengths. $\alpha = 70^{o}$

An inspection of these four figures and the design curves in Reference 3 indicate that an antenna design based only on impedance characteristics would permit a size reduction of up to 18 or 20 percent when using the thin arm zigzag geometry. However, as we have seen in the preceding discussion, the size of the antenna will probably be controlled by the radiation characteristics, and the use of any other criterion for size reduction will result in less than optimum radiation performance.

The measured VSWR and the magnitude of the reflection coefficient of these antennas, referred to a 100 ohms balanced feed system, is shown in Figures 46 through 49. This 100 ohm balanced feed is the simplest practical feed for these antennas. It consists simply of a broadband 50 ohm coaxial hybrid with the sum port terminated in a matched load, and two equal length 50 ohm coaxial lines carried along the antenna axis to form a balanced 100 ohm feed.[5]

1.6 Summary

We have been concerned with investigating the characteristics of conical spiral antennas, of relatively loose wrap (α = 65 and 70°), constructed with arms modified into a zigzag slow-wave geometry. For this admittedly quite limited range of conical spiral antennas, a large discrepancy was observed between the geometrical and electric slowing factors.

Geometrical slowing factors of as much as 3.5:1 yielded electrical slowing factors of no greater than 1.14:1, when performance was based upon radiation characteristics. This implies the possibility of reducing the size of the antennas by 14 or 15 percent. If impedance characteristics were to be the controlling factor this reduction could be increased to 20 percent.

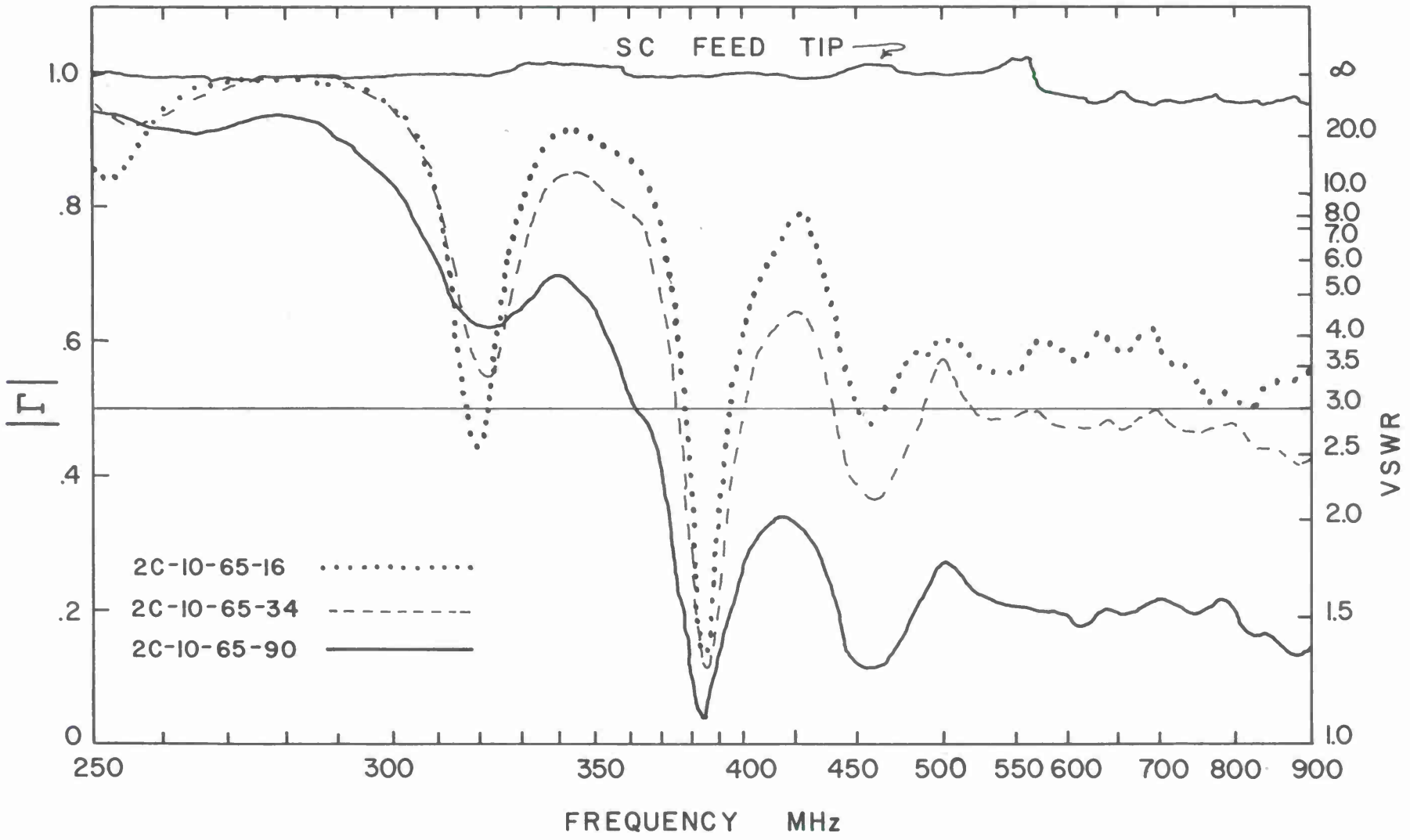

Figure 46. VSWR as a function of frequency for normal spiral antennas (α = 65°). (Z_o = 100 ohms.)

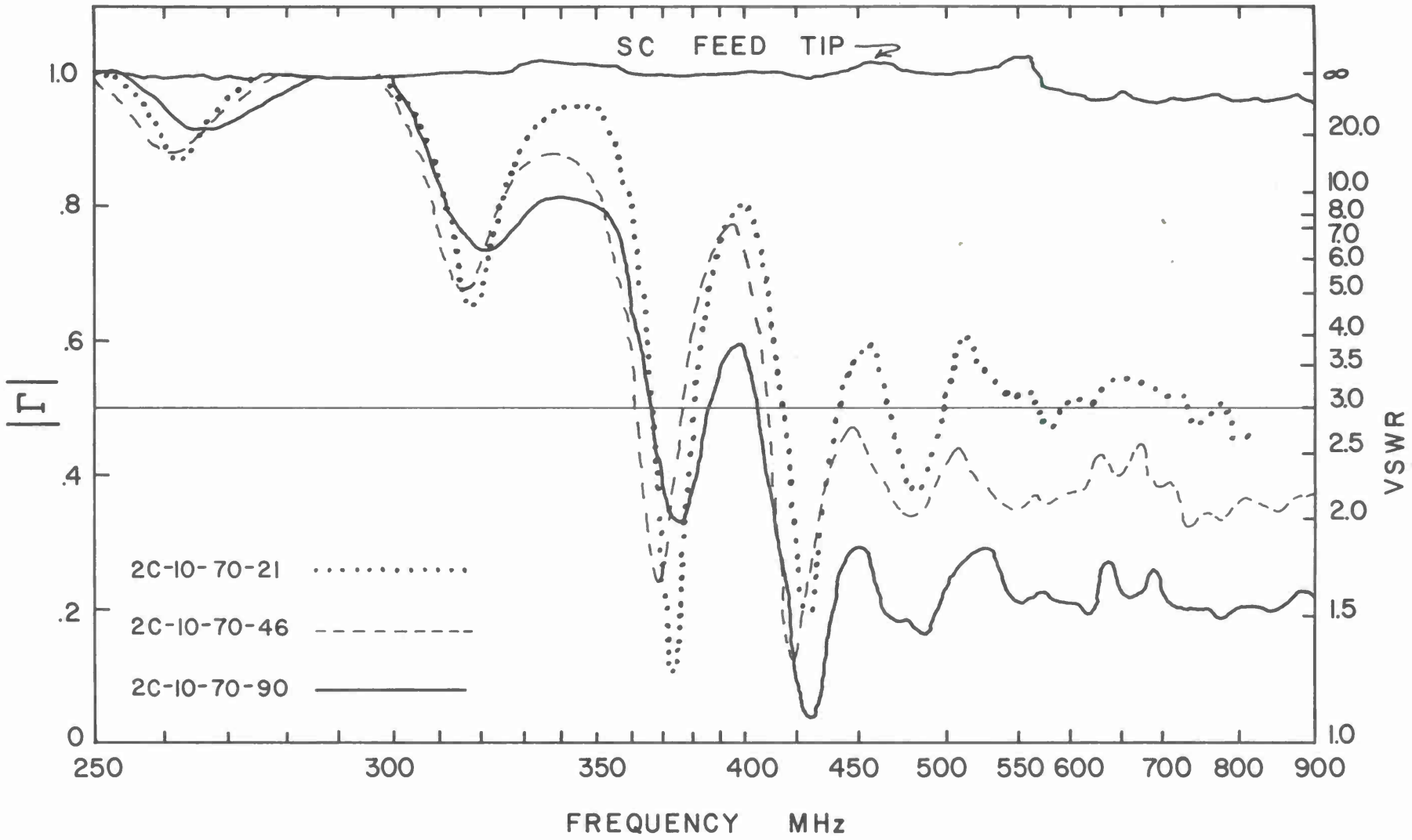

Figure 47. VSWR as a function of frequency for normal spiral antennas ($\alpha = 70°$). ($Z_o = 100$ ohms.)

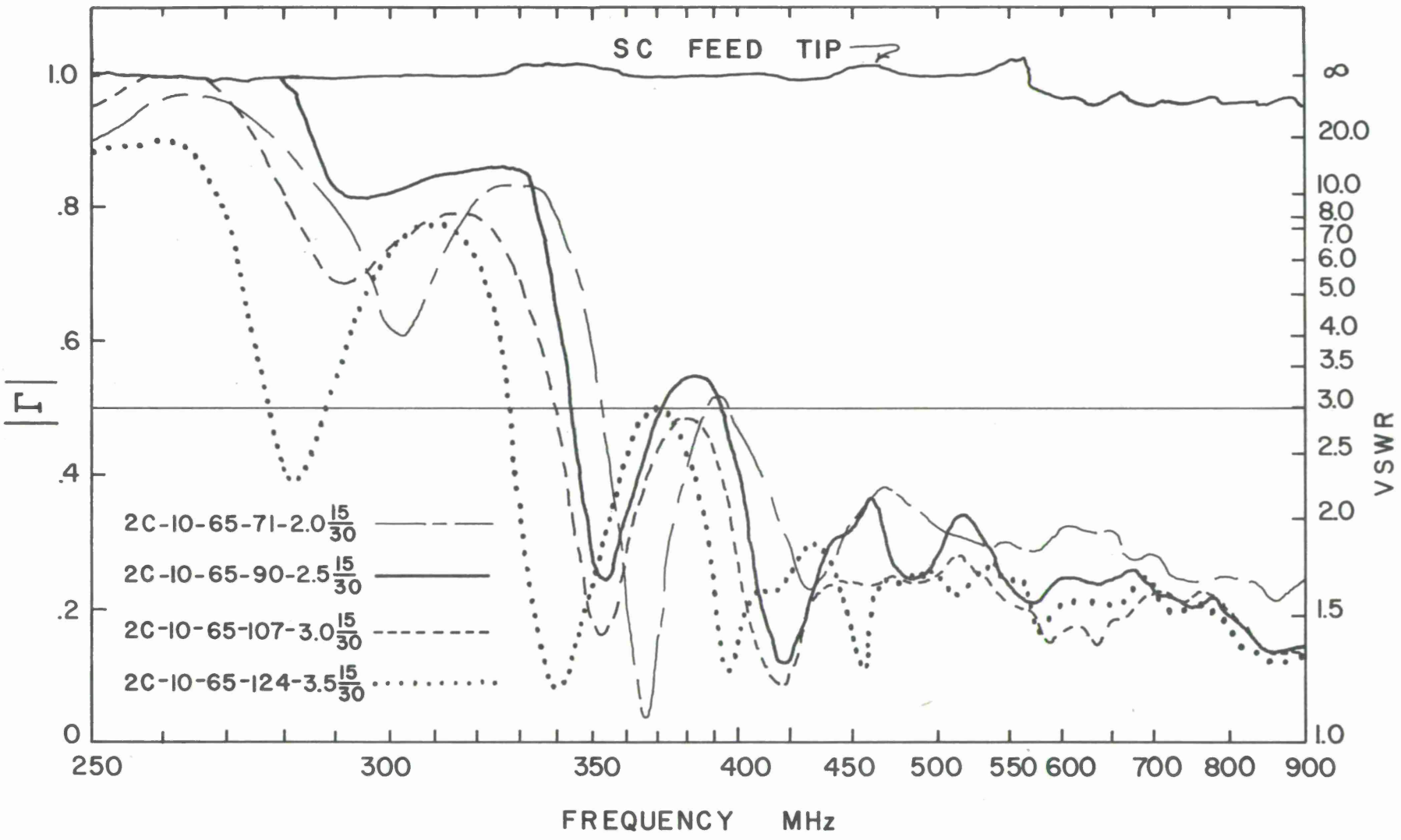

Figure 48. VSWR as a function of frequency for wide zigzag antennas, for all geometrical slowing factors ($\alpha = 65°$). ($Z_o = 100$ ohms.)

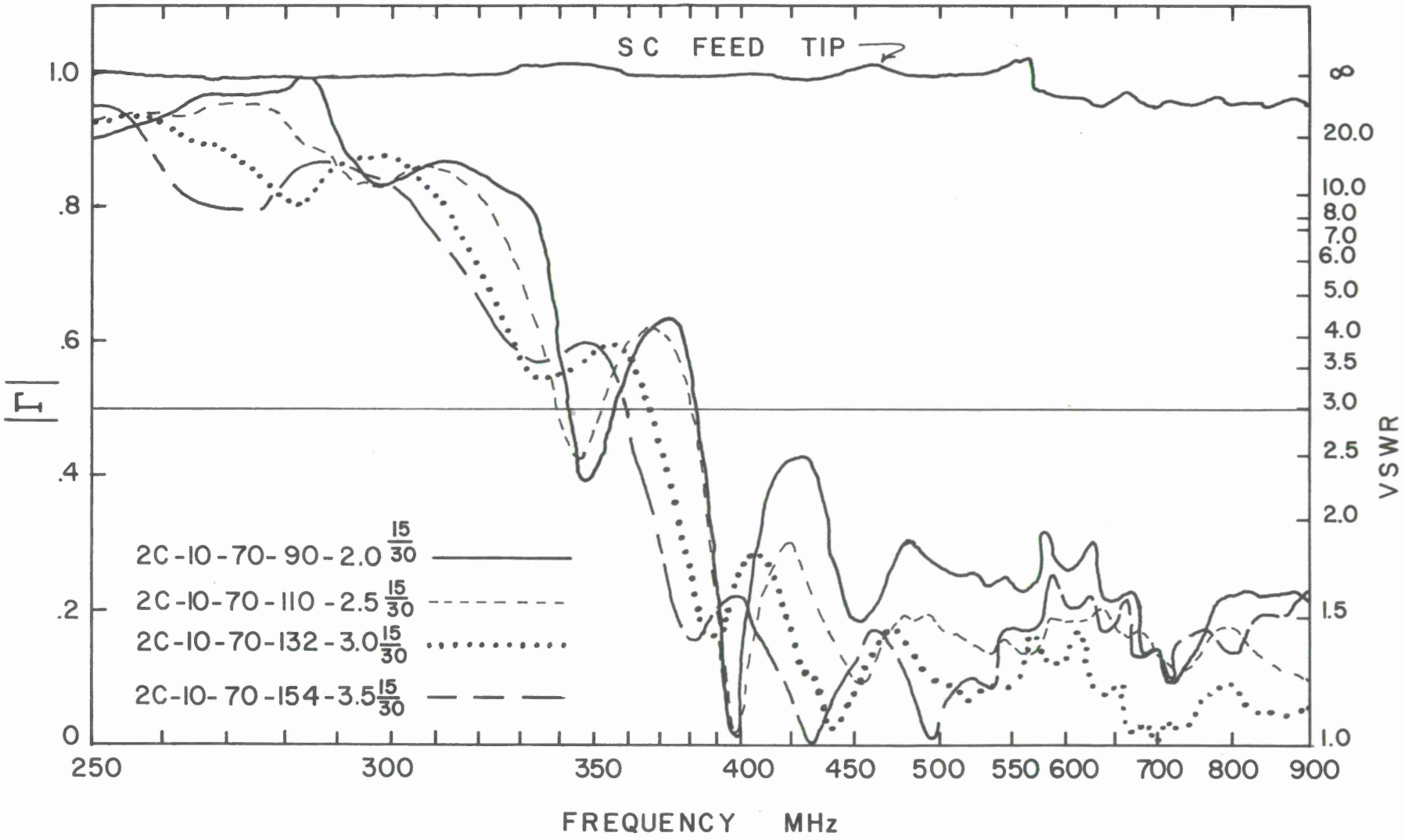

Figure 49. VSWR as a function of frequency for wide zigzag antennas, for all geometrical slowing factors ($\alpha = 70°$). ($Z_o = 100$ ohms.)

The use of the zigzag slow-wave geometry,which was studied,also resulted in an increase in beamwidth and a change in characteristic impedance level. These changes may or may not be desirable depending upon the intended application.

The study and its results should prove of use for the design of conical antennas intended for specific applications. However, possibly the most significant result is the knowledge that there appears to be this high ratio of geometric slowing required to make major changes in the effective propagation constant along the spiral geometry of the arms of this type antenna. This information was the basis for a limited study of one slow-wave helix antenna. This study is considered in part II of this report.

PART II. A SLOW-WAVE HELIX

2.1. Introduction

The annual report, dated September 1971[6], which was submitted under the prior contract, was concerned with the study of the small unbalanced conical spiral antenna (CUSP). In that report it was suggested the radiation from this type antenna might be controlled by constructing the complete arms with a slow-wave geometry. Since there is little documented information available on the use of slow wave structures for the spiral arms of these antennas, the study that forms Part I of this report was carried out.

In that earlier study it was discovered that the radiation from the CUSP antenna, in the range of wavelengths of prime interest (i.e. when the antenna was small in wavelengths), originated from effectively feeding one arm of this structure against the inner metal core which housed the electronic equipment. The second arm of the two arm conical antenna merely served as part of the feed mechanism. Thus although it was a two arm structure fed at the apex of the cone, it was operating as a monofilar base-fed helix. And, since the maximum diameter was small in wavelengths, the maximum of radiation was broadside to the axis of the cone as for a normal-mode helix.

In the light of this knowledge, and that which we gained from the study of the slow-wave conical spiral, we concluded that the axial-mode type of pattern coverage that might be desirable from this relatively small structure could be obtained by simply constructing a single slow-wave arm antenna and feeding this single arm against an inner metal core.

2.2 The Antenna

We made a very limited study of a small diameter conical antenna (with maximum circumference of approximately 1/4 wavelength) operated as a slow-wave base-fed end-fire helix. To obtain a maximum of radiation along the axis of this antenna the propagation constant along the arms would have to be changed by a factor of approximately 4 to 1 so that approximately 2π radians of phase shift could be accumulated in one turn of the arms. Without this change in propagation constant, as indicated above, an antenna of this diameter would radiate a maximum of energy broadside to the antenna axis, as a normal-mode helix. Using the results of the previous work on the slow-wave spiral antennas, and some preliminary checks on the helix-type structure, we estimate that it would require a geometric slowing factor of at least 9 or 10 to 1 to achieve an electric slowing factor of approximately 4 to 1.

A monofilar conical helix of 2 1/4 turns was constructed with a geometric slowing factor of 9.2:1. This antenna, with its inner metal core removed, is shown in Figure 50. The antenna was constructed by etching the arm on a 0.010 inch Teflon impregnated fiber glass cone, clad with 1 mil. of copper on one side. The cone has an included cone angle of 10.8 degrees and a base diameter of 19.3 cm., a truncated tip diameter of 5.3 cm, and an axial length of 73 cm. The respective dimensions of the metal core are 15.3 cm, 6 cm, and 41 cm.

2.3 Radiation Characteristics

Radiation patterns recorded from 130 MHz to beyond 200 MHz indicated that this antenna was basically an axial-mode radiator. Patterns taken at 150, 160, and 180 MHz are shown in Figures 51-53. For those patterns the antenna axis is along the $\theta = 0$ and 180° line, and the apex of the cone is

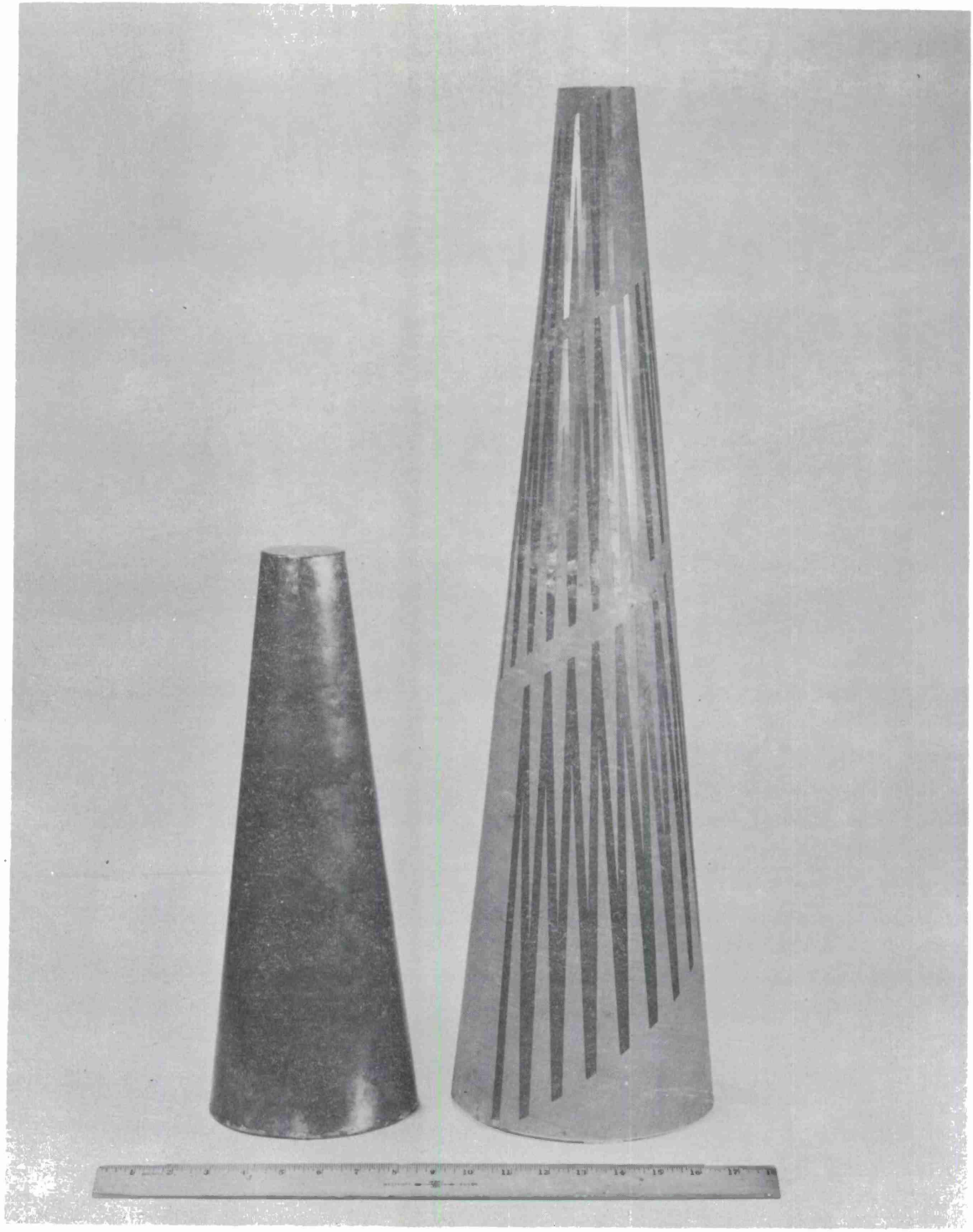

Figure 50. Photograph of the zigzag slow-wave conical helix antenna with the inner metal core removed.

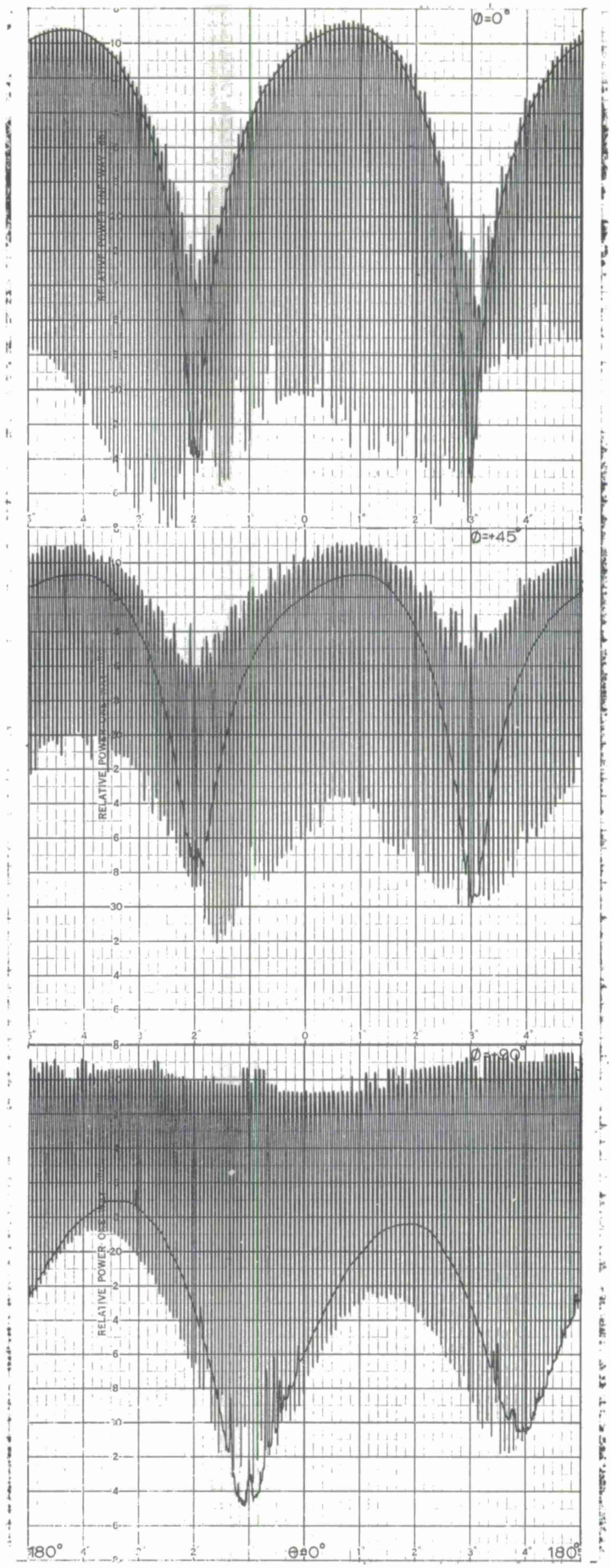

Figure 51. Radiation patterns of zigzag slow-wave conical helix. 150 MHz. Single curve is E_θ polarization.

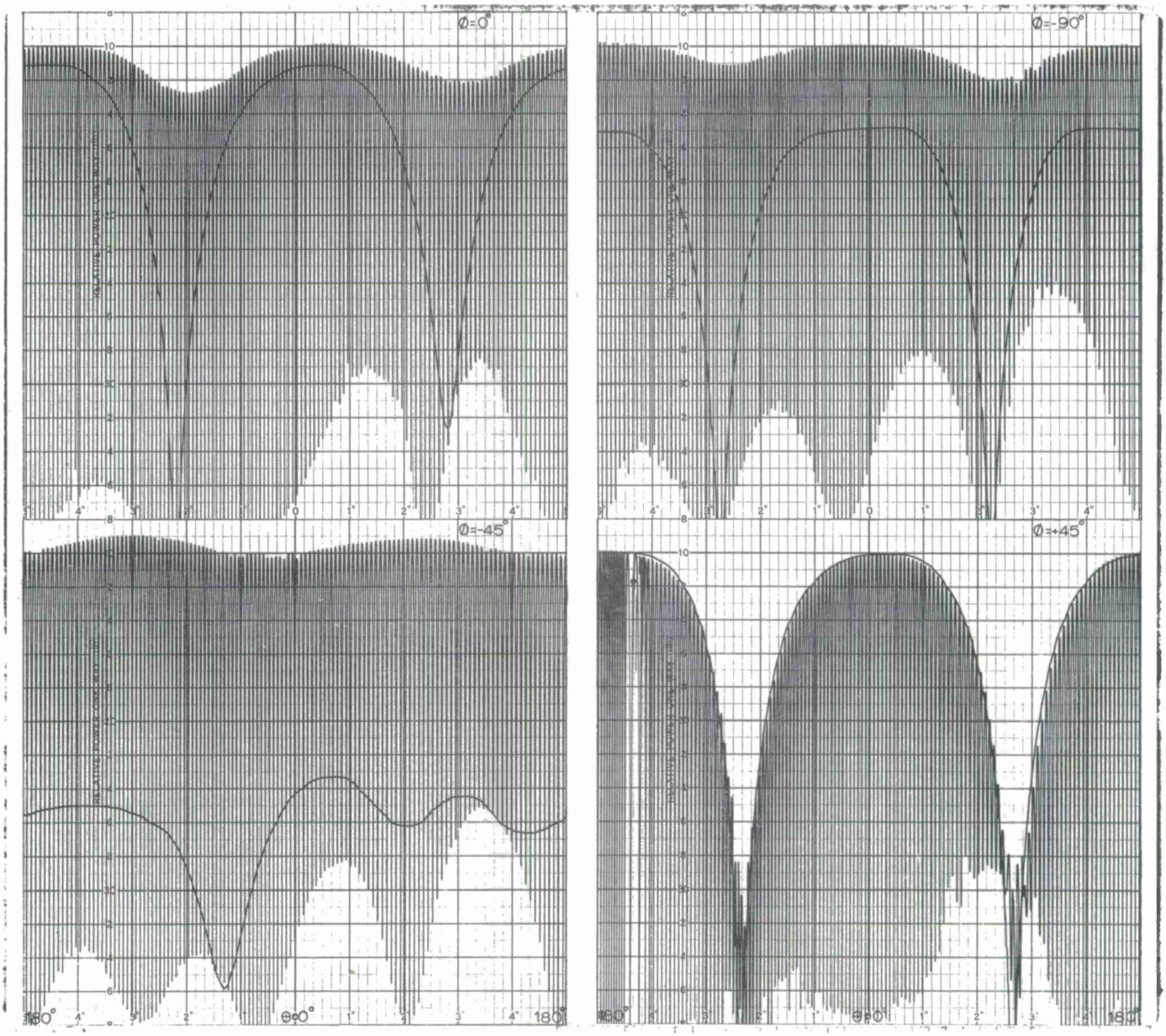

Figure 52. Radiation patterns of zigzag slow wave conical helix. 160 MHz. Single curve is E_θ polarization.

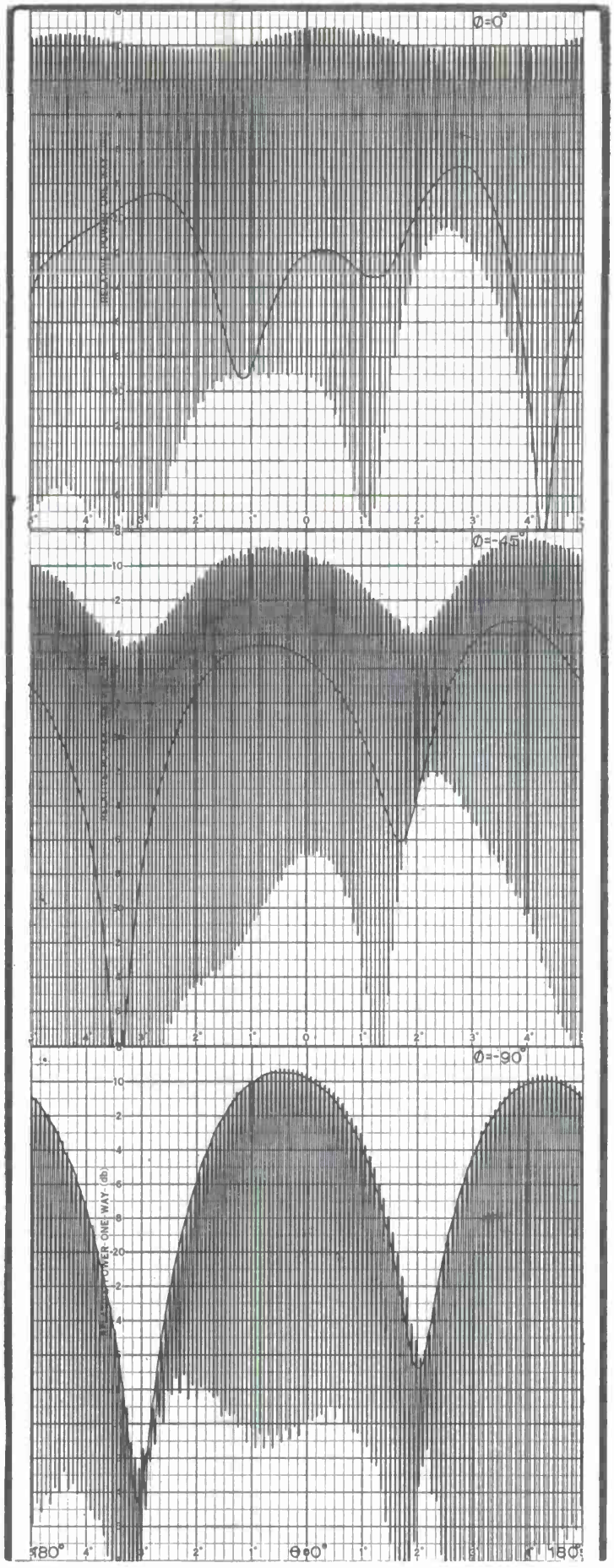

Figure 53. Radiation patterns of zigzag, slow wave conical helix. 180 MHz. Single curve is E_θ polarization.

at $\theta = 0^{o}$. The vertical scale is in dB with 2 dB per major division.

A battery powered oscillator and the associated electronics were contained in the inner metal core. There were no wires or cables connected to the cone. The slow-wave conical helix was excited at the base end against the inner metal core as shown in Figure 54. The patterns were recorded with a constantly rotating linearly polarized receiving antenna, and hence the difference between the maximum and minimum excursions of the fine structure at any point on the pattern is the axial ratio of the field in that particular direction. Patterns were also recorded with a fixed plane of polarization of the receiving antenna (E_{θ}, i.e. polarized in a plane which contains the cone axis), and these are the single line curves.

As indicated in these figures,this is essentially a linearly polarized bidirectional radiator. The pattern coverage along the axis of the antenna is excellent, although there is some change in the plane of polarization with change in direction and frequency. This latter characteristic will be discussed later.

The power gain, on-axis, without matching, was recorded at 150, 163, and 180 MHz as -8.7, -5.5, and -12.9 dB with respect to an isotropic level. This will also be discussed after considering the mismatch of the antenna to the 50 ohm feed line.

2.4. VSWR Measurements

The VSWR of the antenna, was measured using the non-metallic cable system described in reference no. 6. As shown in Figure 55, it was quite high, referenced to 50 ohms, indicating a sizable mismatch loss. Table III below shows the VSWR and mismatch loss between the generator and the antenna, at the three frequencies when the gain was directly measured.

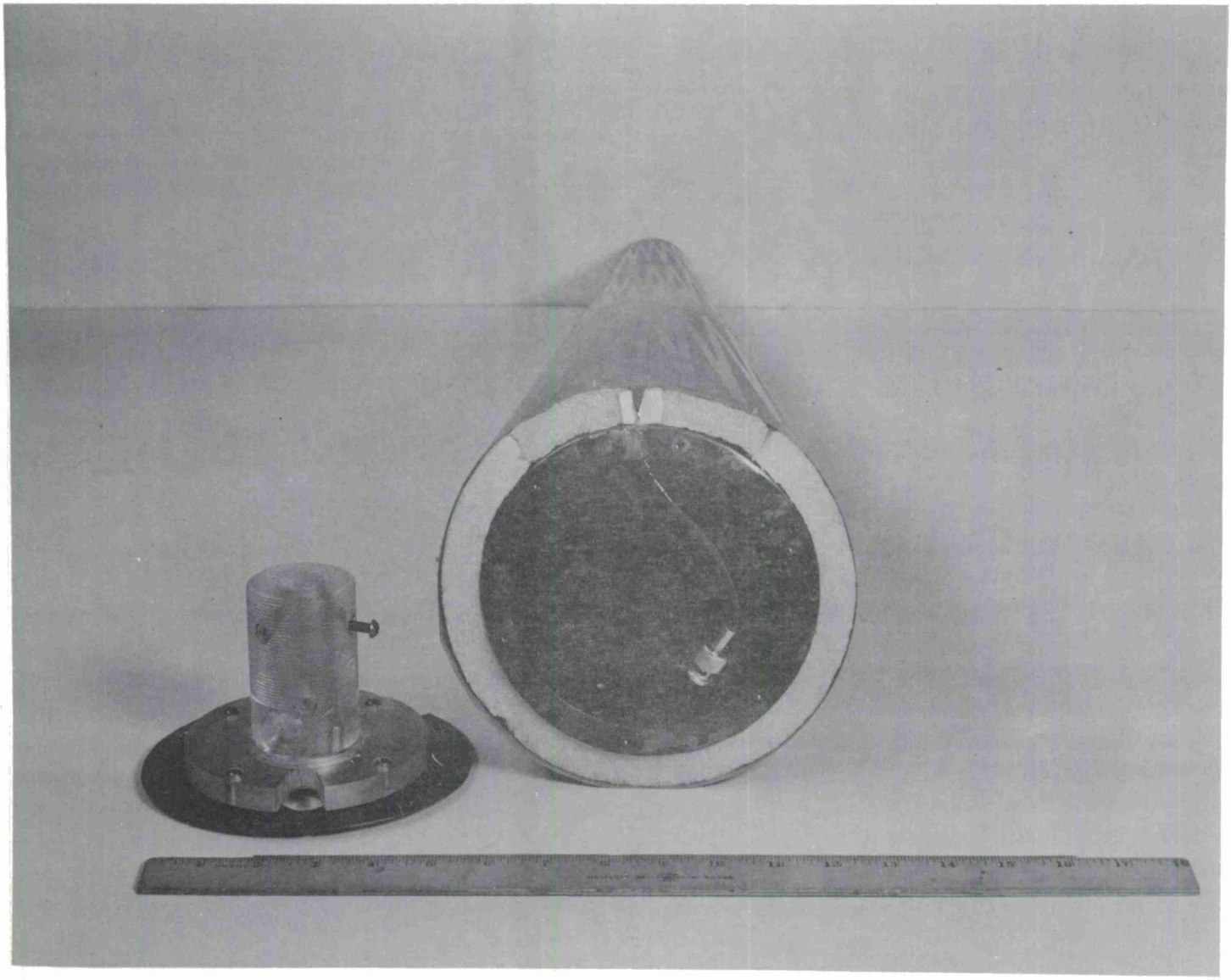

Figure 54. Base view of slow-wave helix showing inner metal cone. The coaxial feed cable center conductor extends through the metal cone and connects to helix.

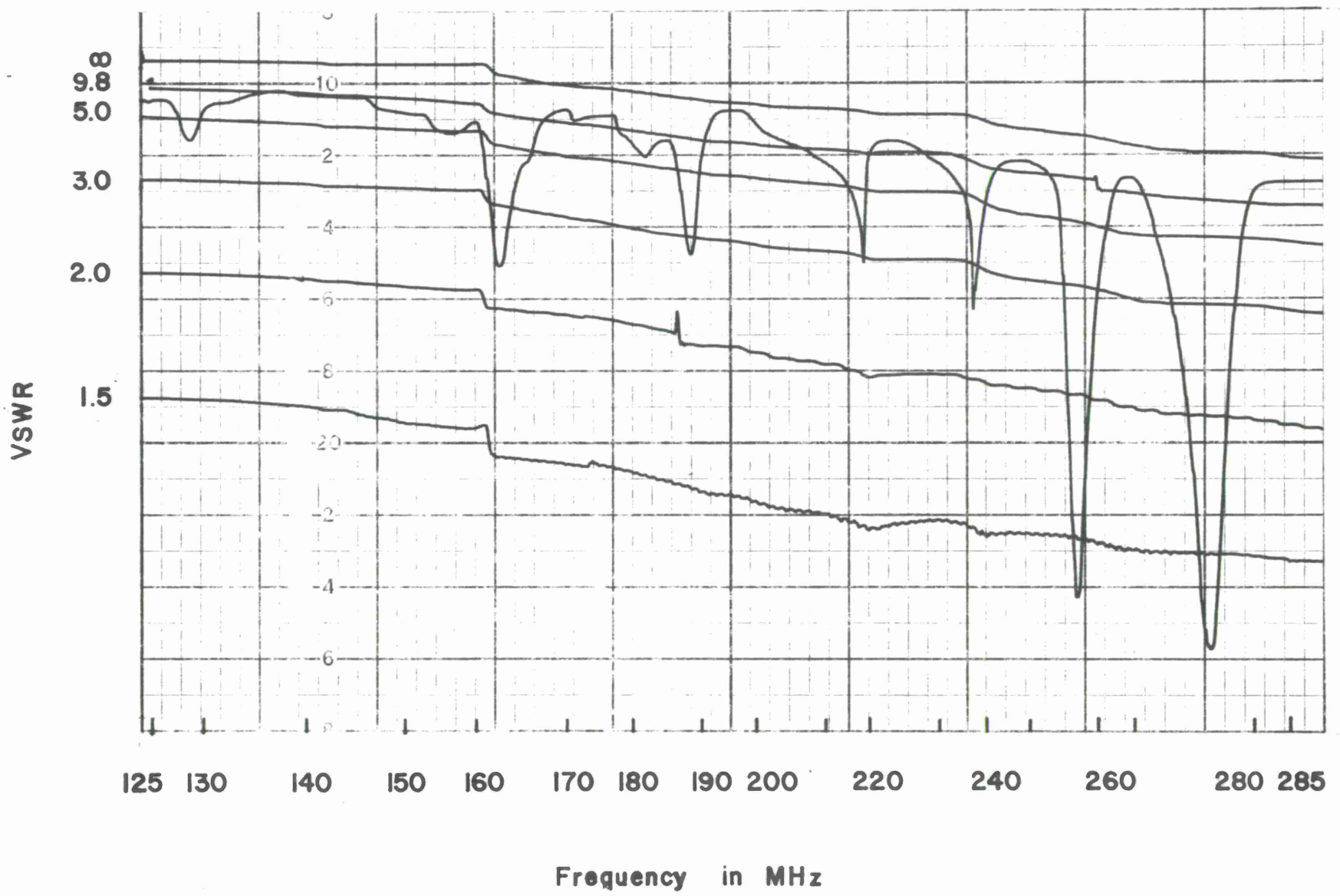

Figure 55. Measured VSWR referred to 50 ohms of one slow wave conical helix antenna (constructed with zig-zag geometry).

Table No. III. Gain, VSWR, and Mismatch Loss of the Slow Wave Conical Helix Antenna.

Freq. MHz	BBPG dB (RTI)	VSWR	Mismatch loss dB	Gain (BBPG corrected for mismatch) dB
150	-8.7	7.0	-3.5	-5.2
163	-5.5	2.5	-.9	-4.6
180	-12.9	8.0	-4.0	-8.9

2.5. Near-Field Measurements

The relative phase and amplitude of the normal component of the electric field (E_N) near the surface of the cone were recorded at 150 MHz, with the set-up described in Part I of this report. These measurements, made along the center line of the envelope of the zigzag geometry, indicated a standing wave with nulls approximately 21 cm apart near the base, increasing to approximately 25 cm apart near the apex. Thus the guide wavelength (λ_g) on the cone was between approximately 42 and 50 cm, compared with the free space wavelength (λ_o) of 200. This indicated an electrical slowing factor of from 4 to 4.75:1, from a geometrical slowing factor of 9.2:1. The variation in the electrical slowing factor can be accounted for by the changing geometry of the spiral arms. For arms, with a constant width envelope, wrapped on a cylinder, this slowing factor should remain constant.

This first version of the slow-wave helix did have approximately the electrical slowing that we desired, and did indeed have axial directed radiation. It is not however an optimum design. The standing wave of antenna current, and hence electric field along the envelope of the arm,

tended to prevent the antenna from having radiation characteristics that are symmetrical about the antenna axis.

Figure 56 shows this standing wave along the spiral arm. In this figure we show a scale drawing of the development of the conical surface of this antenna reduced by a factor of 1/25.3. The envelope of the slow-wave arm is shown on this development of the cone. The path along which E_N was measured is shown as a dotted line and the standing wave of E_N which was recorded has been drawn along this path.

We also probed E_N along radius vectors on the conical surface. These probe lines are shown on the development of the cone, in Figure 57. In this figure we have shown the standing waves along the arm, and those observed along the radius vectors. These latter amplitude (and implied phase, since alternate lobes are out of phase) distributions form the aperture distribution that controls radiation in the axial direction. The lack of symmetry, with the angle ϕ around the antenna, is evident.

2.6. Conclusions

The initial purpose of this investigation was to show that the major radiation from this small conical structure could be directed in an axial direction, by constructing a monofilar slow-wave helix on the surface of the cone, and exciting this helix against an inner metal core.

This effort was successful and it shows good promise. No effort was made to show performance over a complete octave bandwidth, although that shown is representative of such performance. This antenna was considered a first effort only. Based upon this start we feel that improvements can be made in the input reflection coefficient, with and without matching, and hence the "broadband power gain" on axis.

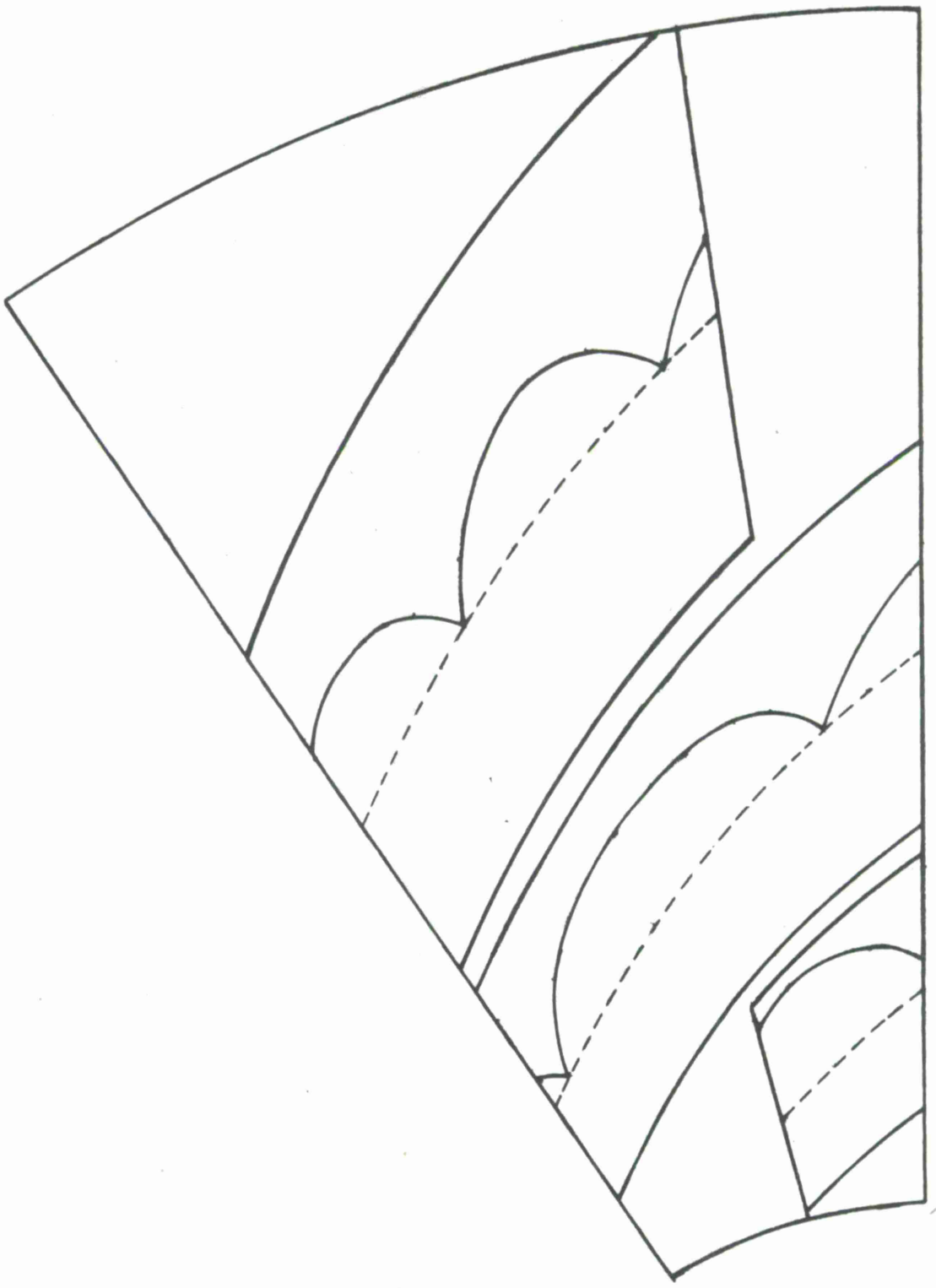

Figure 56. Development of the conical surface of the slow-wave helix with only the envelope of the arms shown. Probe line and measured standing wave of E_n is shown along this envelope. 150 MHz.

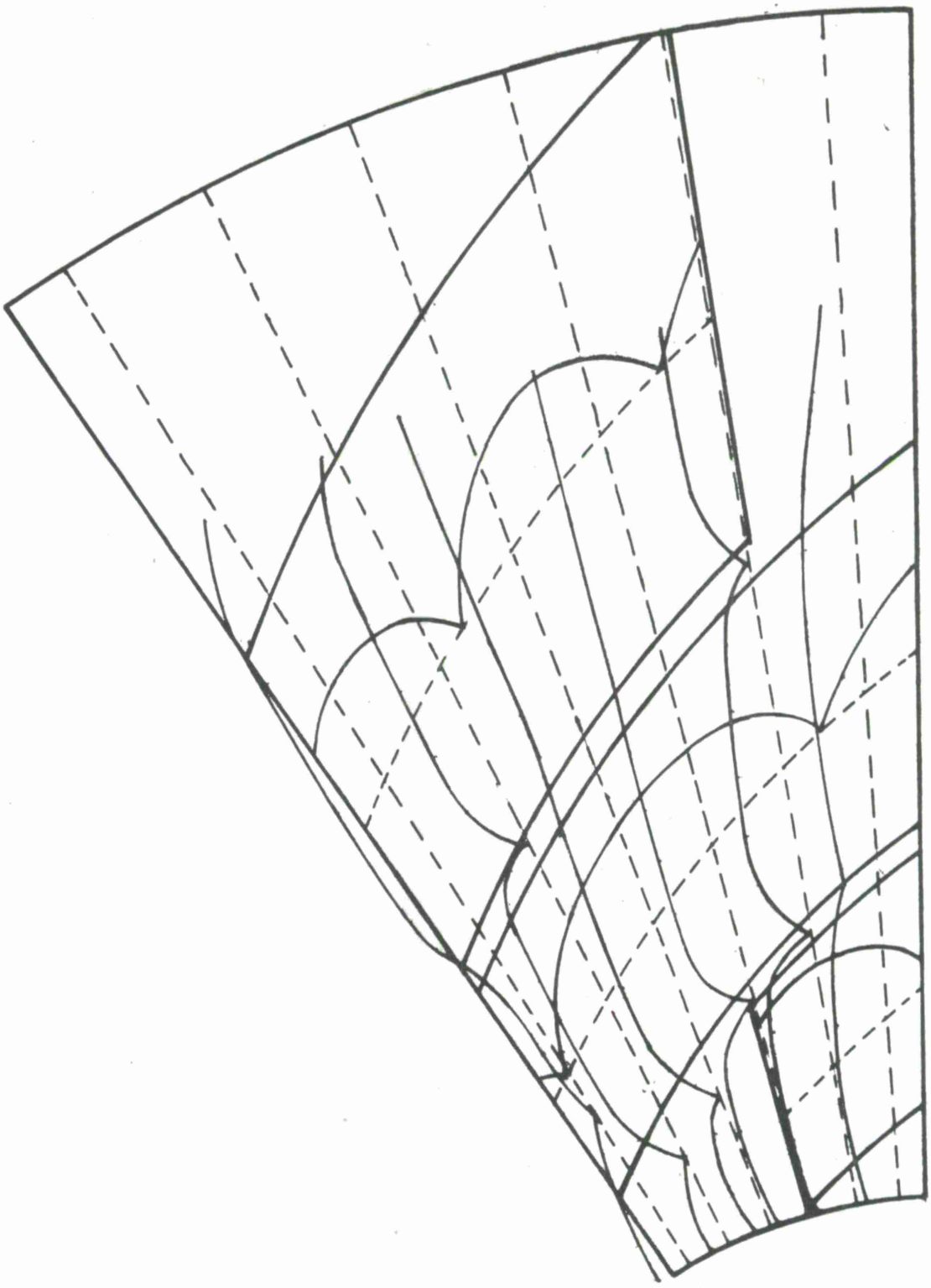

Figure 57. Development of the conical surface of the slow-wave helix with envelope of slow wave arm shown. Probe lines and measured standing waves of E_n along arm and along radius vectors are shown. 150 MHz

These improvements could come from constructing the antenna with an undulating geometry, rather than the sharp zigzags which were used. This should reduce the discontinuities along the arm.

The antenna, as described here, is not radiating in a traveling wave mode which is characteristic of the axial beam helix. Control of the phase velocity along the structure, by a different choice of geometry and geometrical slowing factor, should make the realization of this traveling wave mode possible. If realizable, this traveling wave antenna should have more constant input impedance and more symmetrical radiation characteristics. These factors should be investigated, but this could not be accomplished within the time limitation of the present contract.

REFERENCES

1. G. G. Rassweiler, "Helical and Log Conical Helical Antennas Loaded with an Isotropic Material," Dept. of E.E., The University of Michigan, Ann Arbor; Third Q.R. Contract AF33(615)3609, Project 6278, November 1966(DDC No. AD806094).

2. E. T. Roland and W. F. Patterson, "A Slow-Wave Flat Spiral Antenna," Abstracts, Seventeenth USAF Antenna Symposium, sponsored by A. F. Avionics Lab., at Monticello Ill., Univ. of Ill., November 1967.

3. S. L. Mathews, "Physical Size Reduction of the Conical Log-Spiral Antenna by Use of a Zigzag Geometry," M.S. Thesis, Electrical Engineering Dept., Univ. of Illinois, Urbana, Ill., 1972.

4. J. D. Dyson, "The Characteristics and Design of the Conical Log-Spiral Antenna," TR No. 86, Antenna Lab., University of Illinois, Contract AF 33(657)-10474, May 1965.

5. J. D. Dyson and R. Ginyovszky, "Balanced Transmission-Line Measurements Using Coaxial Equipment," IEEE Trans. Microwave Theory Tech., vol. MTT-19, No. 1, pp. 94-96, January 1971.

6. J. D. Dyson, "Investigation of Some Electrically Small Conical Log-Spiral Antennas," (UIAL-71-14) ESD-TR-71-297, Annual Report on Purchase Order CC401, (Prime Contract No. F19628-70-C-0230) Antenna Laboratory, University of Illinois, Urbana, Ill., September 1971.

APPENDIX A

CONSTRUCTION OF ZIGZAG GEOMETRY

The zigzag is drawn within the envelope formed by a single spiral arm of the normal conical log-spiral antenna. Figure A1 shows the relationship between the zigzag geometry and the parameters of the log-spiral arm.

The spiral arm is at an angle α to a radius vector extending from the apex to the base along the surface of the cone, and has an angular width of δ', according to the conventions previously established[4]. The zigzag should have equal widths for each arm in order to maintain a relatively constant impedance to the current wave traveling down the cone surfaces. Therefore w, the perpendicular width of a zig, should equal W, the perpendicular width of the adjoining zag.

The problem of determining the zigzag relationship is simplified by placing the boundaries of the zigs colinear with the radial vectors, and assuming straight-line approximations.* The endpoints of the zigs are connected to the endpoints of the zags so as to maintain the equal perpendicular widths. The boundaries of the zags form an angle β to the radius vector, measured in the opposite direction to α.

The concept of slowing factor can be illustrated by Figure A2. The electric current will travel a distance Q along a zag, and a distance R along a zig, compared to the distance P on a normal spiral

*This is a valid assumption since the widths are always much smaller with respect to the cone circumference at any point along the cone surface.

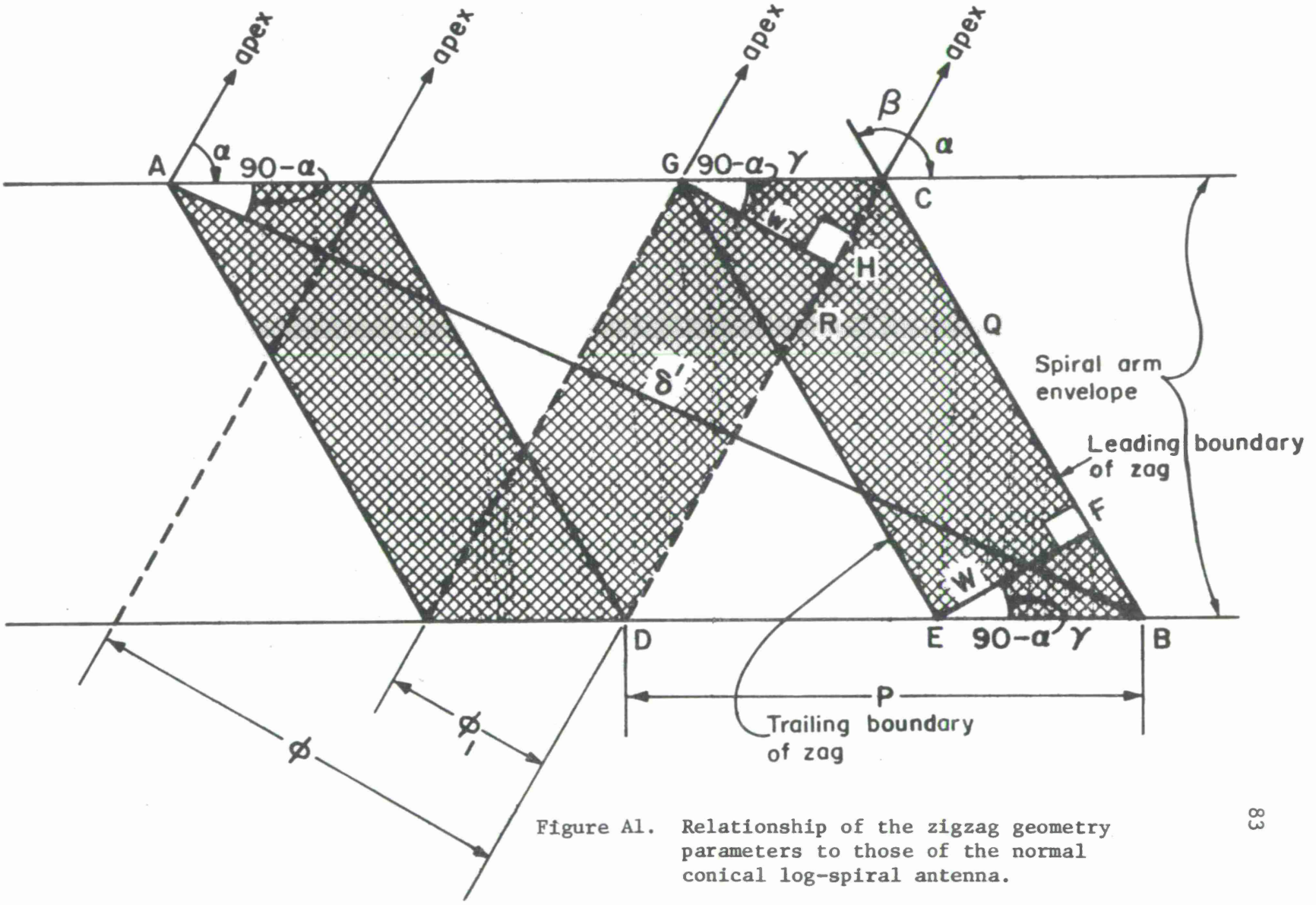

Figure A1. Relationship of the zigzag geometry parameters to those of the normal conical log-spiral antenna.

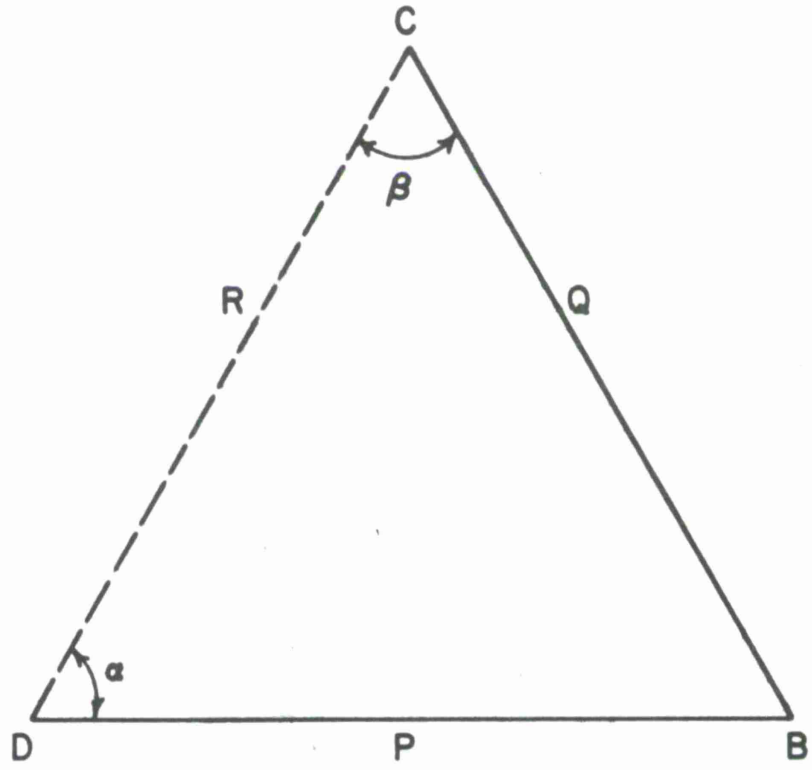

Figure A2. Diagram illustrating the slowing factor concept.

arm. The time to travel the distance Q + R will be longer than that for P, and we therefore can say that the electric current requires a time factor $\frac{Q + R}{P}$ longer to travel the zigzag path:

$$\text{Slowing factor, } \zeta = \frac{Q + R}{P} . \qquad (1)$$

That is, the electric current has been slowed by a factor ζ.

Figure A1 indicates the relationship between P and ϕ, where ϕ is the angular distance between the leading boundaries of adjacent zigs (or similarly, between the leading boundaries of adjacent zags), measured with reference to the apex:

$$P = \frac{\phi}{\sin \alpha} . \qquad (2)$$

Referring to triangle ABC in Figure A1, and applying the Law of Sines,

$$\frac{Q}{\sin (90 - \alpha)} = \frac{\delta'}{\sin (\alpha + \beta)}$$

$$Q = \delta' \frac{\cos \alpha}{\sin (\alpha + \beta)} .$$

Using the Law of Sines again on triangle BCD in Figure A2,

$$\frac{Q}{\sin \alpha} = \frac{R}{\sin[180 - (\alpha + \beta)]}$$

$$R = \frac{Q \sin (\alpha + \beta)}{\sin \alpha} .$$

Substituting the values for Q and R into the slowing factor equation, (1) reduces to

$$\zeta = \frac{\delta'}{\phi} \left[\frac{\cos \alpha \sin \alpha}{\sin (\alpha + \beta)} + \cos \alpha \right] . \qquad (3)$$

We note that triangles GHC and EBF in Figure A1 are congruent.

Consequently,

$$\text{angle CGH} = \text{angle FEB} \qquad \text{(a)}$$

$$\text{angle GCH} = \text{angle FBE} \qquad \text{(b)}$$

$$\text{angle CGH} = 90 - \alpha$$

$$\text{angle GCH} = \alpha$$

$$\text{angle FEB} = \alpha + \beta - 90$$

$$\text{angle FBE} = 180 - (\alpha + \beta) \quad .$$

Equating the respective equal angles, (a) and (b), both sets of angles reduce to

$$\beta = 180° - 2\alpha \quad . \qquad (4)$$

Therefore, the angle the radius vector makes with the boundary of the zag, β, is determined by the angle of wrap, α.

Substituting (4) into (3), the slowing factor equation reduces to

$$\zeta = \frac{2\delta'}{\phi} \cos \alpha \ . \qquad (5)$$

This result suggests a large variety of methods for determining a zigzag geometry. For example, there are several ways to achieve a specific geometric slowing factor, if reasonable values are chosen for δ', ϕ, and α. Care should be taken in specifying ϕ so that it divides rationally into 360°, permitting zigs to match up with zags along a radius vector where a physical joint might be placed, and selecting an appropriate α and δ' for a given included cone angle to produce directive radiation patterns.

For the results presented in this paper, ϕ and α were fixed, with δ' being determined from a given ζ.

It should be noted that a drawing of a normal spiral must be created so that the zigzag geometry can be constructed within the envelope of the spiral arm.

A master is created by drawing on the development of a conventional cone radius vectors spaced according to the spacing chosen for the zigzag geometry. The normal spiral arm drawing is placed on top of the master, and the zigzags are ready to be drawn.

Figure A3 illustrates the construction of the zigzag geometry. A fixed triangle edge is placed along a radius vector, with the right-angled corner at the upper left. An adjustable-angle triangle is set for the angle β, and it is placed along the left edge of the fixed triangle such that an angle β is made to the radial line, measuring counterclockwise. We began the zag boundary line from the bottom-most part of the spiral envelope, although the upper part could be the starting point. (The choice should be consistent throughout the construction of the zigzag geometry.) This line can be called the leading boundary of the zag.

The trailing boundary of the zag is drawn in the same manner, with the exception that the fixed square is realigned with a new radius vector corresponding to the angular arm width of the zag ϕ_1. ϕ_1 is an arbitrary value, but should be less than half the length of a zigzag cell, ϕ, in order to achieve a good electric slowing factor.

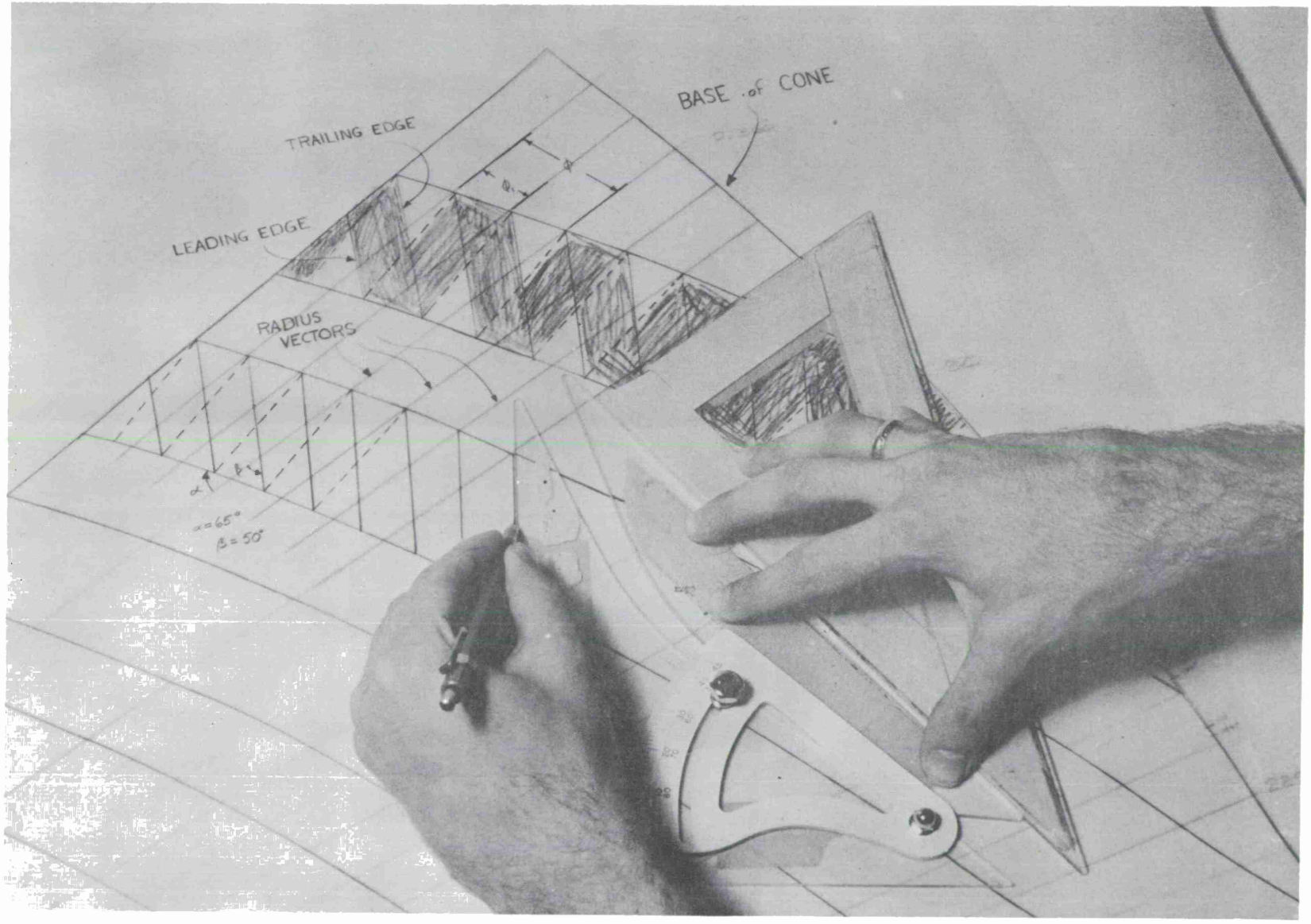

Figure A-3. Construction of zigzag geometry.

The zigs can be made once the leading and trailing edges of the zags are drawn by simply connecting the end of a leading edge to the beginning of a trailing edge, for example, points C and D in Figure A1. Generally, these lines will not lie along a radius vector, as assumed, but the error is only a few degrees, depending upon the cone and zigzag geometry parameters. It should also be noted that the zig arm width will not be equal to the zag arm width due to logarithmic growth, but the difference is extremely small and will have negligible effect on the electric slowing factor.

APPENDIX B

CALCULATION OF "EQUIVALENT" SPIRAL ARM WIDTH FROM ZIGZAG

The "equivalent" spiral arm width has a perpendicular width of w, the width of the zigzag arm, and makes an angle of α to any radius vector. This is the same as taking a zig or zag and "bending" it up to the angle of wrap, α, made by the zigzag envelope. The problem reduces to finding the δ' of the "equivalent" spiral arm.

We define the "equivalent" spiral width to be δ''. (See Figure B1.) The Law of Sines for Spherical Triangles can be used to compensate for the cone curvature in solving for δ'':

$$\frac{\sin w}{\sin(90-\alpha)} = \frac{\sin \delta''}{\sin \alpha}$$

All widths are in terms of degrees.

$$\delta'' = \sin^{-1} [\sin w \tan \alpha] .$$

The Law of Sines for Plane Triangles can also be used, although the two values of δ'' will differ by a few degrees. This difference will be unnoticeable in terms of the resultant near-field characteristics:

$$\delta'' = w \tan \alpha .$$

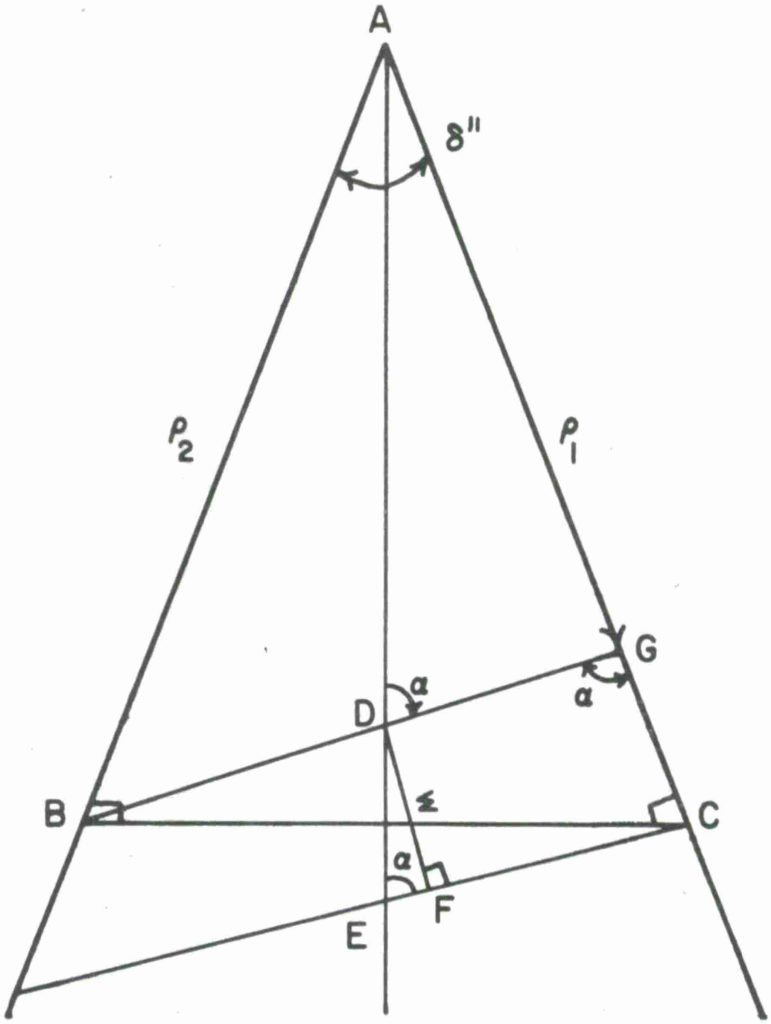

Figure B-1. Determination of the "equivalent" spiral arm width of the wide and thin arm zigzag geometries.

APPENDIX C

CALCULATION OF ELECTRIC SLOWING FACTOR AND PERCENTAGE SIZE REDUCTION OF ZIGZAG ANTENNAS

The -15 dB points on the surface of the cone were determined for three frequencies and an average value used for both the normal spiral antennas (references) and the zigzag antennas. The shifts of the -15 dB points of the zigzag antenna relative to the -15 dB points of the reference antennas are then expressed as a percentage of zigzag size to the size of the reference antenna:

$$\text{Percent Size Reduction} = \frac{\rho_{REF} - \rho_{ZZ}}{\rho_{REF}} \times 100$$

where ρ is the distance measured from the apex to the -15 dB point on the surface of the cone.

The electric slowing factor can be determined from the previous result:

$$\text{Electric slowing factor} = \frac{100}{(100\% - \%\ \text{Size Reduction})} .$$

APPENDIX D

Radiation Patterns of Conical Spiral Antennas

(Refer to Section 1.4.1, page 27)

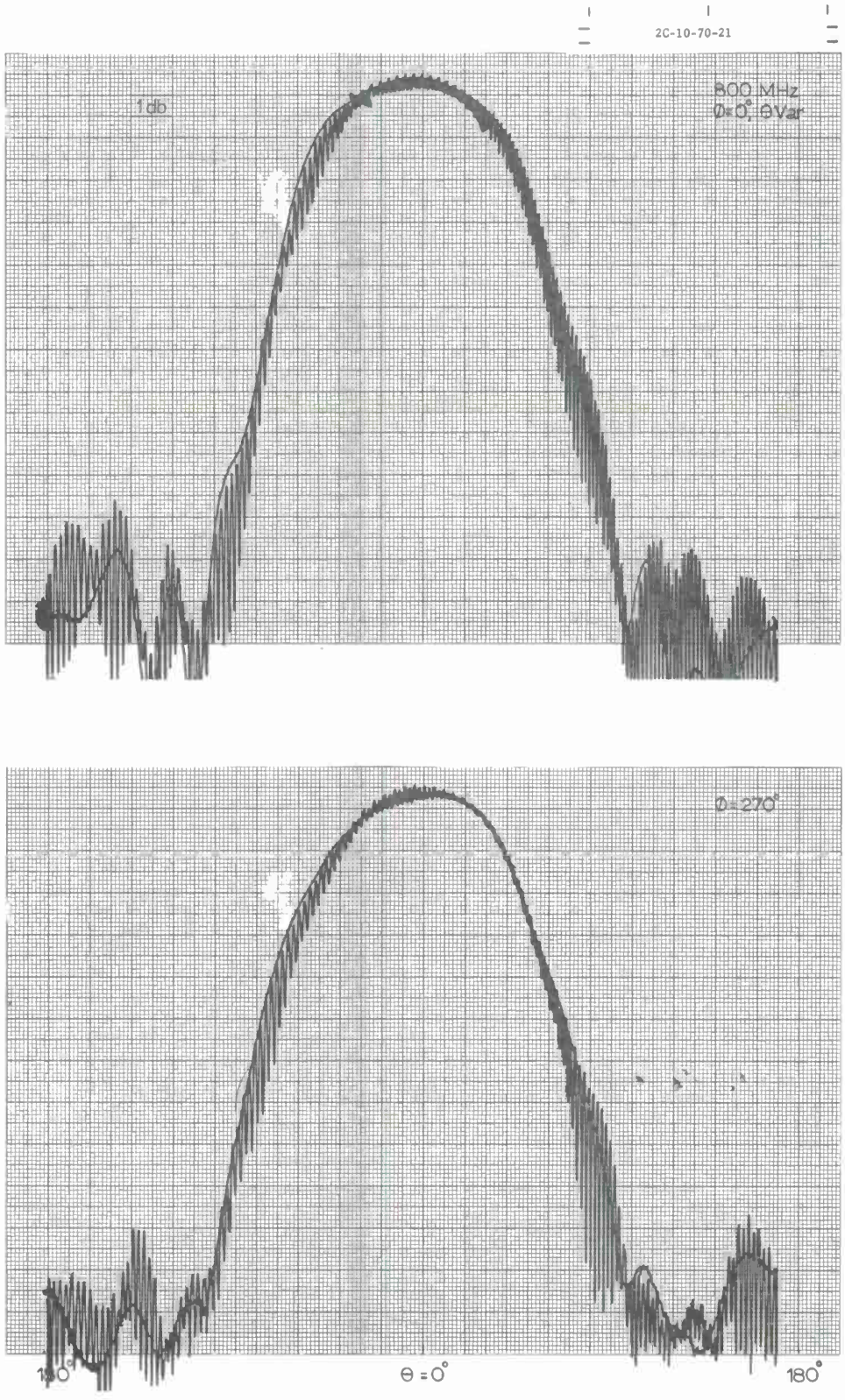

Figure D-1. Radiation patterns of conventional conical spiral antenna, $\alpha = 70°$, $\delta' = 21°$. Recorded with continually rotating linearly polarized receiving antenna.

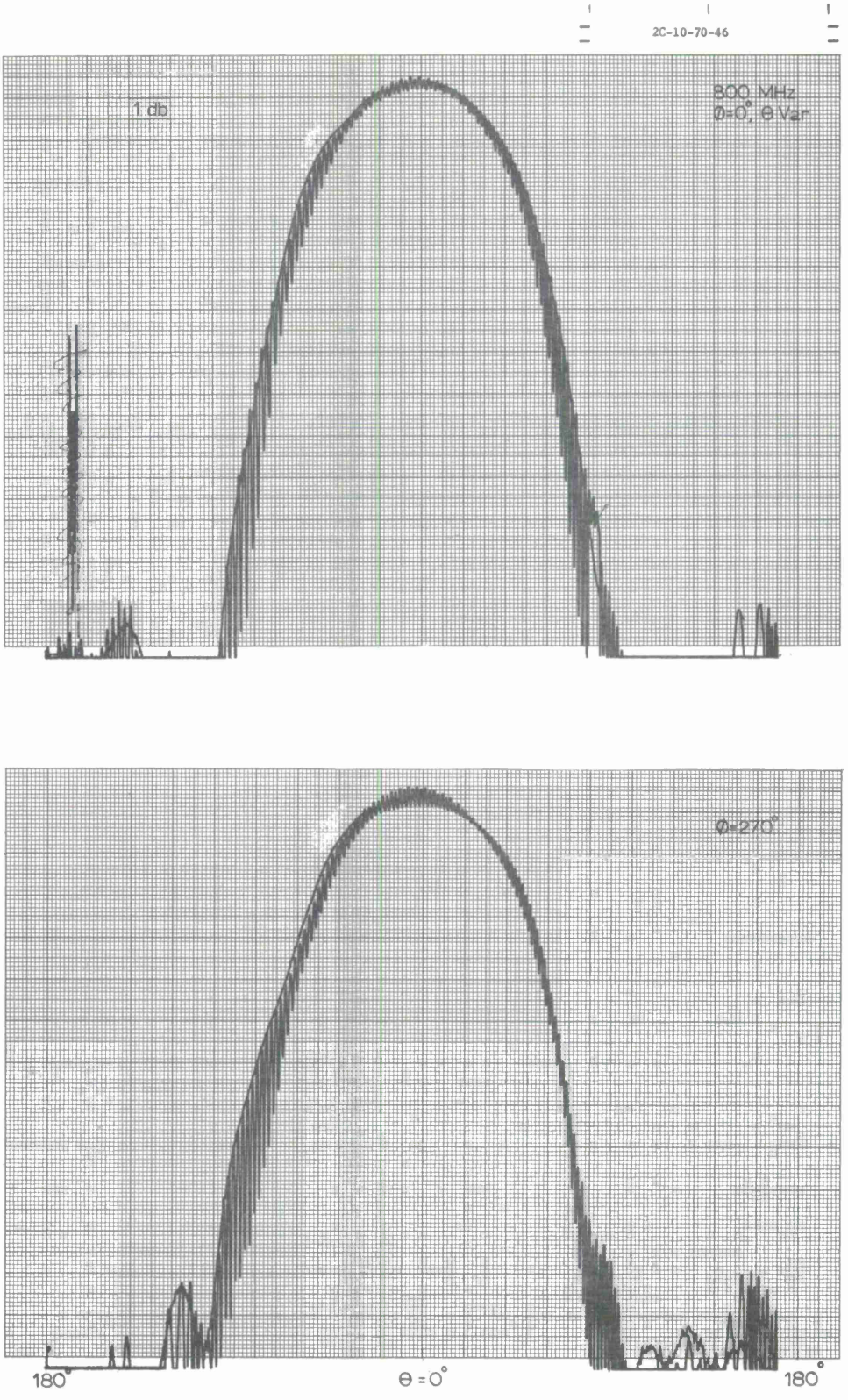

Figure D-2. Radiation patterns of conventional conical spiral antenna, $\alpha = 70°$, $\delta' = 46°$.

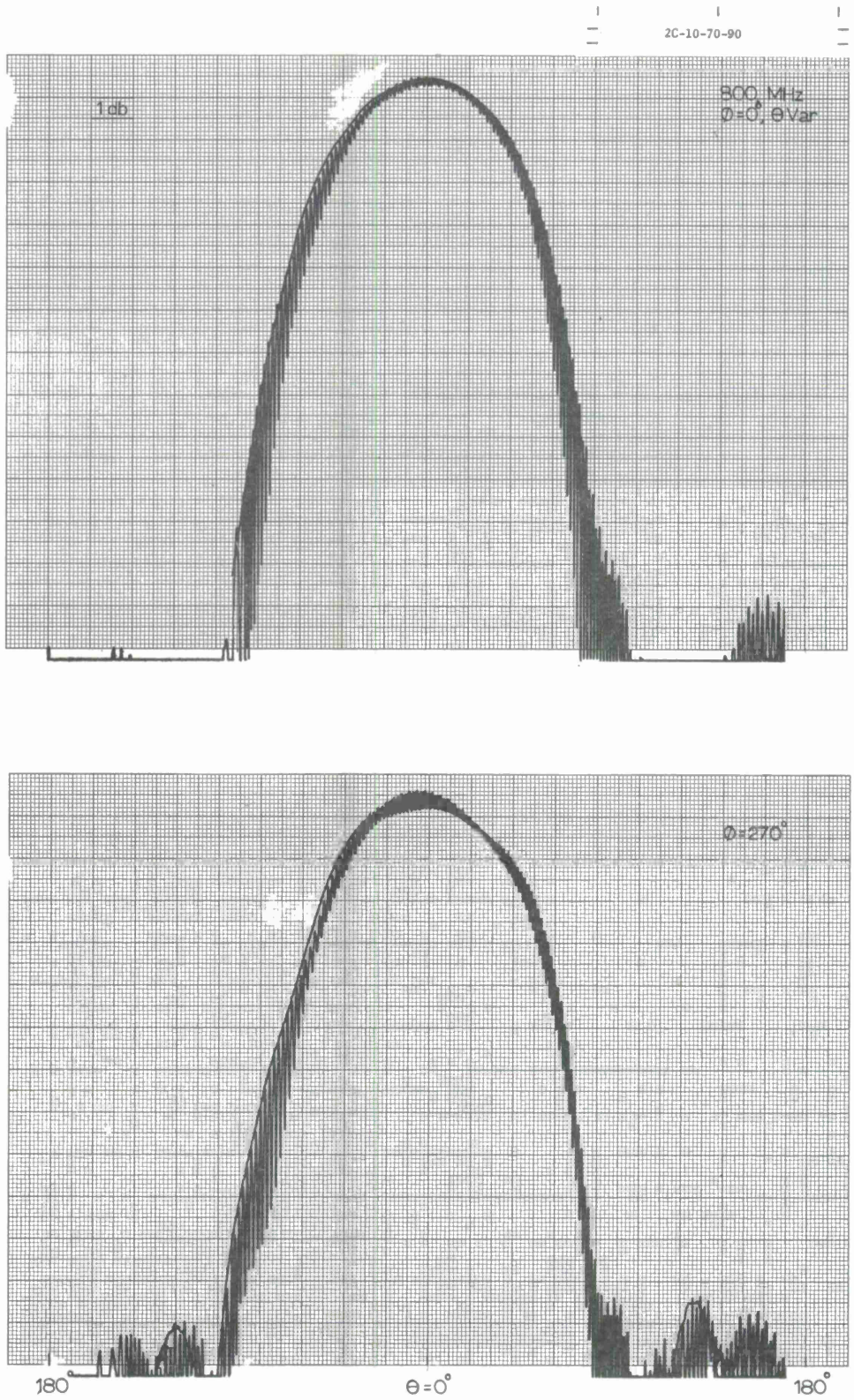

Figure D-3. Radiation patterns of conventional conical spiral antenna, $\alpha = 70°$, $\delta' = 90°$.

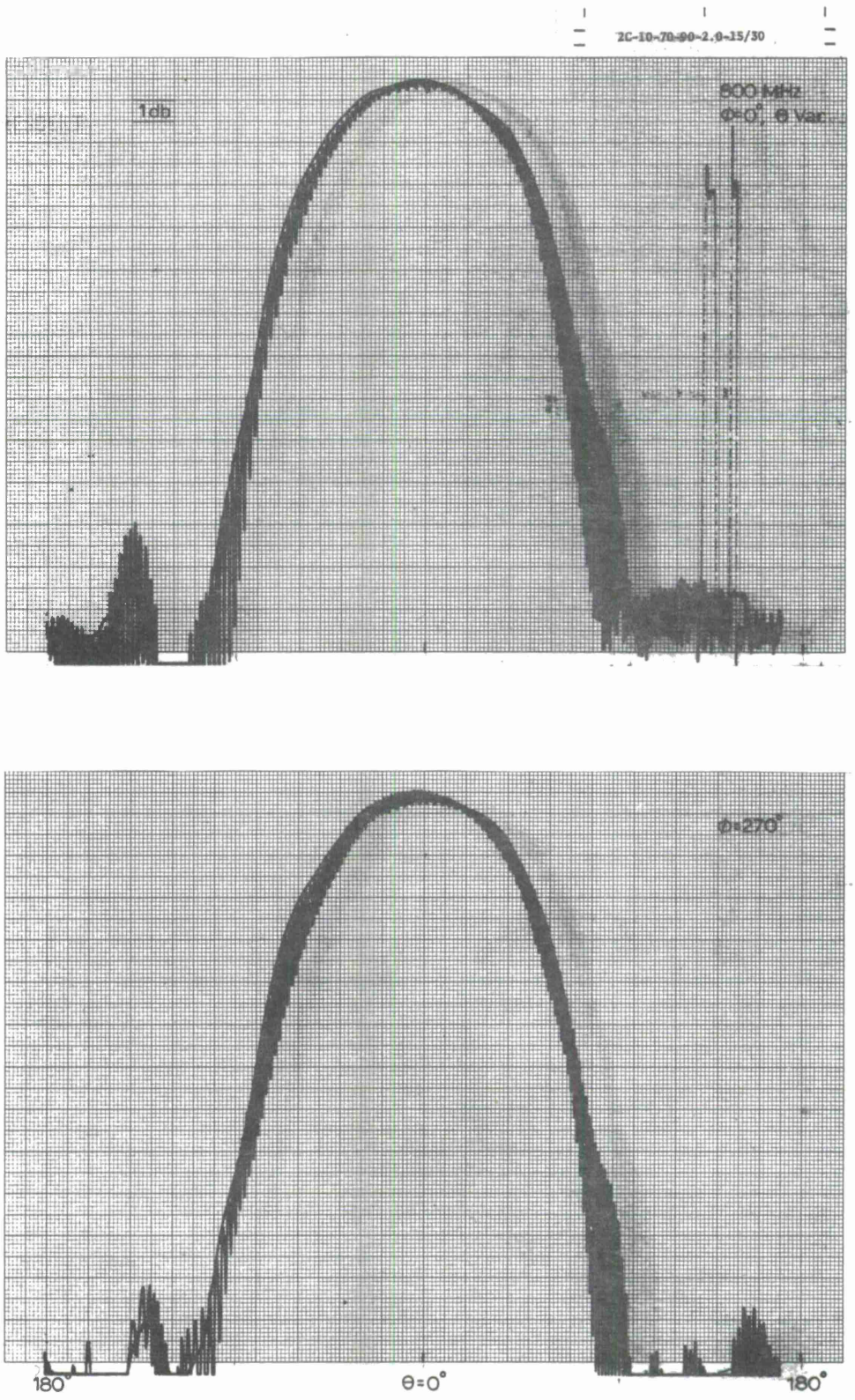

Figure D-4. Radiation patterns of slow-wave conical spiral antenna, $\alpha = 70°$, wide arm width (15/30), slowing factor 2.0.

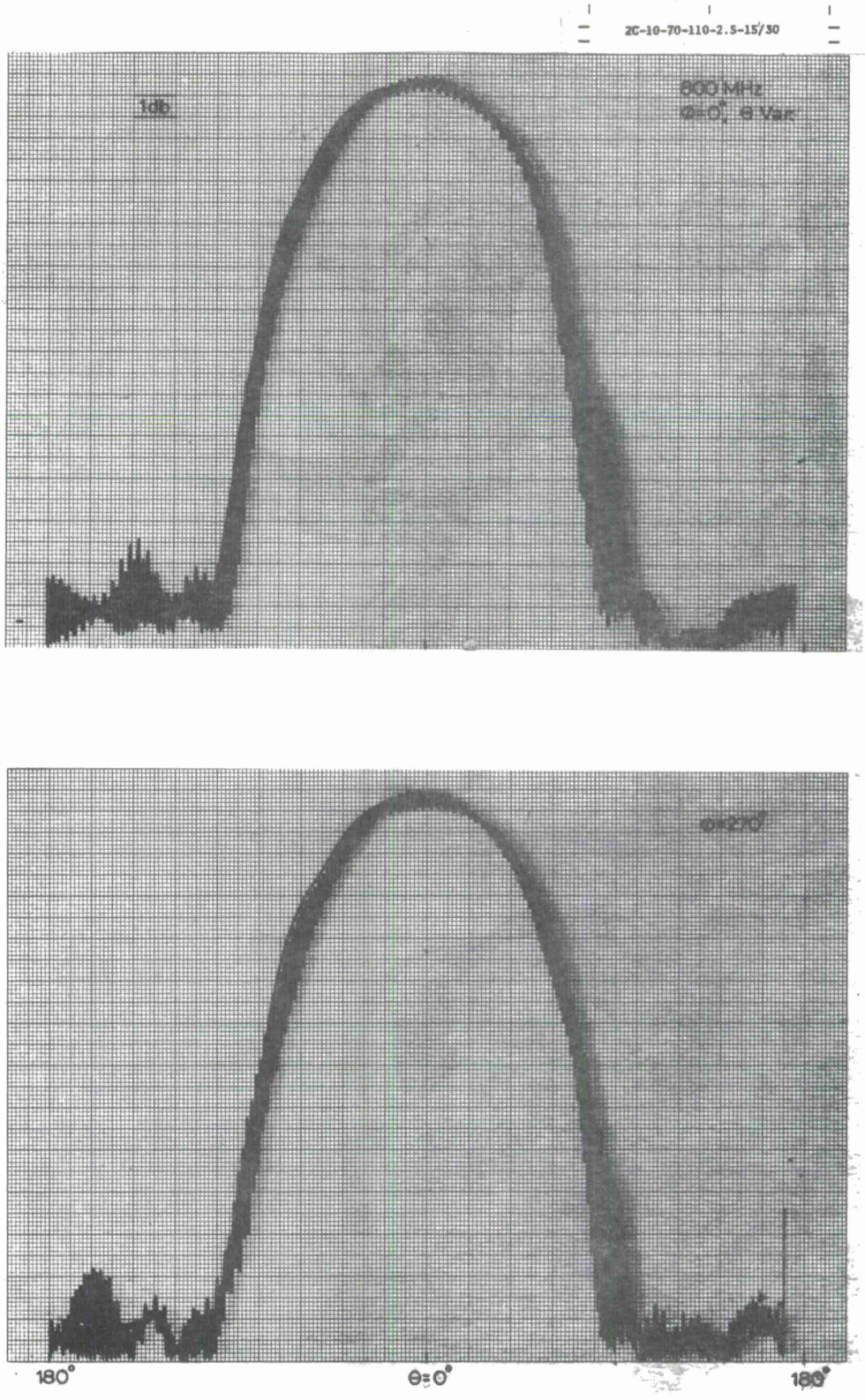

Figure D-5. Radiation patterns of slow-wave conical spiral antenna, $\alpha = 70°$, wide arm width (15/30), slowing factor 2.5.

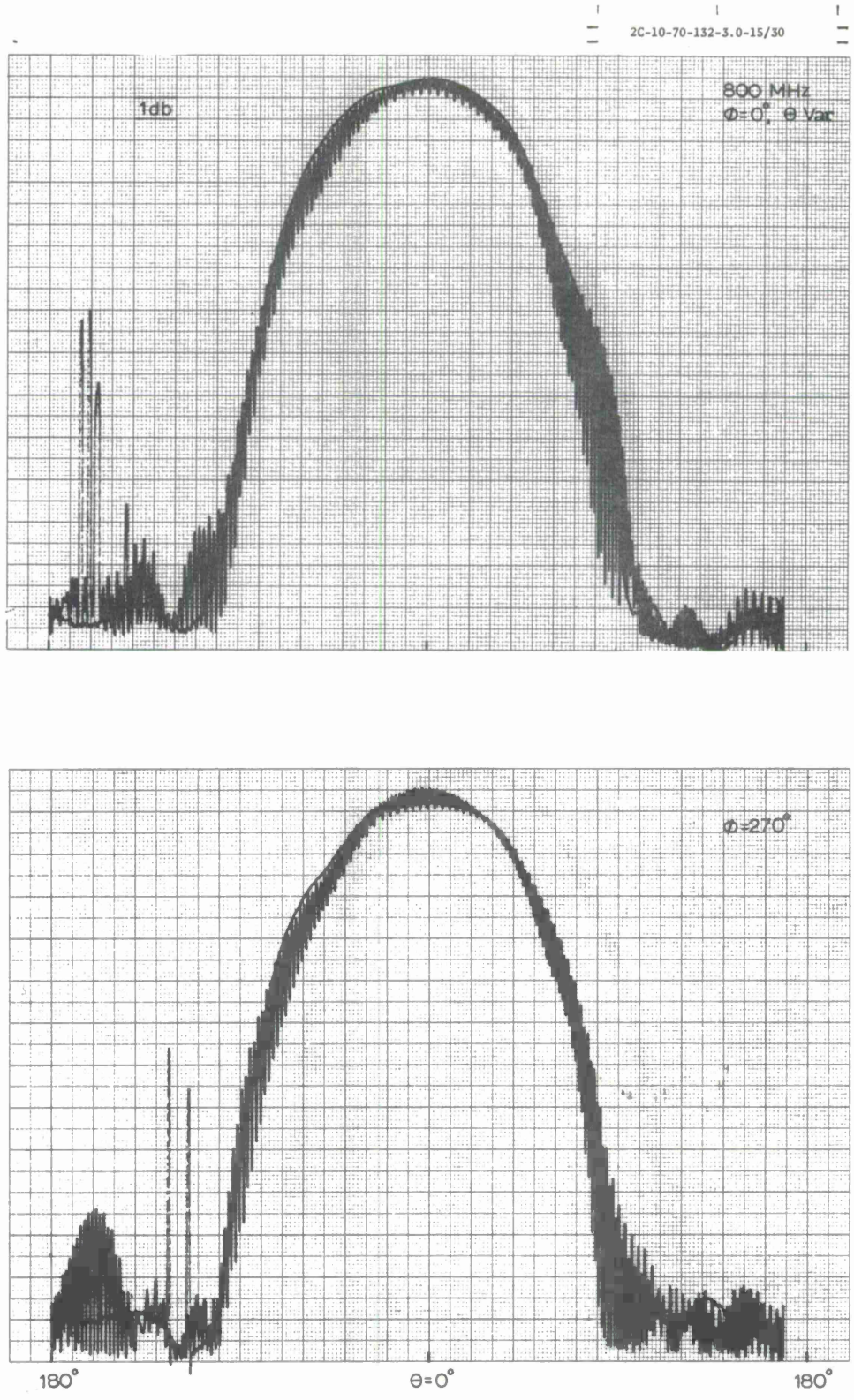

Figure D-6. Radiation patterns of slow-wave conical spiral antenna, $\alpha = 70°$, wide arm width (15/30), slowing factor 3.0.

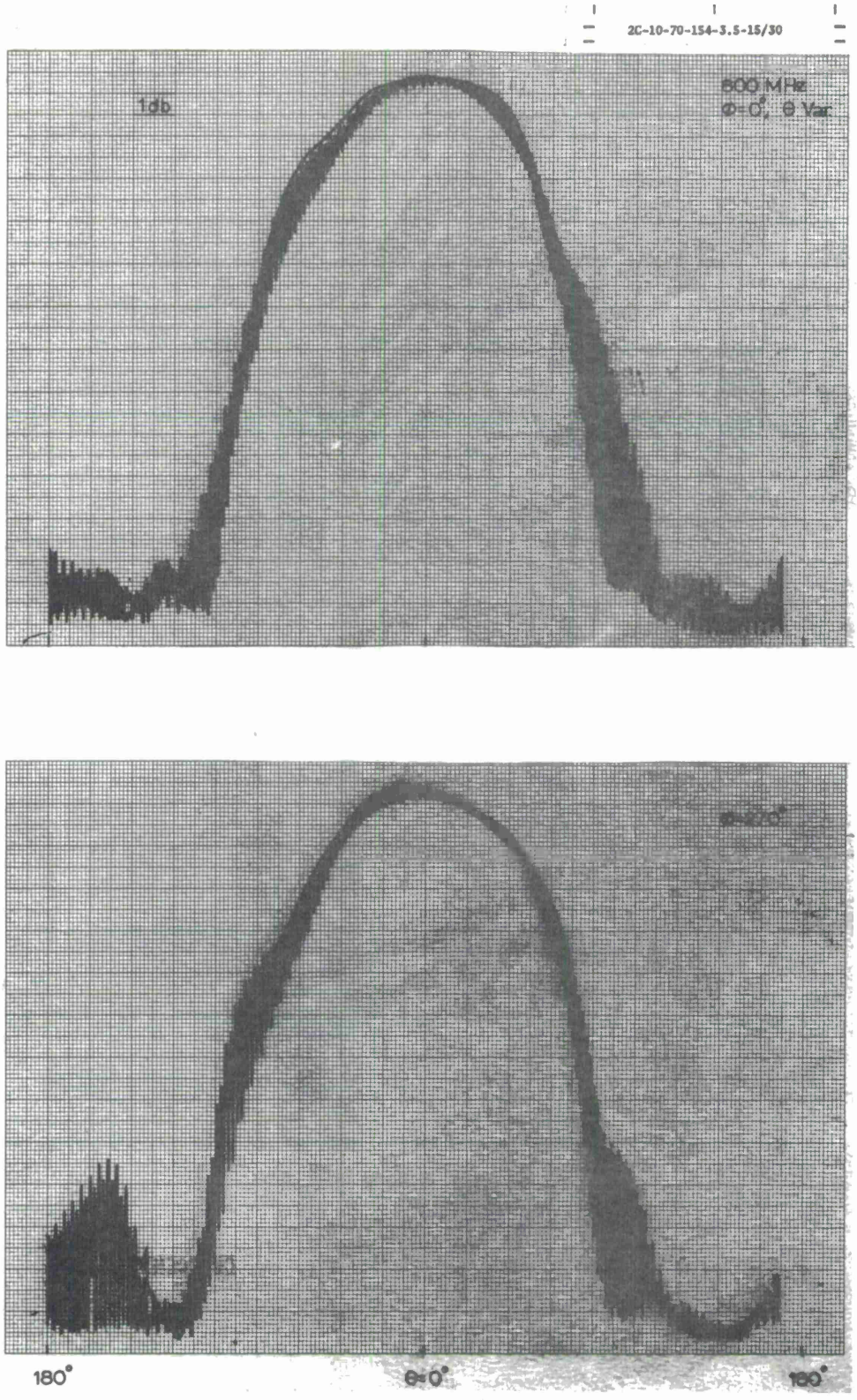

Figure D-7. Radiation patterns of slow-wave conical spiral antenna, $\alpha = 70°$, wide arm width (15/30), slowing factor 3.5.

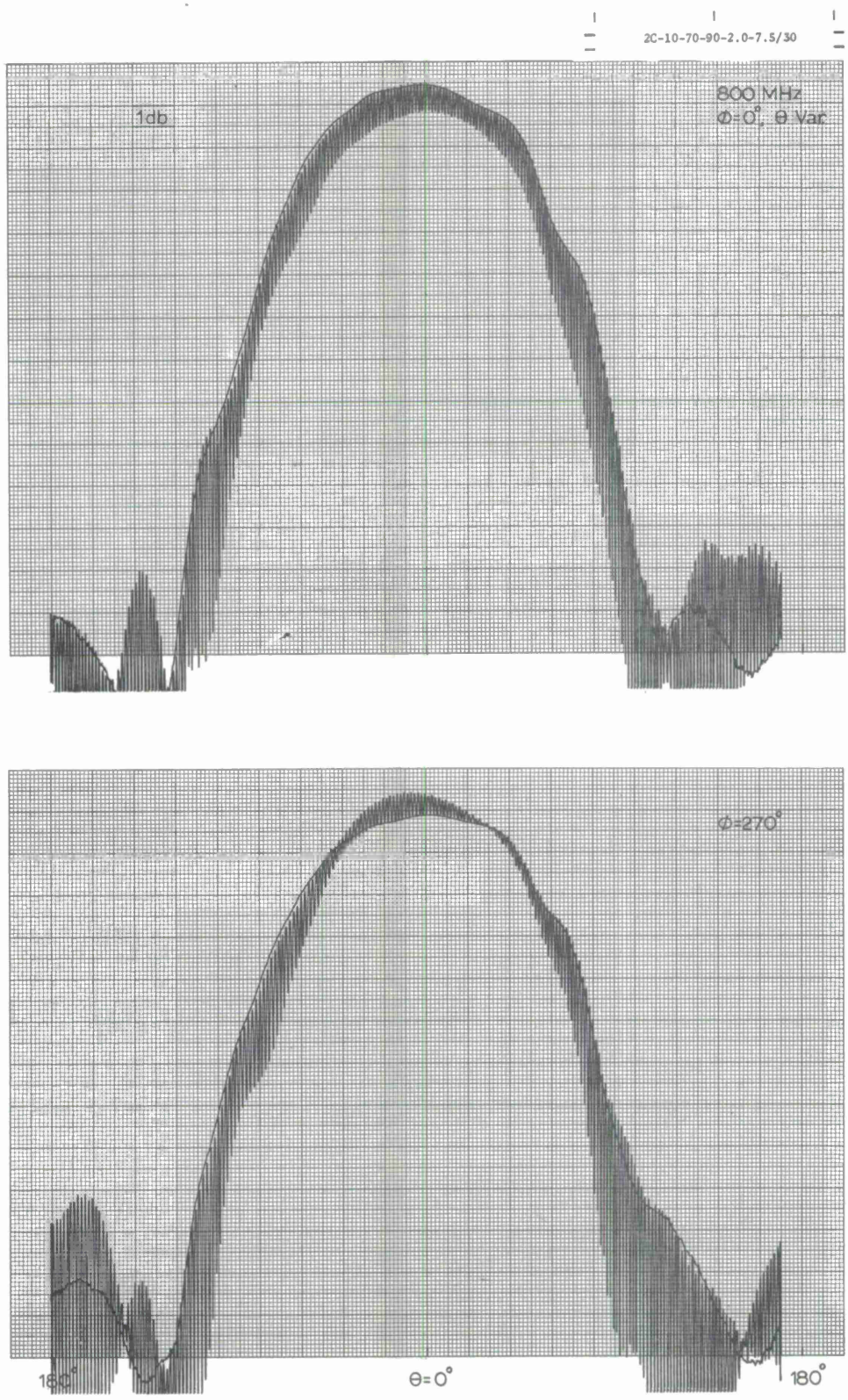

Figure D-8. Radiation patterns of slow-wave conical spiral antenna, $\alpha = 70°$, narrow arm width (7.5/30), slowing factor 2.0.

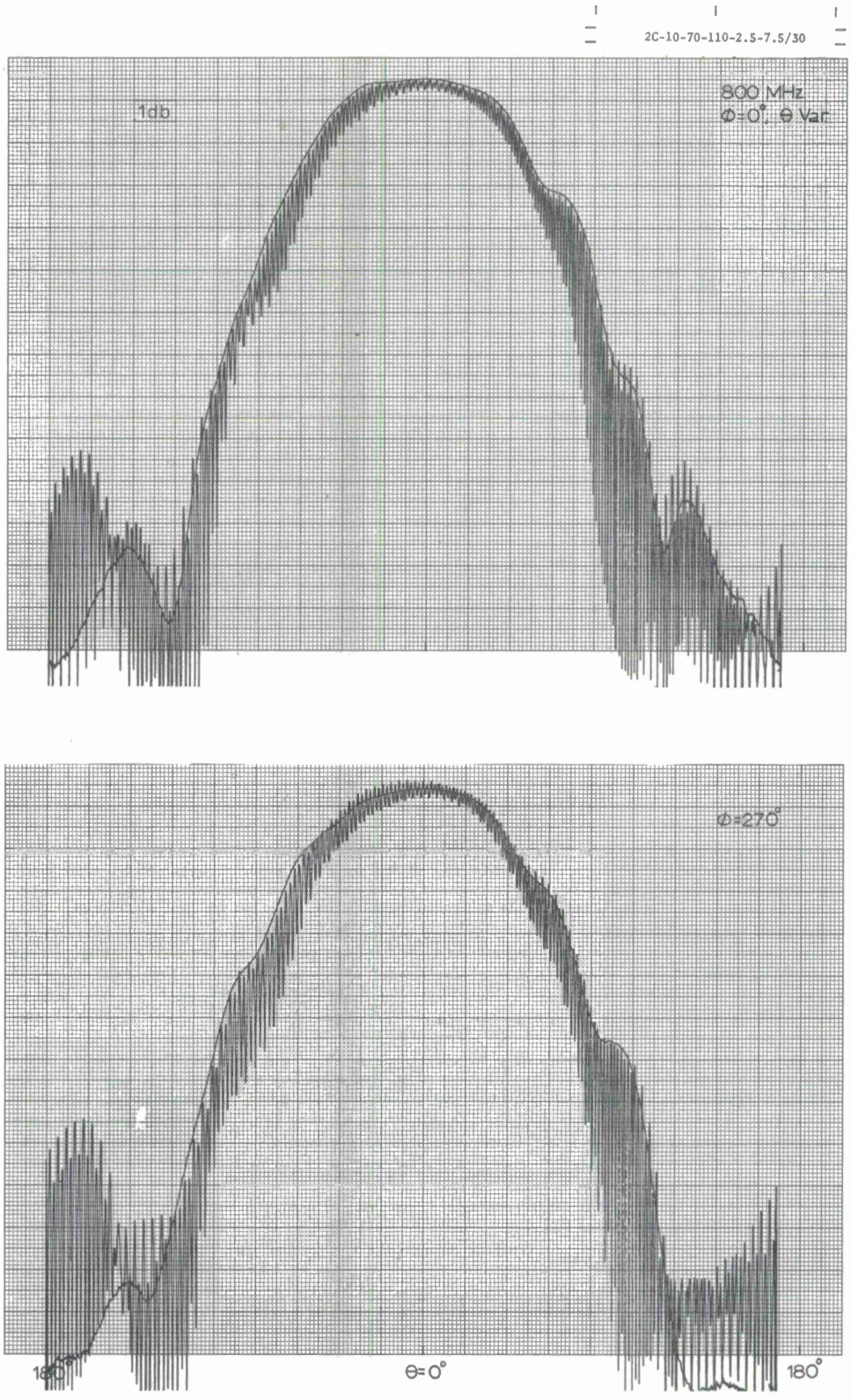

Figure D-9. Radiation patterns of slow-wave conical spiral antenna, $\alpha = 70°$, narrow arm width (7.5/30), slowing factor 2.5.

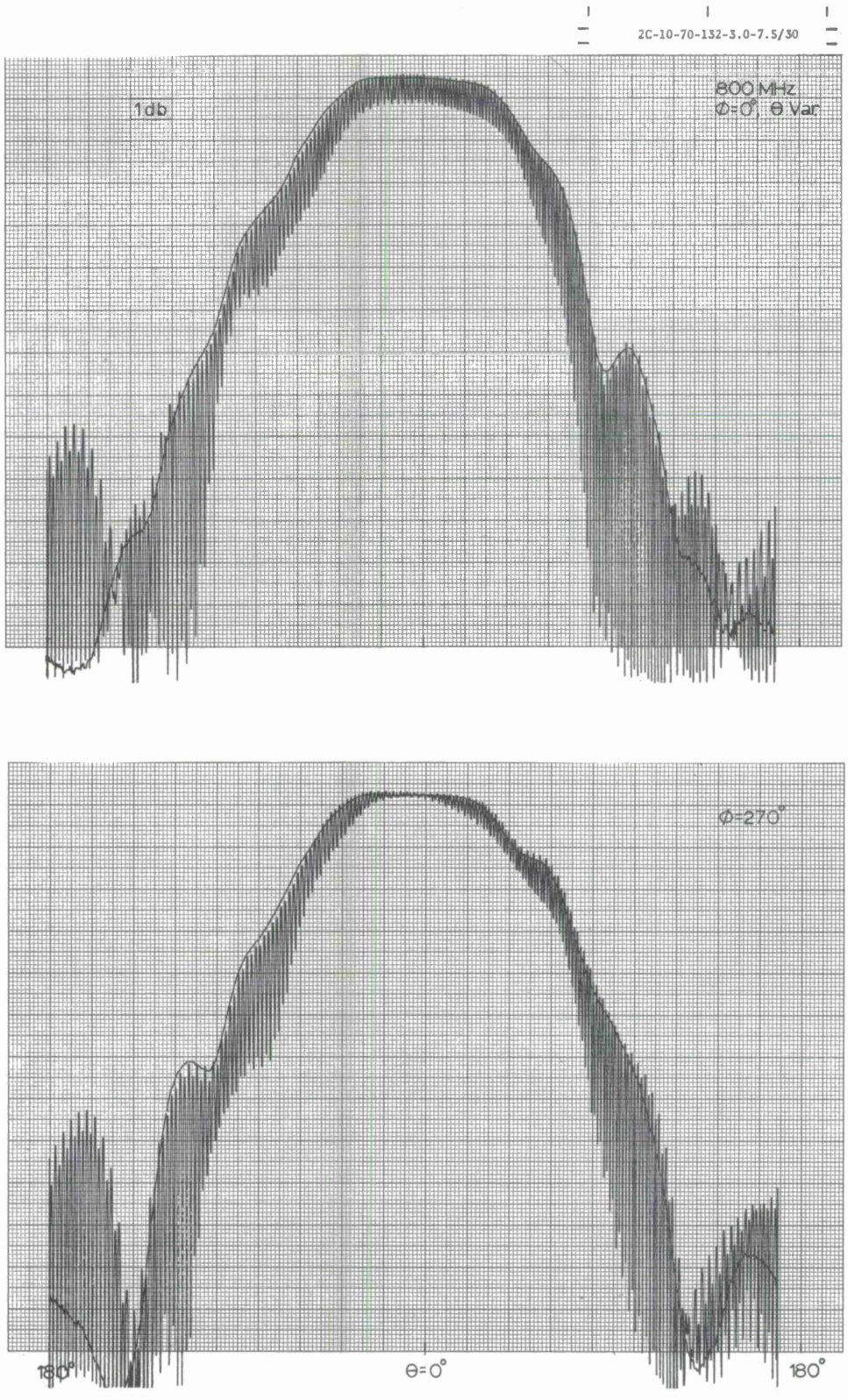

Figure D-10. Radiation patterns of slow-wave conical spiral antenna, $\alpha = 70°$, narrow arm width (7.5/30), slowing factor 3.0.

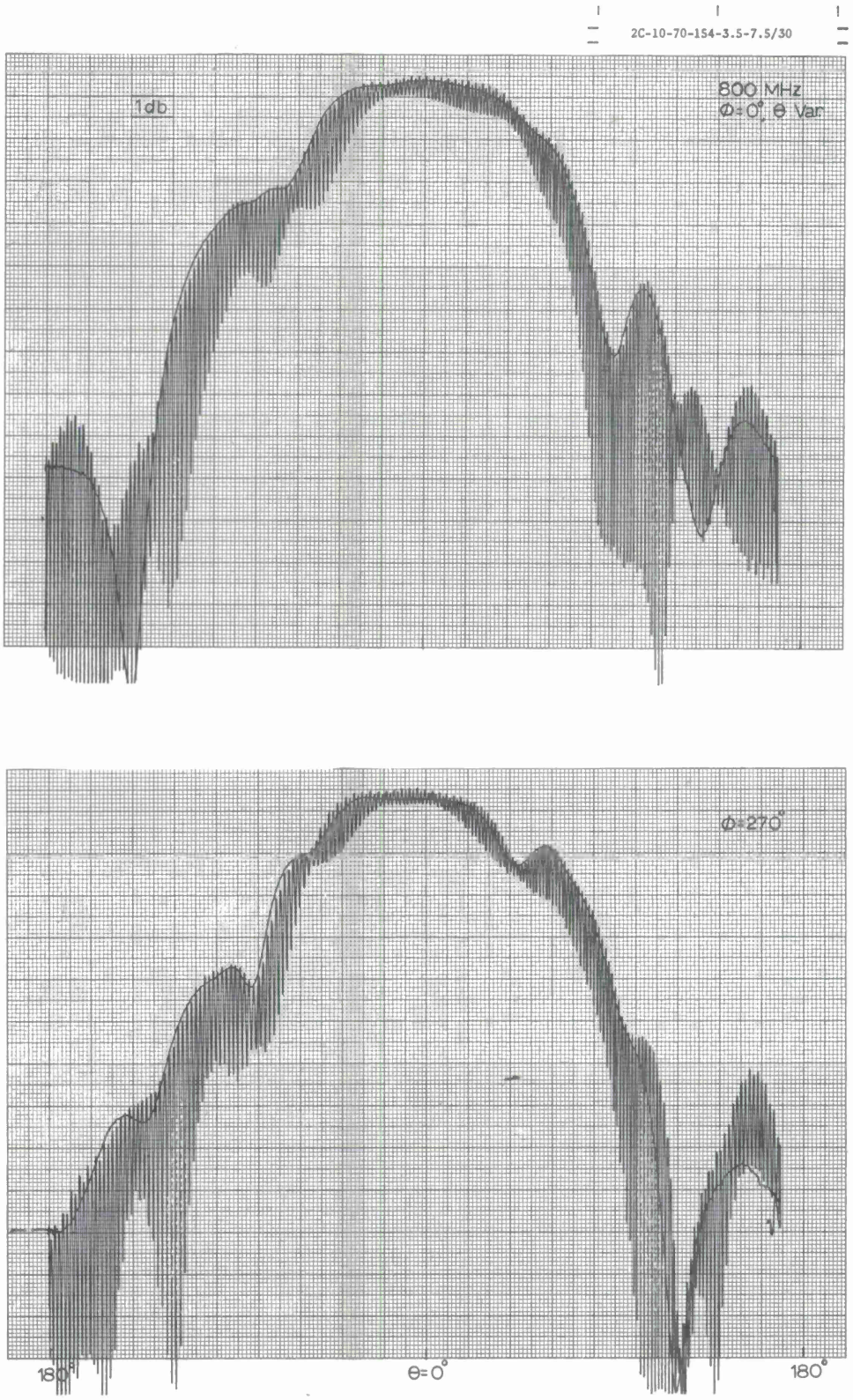

Figure D-11. Radiation patterns of slow-wave conical spiral antenna, $\alpha = 70°$, narrow arm width (7.5/30), slowing factor 3.5.

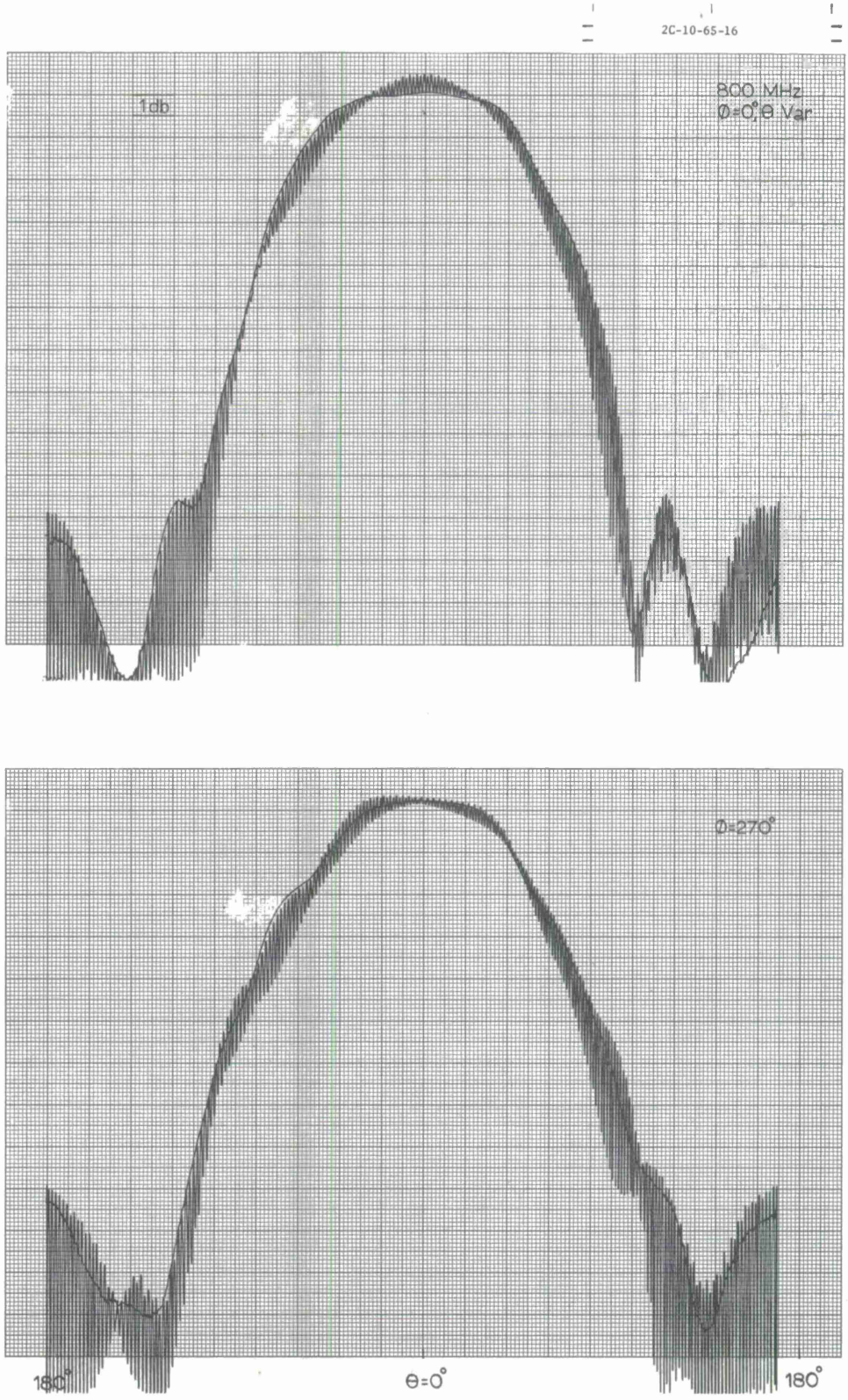

Figure D-12. Radiation patterns of conventional conical spiral antenna, $\alpha = 65°$, $\delta' = 16°$.

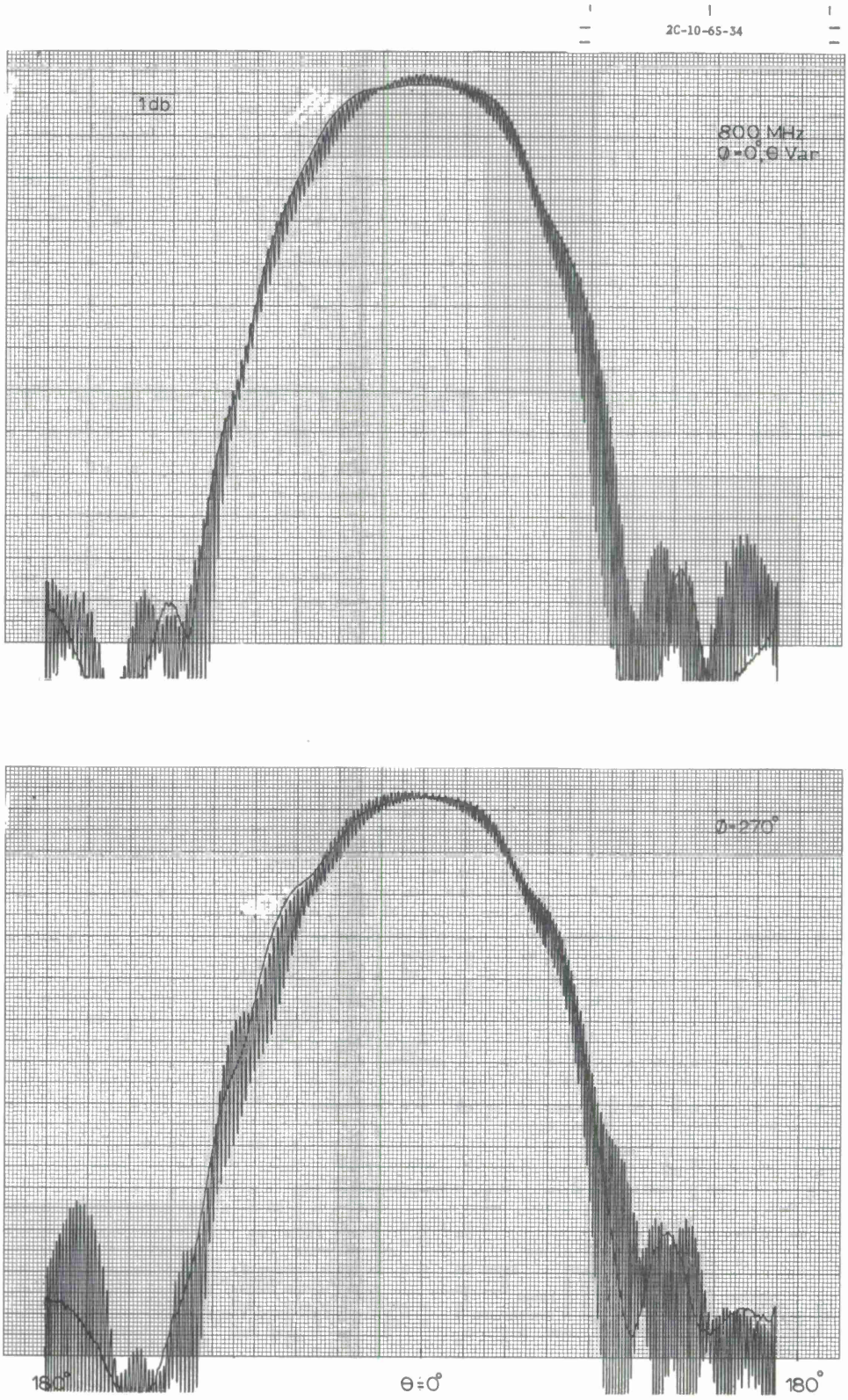

Figure D-13. Radiation patterns of conventional conical spiral antenna, $\alpha = 65°$, $\delta' = 34°$.

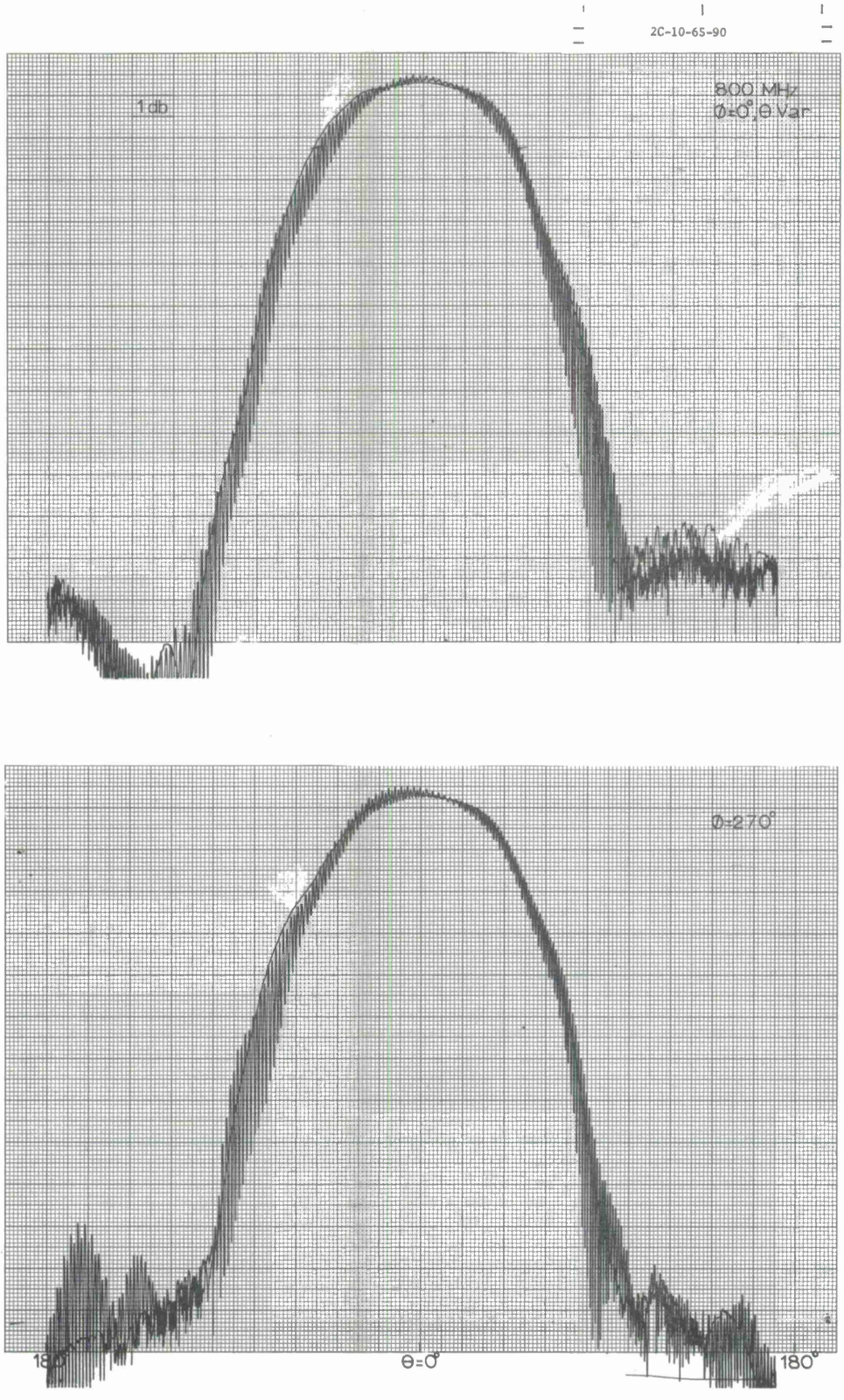

Figure D-14. Radiation patterns of conventional conical spiral antenna. $\alpha = 65°$, $\delta' = 90°$.

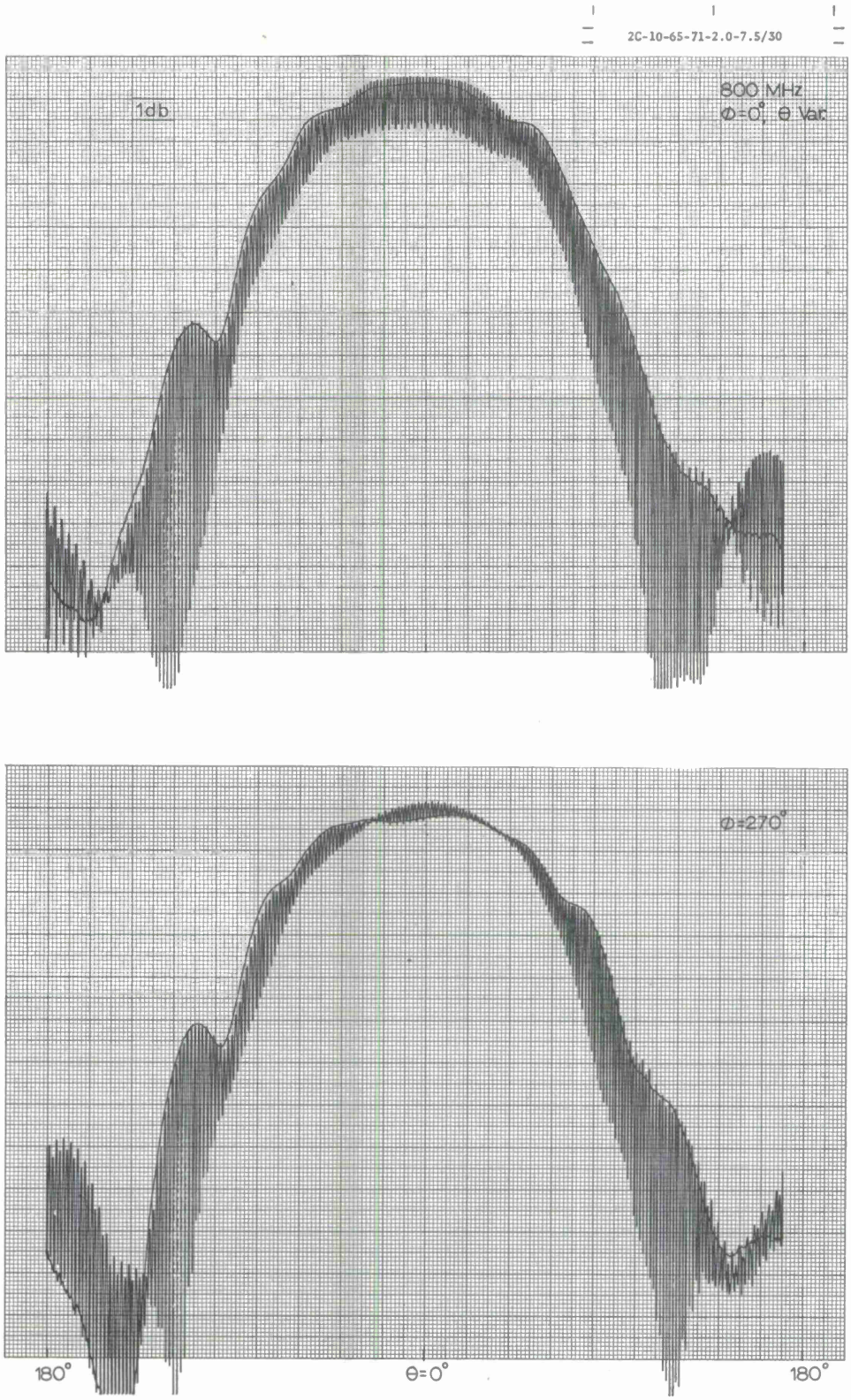

Figure D-16. Radiation patterns of slow-wave conical spiral antenna, $\alpha = 65°$, narrow arm width (7.5/30), slowing factor 2.0.

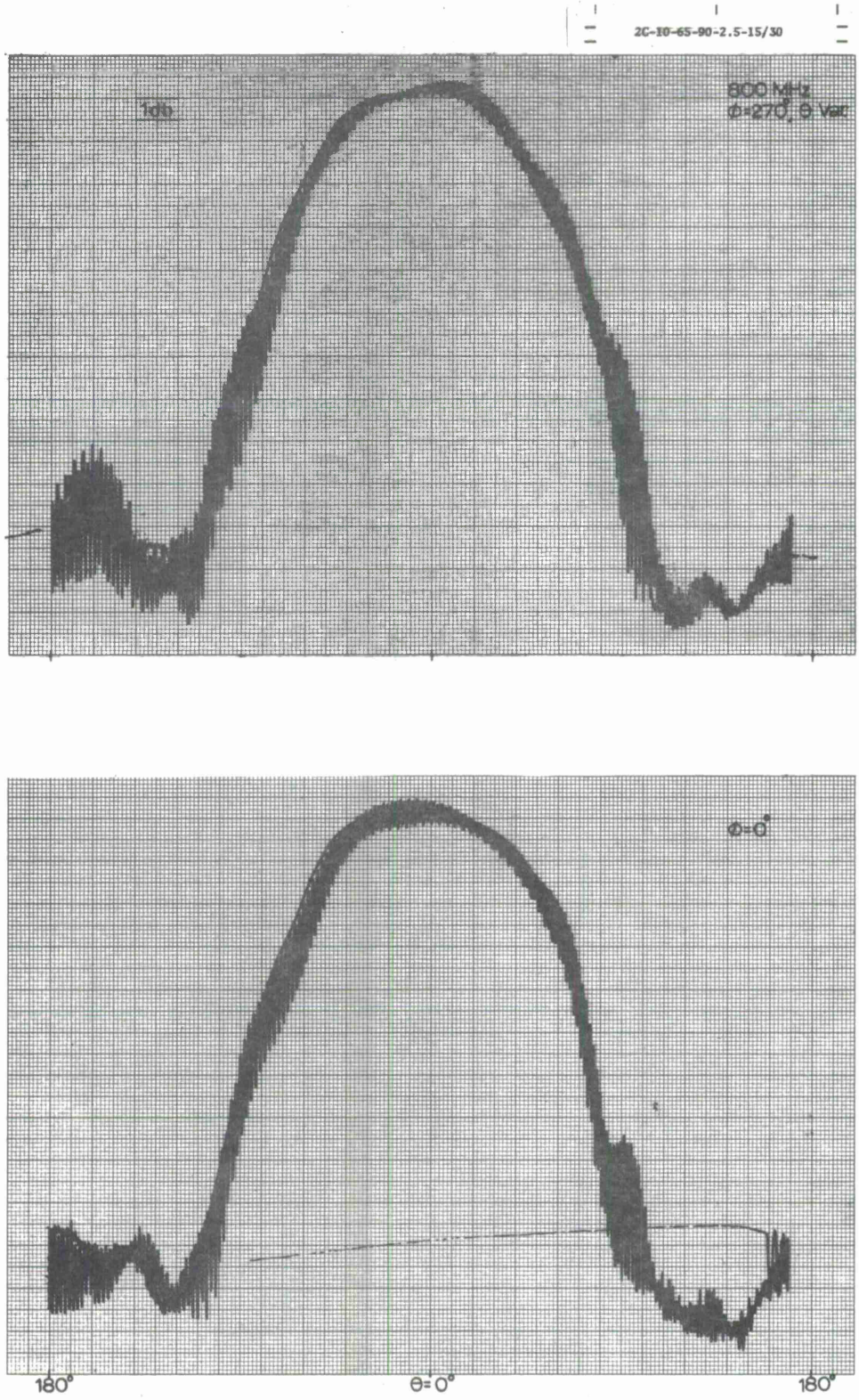

Figure D-15. Radiation patterns of slow-wave conical spiral antenna, $\alpha = 65°$, wide arm width (15/30), slowing factor 2.5.

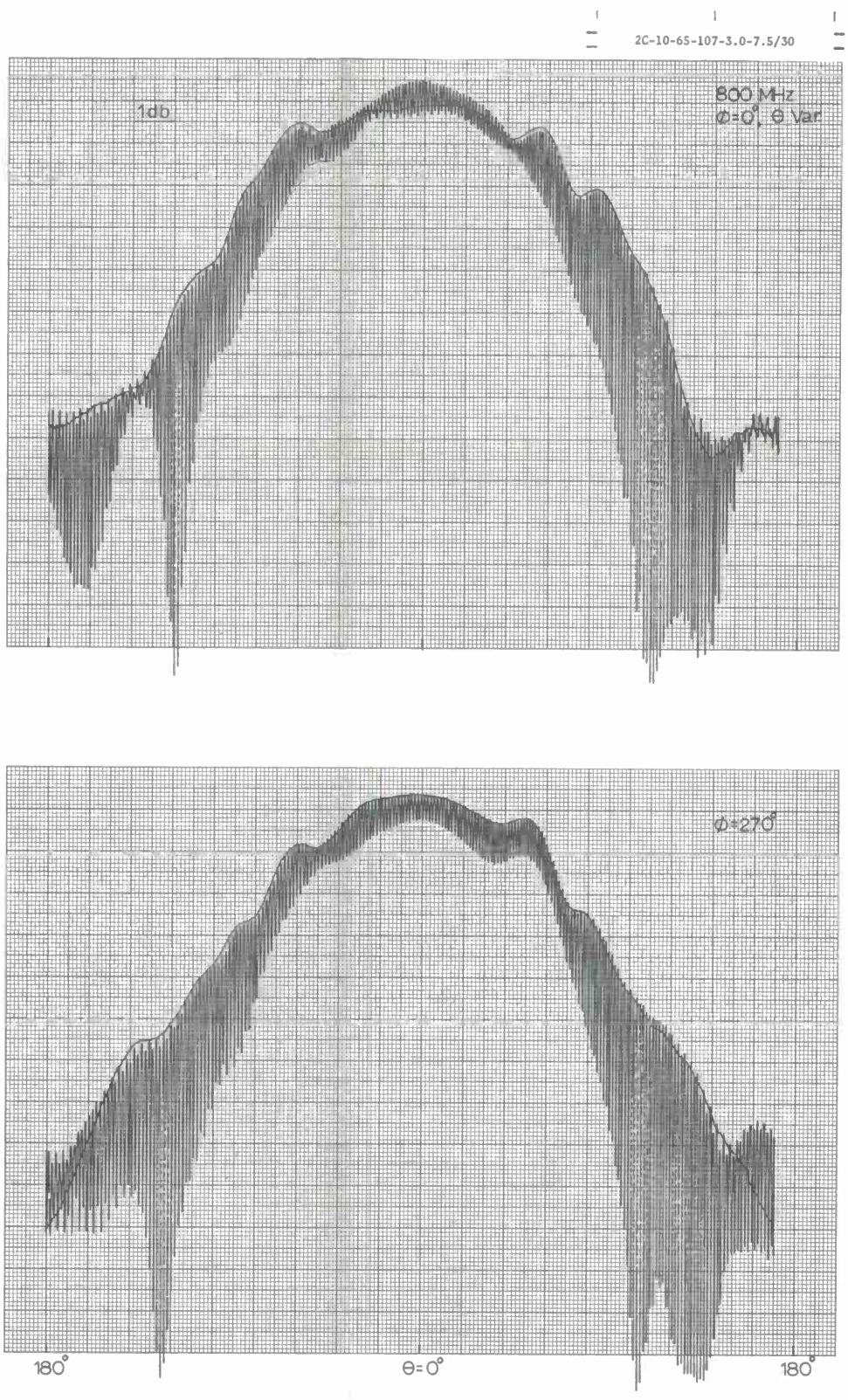

Figure D-17. Radiation patterns of slow-wave conical spiral antenna, $\alpha = 65°$, narrow arm width (7.5/30), slowing factor 3.0.

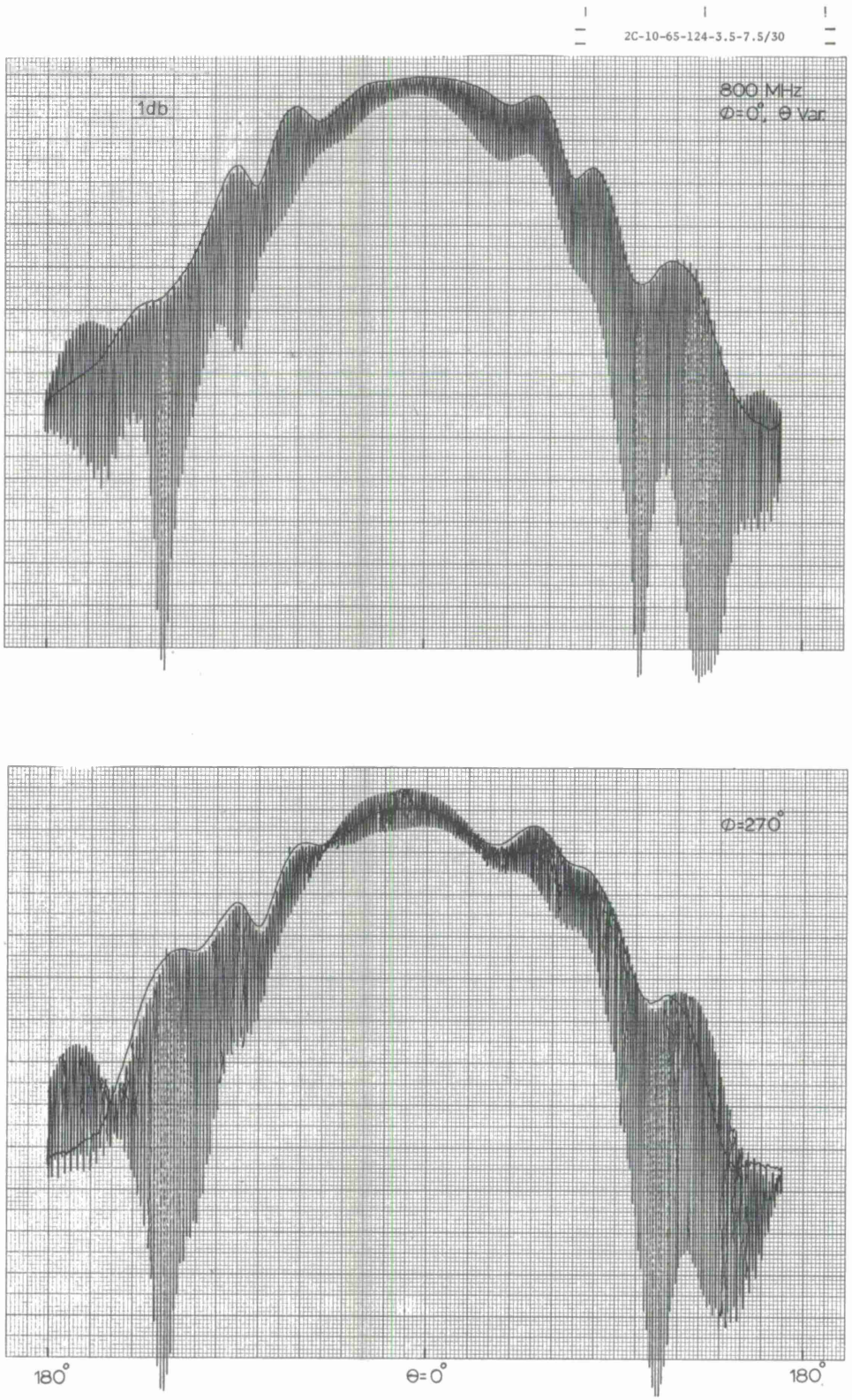

Figure D-18. Radiation patterns of slow-wave conical spiral antenna, α = 65°, narrow arm width (7.5/30). slowing factor 3.5.

APPENDIX E

Relative amplitude of axial radiation from conical spiral antennas as a function of antenna size in wavelengths.

(Refer to Section 1.4.2, page 33).

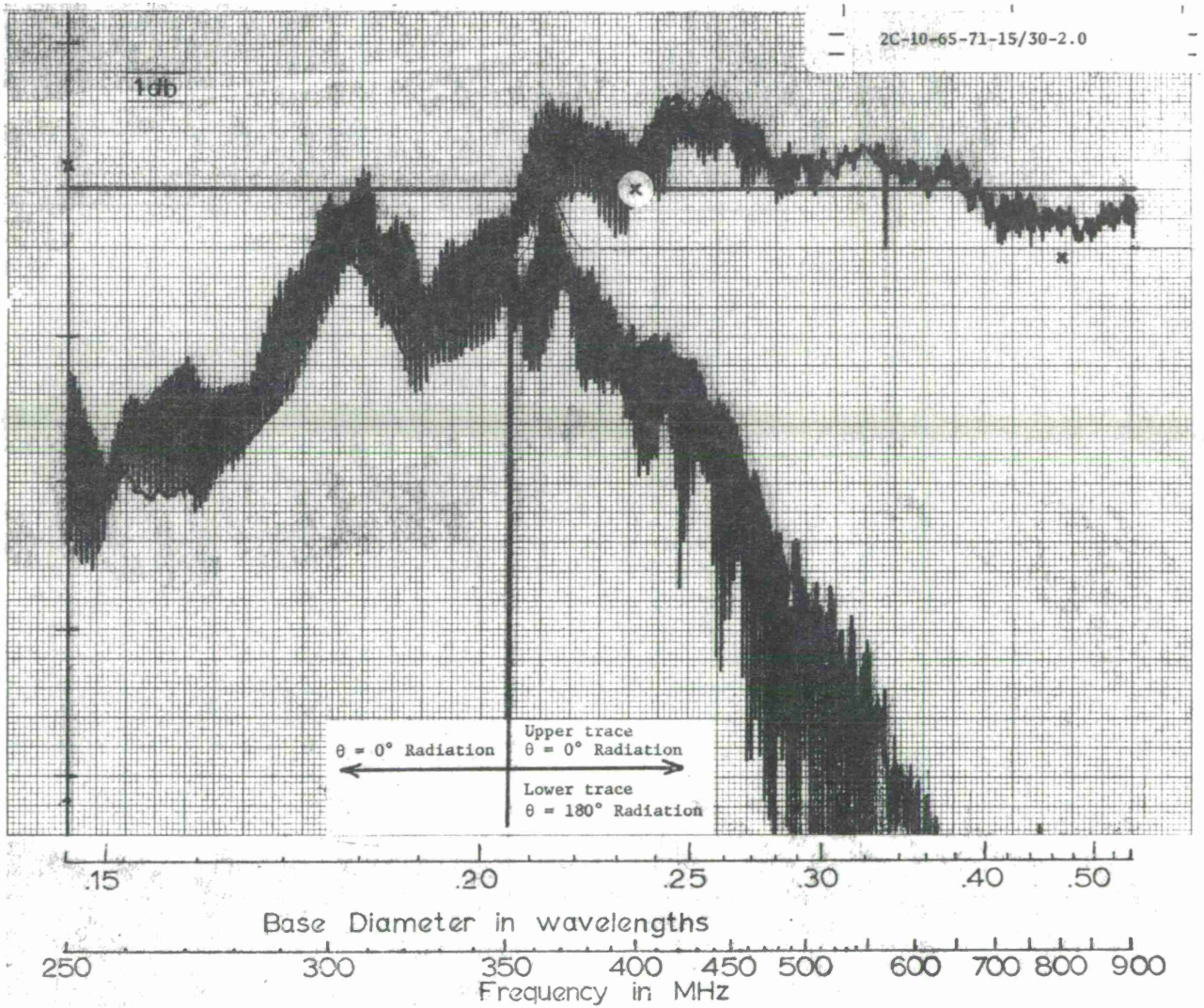

Figure E-1 Relative amplitude of axial radiation from slow-wave conical spiral antenna. $\alpha = 65°$, arm with 15/30, slowing factor 2.0. The 3 data points indicated by an x indicate isotropic level at that point.

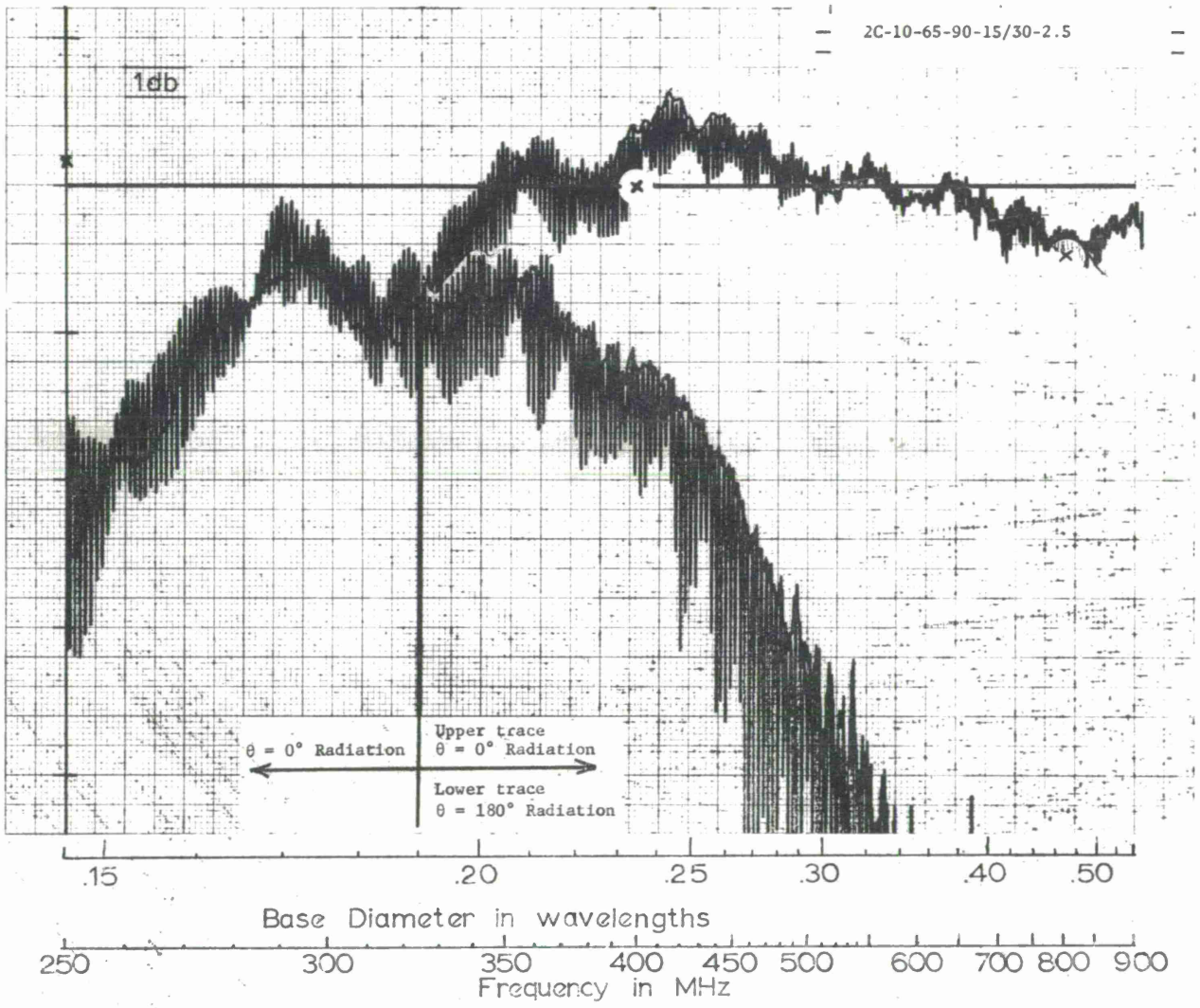

Figure E-2 Relative amplitude of axial radiation from slow-wave conical spiral antenna, $\alpha = 65°$, arm width 15/30, slowing factor 2.5. Data points indicated by x are isotropic levels.

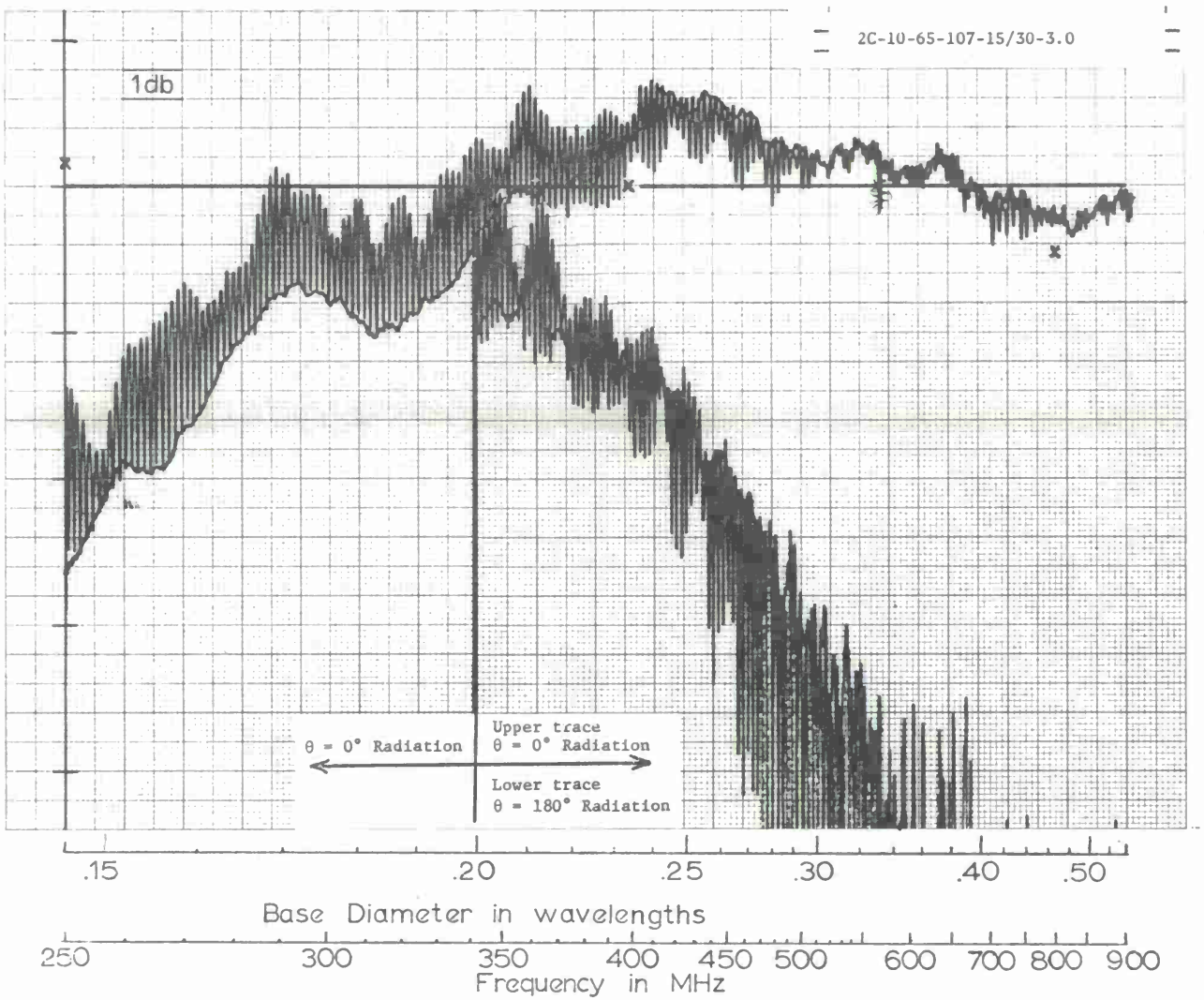

Figure E-3 Relative amplitude of axial radiation from slow-wave conical spiral antenna, $\alpha = 65°$, arm width 15/30, slowing factor 3.0. Data points indicated by x are isotropic levels.

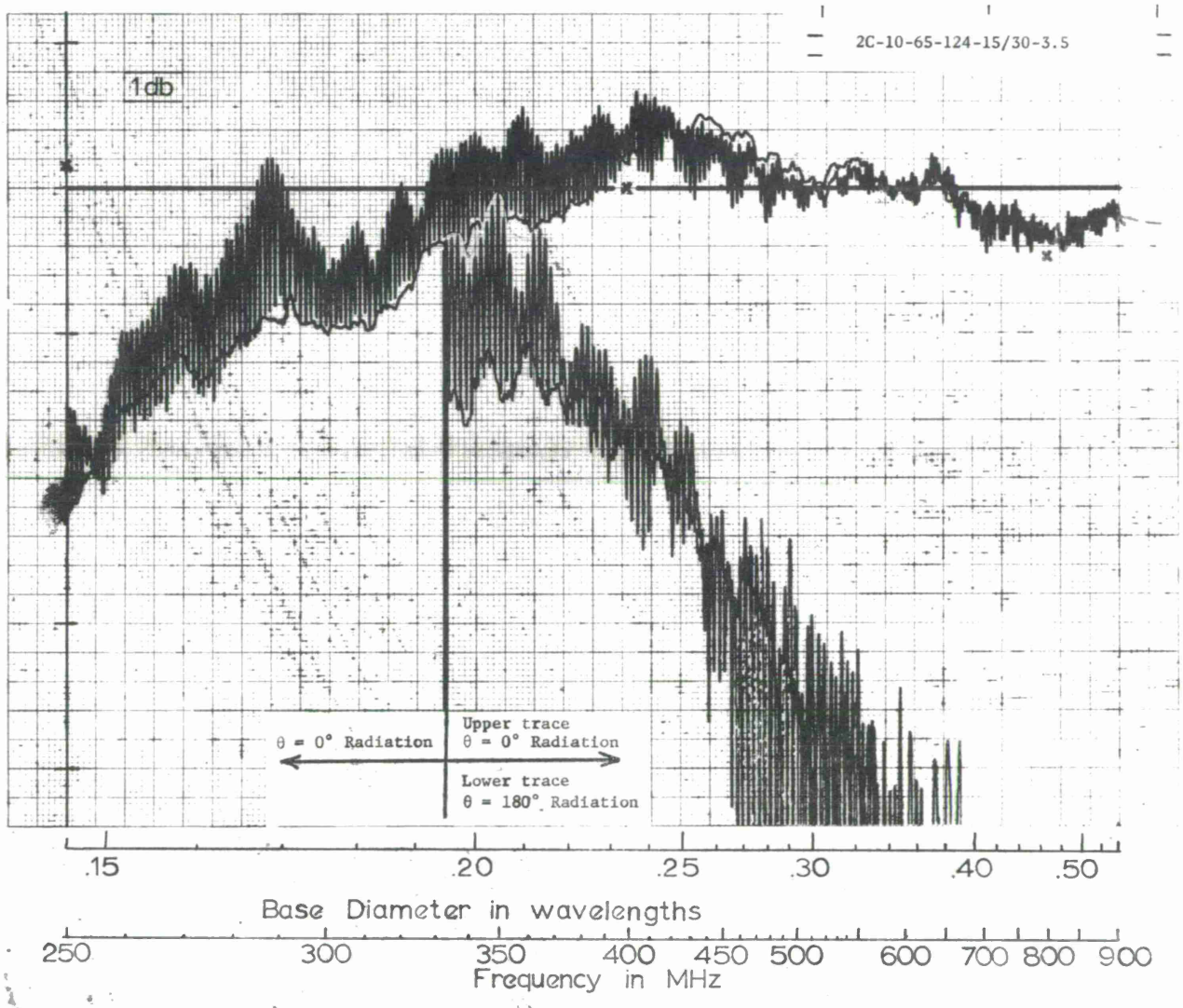

Figure E-4 Relative amplitude of axial radiation from slow-wave conical spiral antenna, $\alpha = 65°$, arm width 15/30, slowing factor 3.5. Data points indicated by x are isotropic levels.

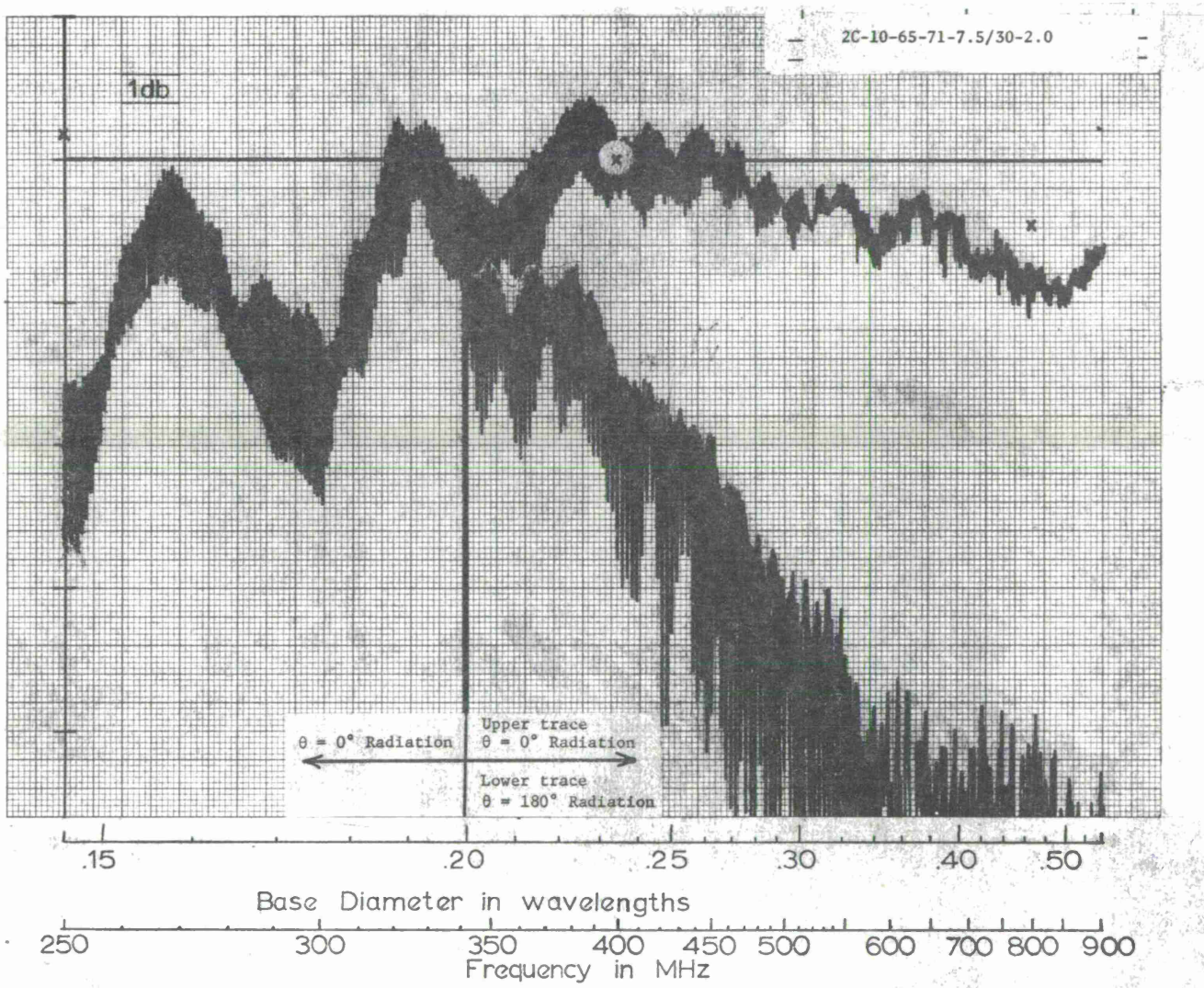

Figure E-5 Relative amplitude of axial radiation from slow-wave conical spiral antenna, $\alpha = 65°$, arm width (7.5/30), slowing factor 2.0. The 3 data points (x) are isotropic levels.

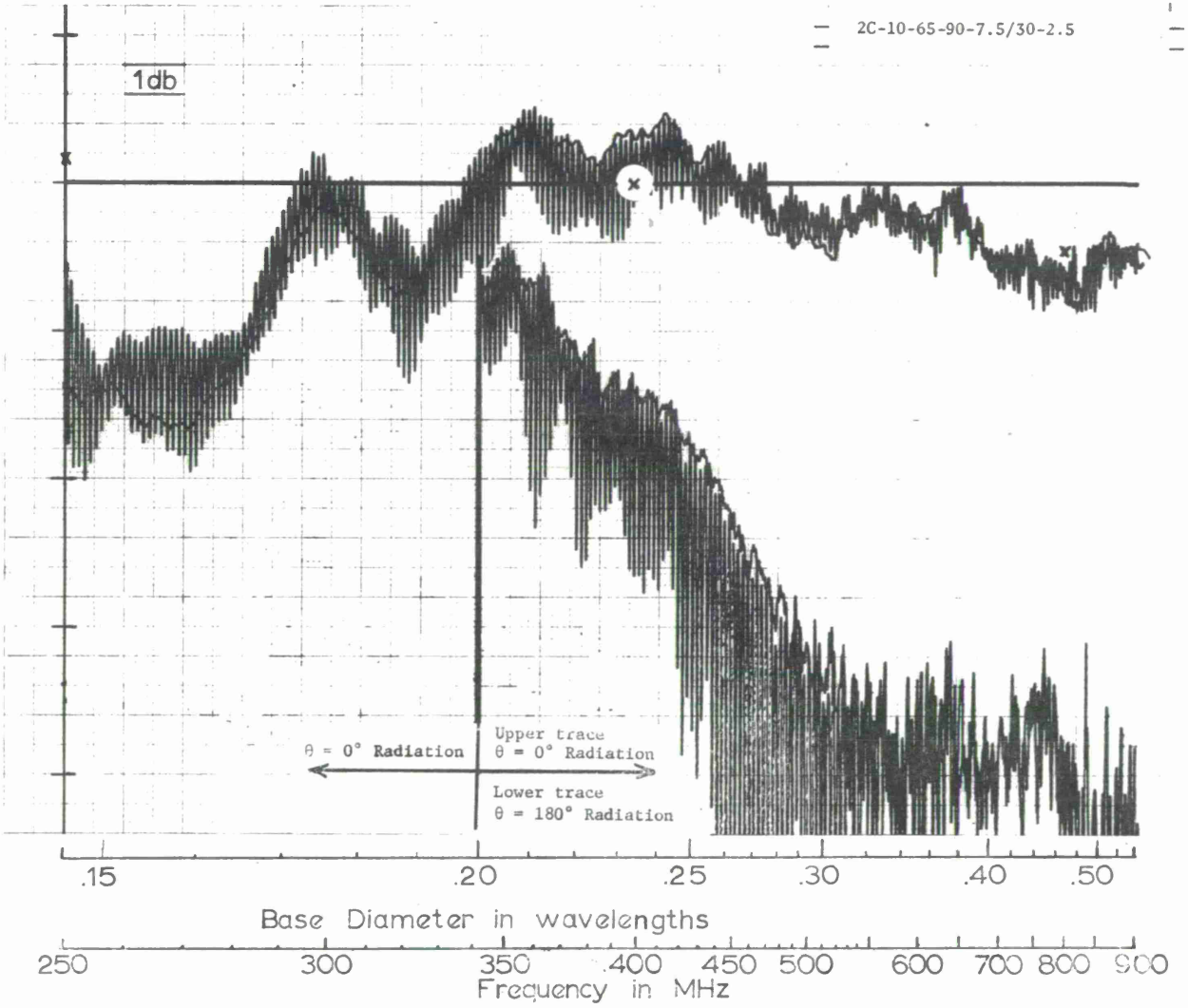

Figure E-6 Relative amplitude of axial radiation from slow-wave conical spiral antenna, α = 65°, arm width (7.5/30), slowing factor 2.5. The 3 data points (x) are isotropic levels.

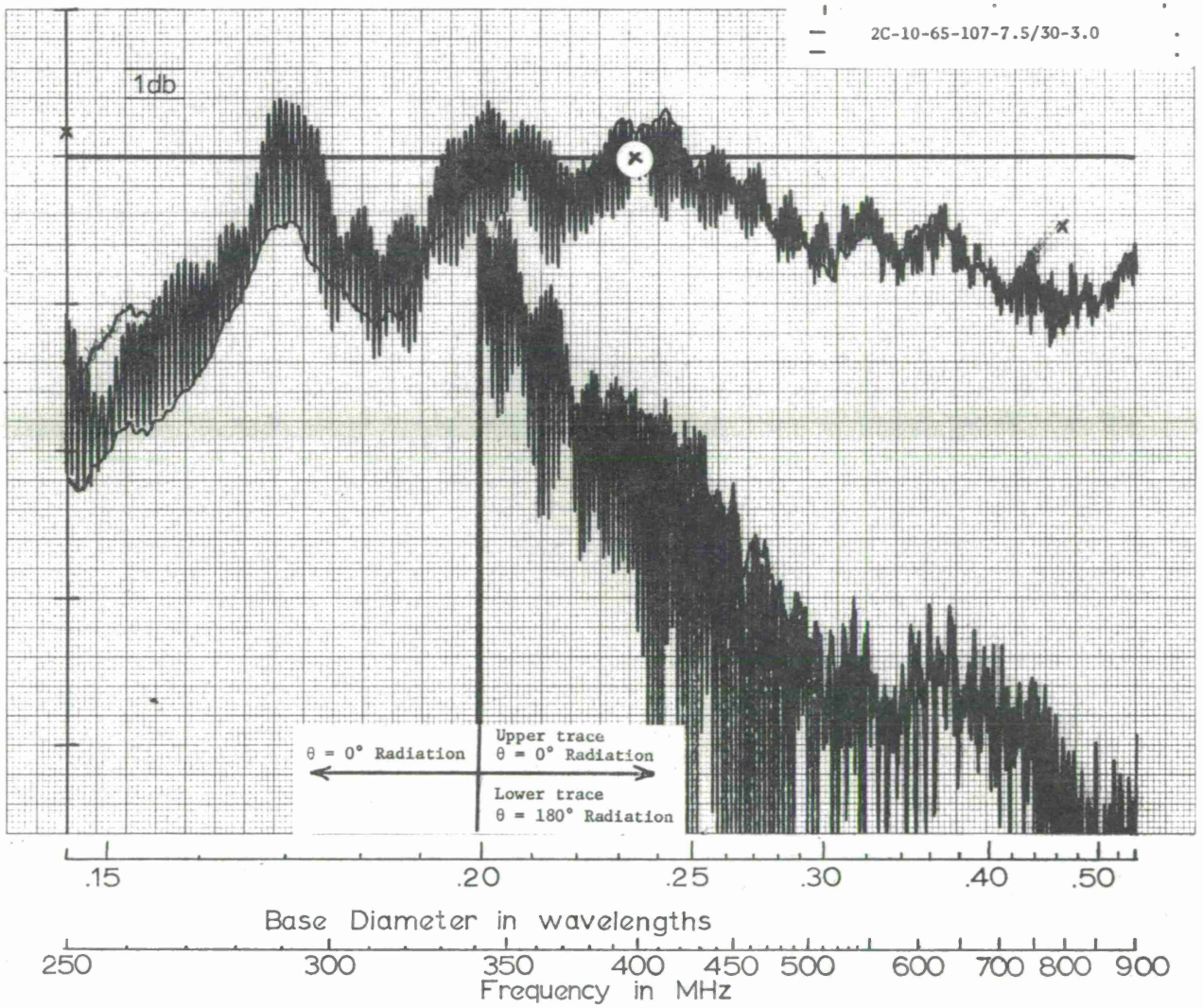

Figure E-7 Relative amplitude of axial radiation from slow-wave conical spiral antenna, α = 65°, arm width (7.5/30), slowing factor 3.0. The 3 data points (x) are isotropic levels.

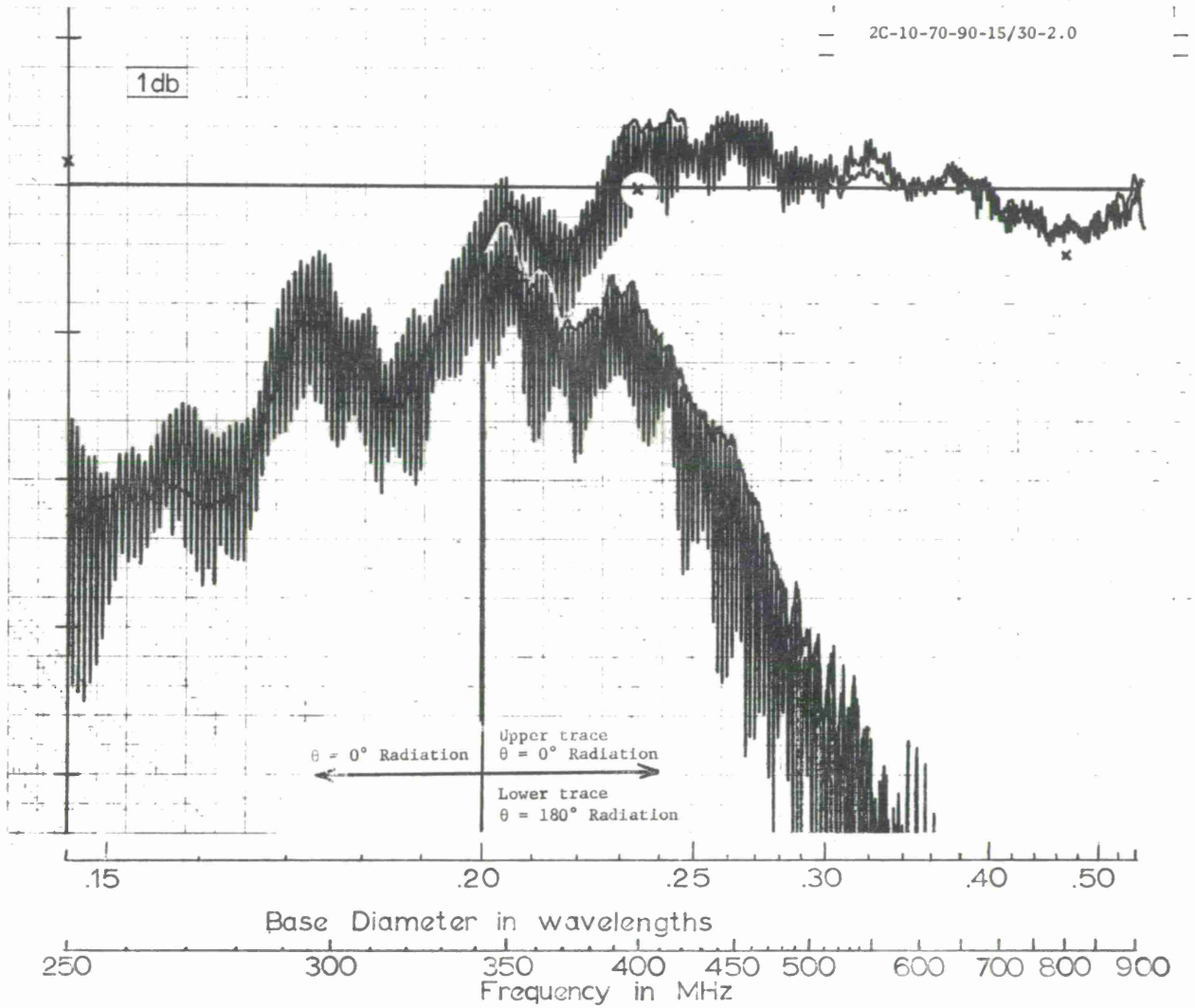

Figure E-8 Relative amplitude of axial radiation from slow-wave conical spiral antenna, $\alpha = 70°$, arm width (15/30) slowing factor 2.0. Data points (x) are isotropic levels.

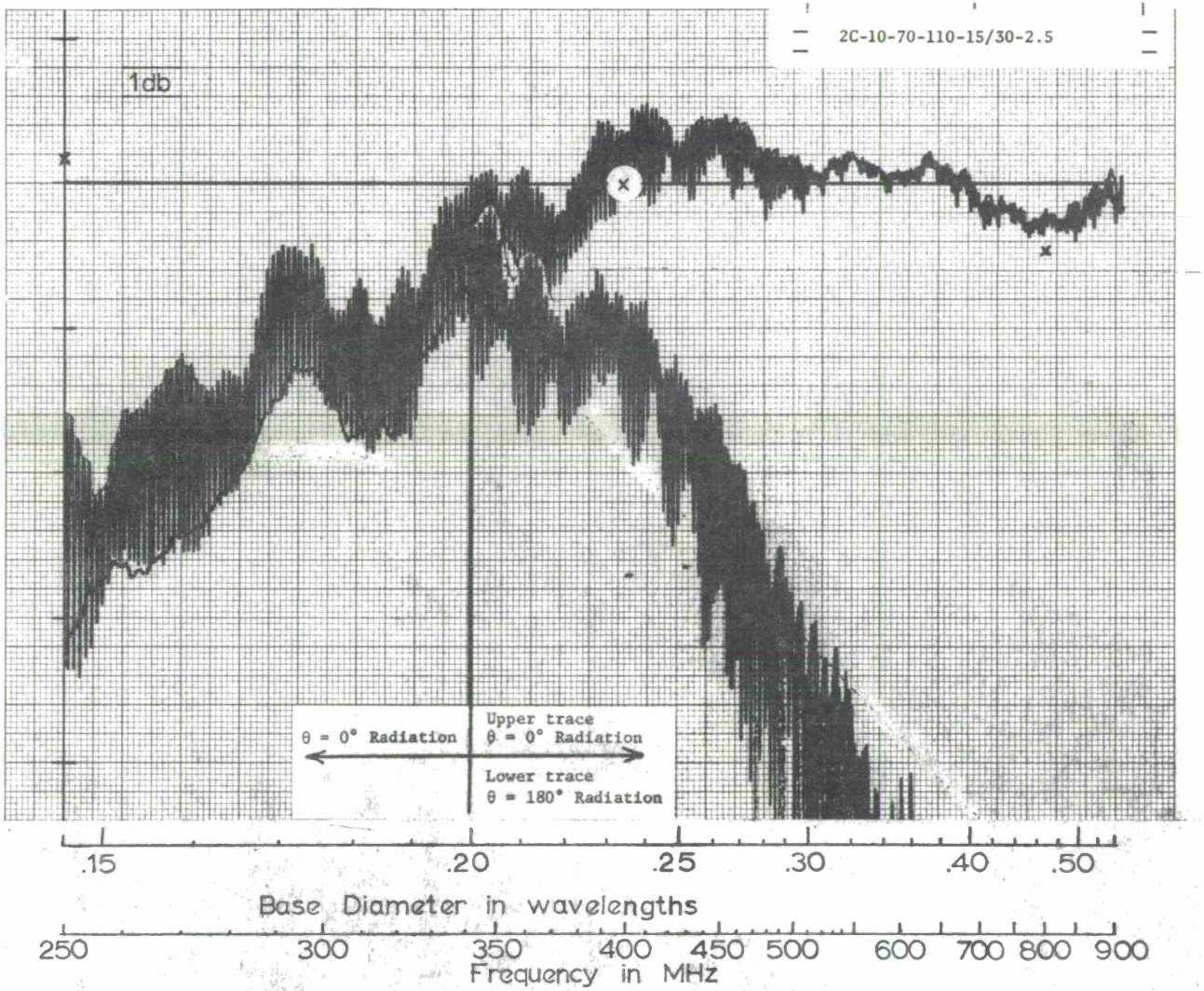

Figure E-9 Relative amplitude of axial radiation from slow-wave conical spiral antenna, α = 70°, arm width (15/30) slowing factor 2.5. Data points (x) are isotropic levels.

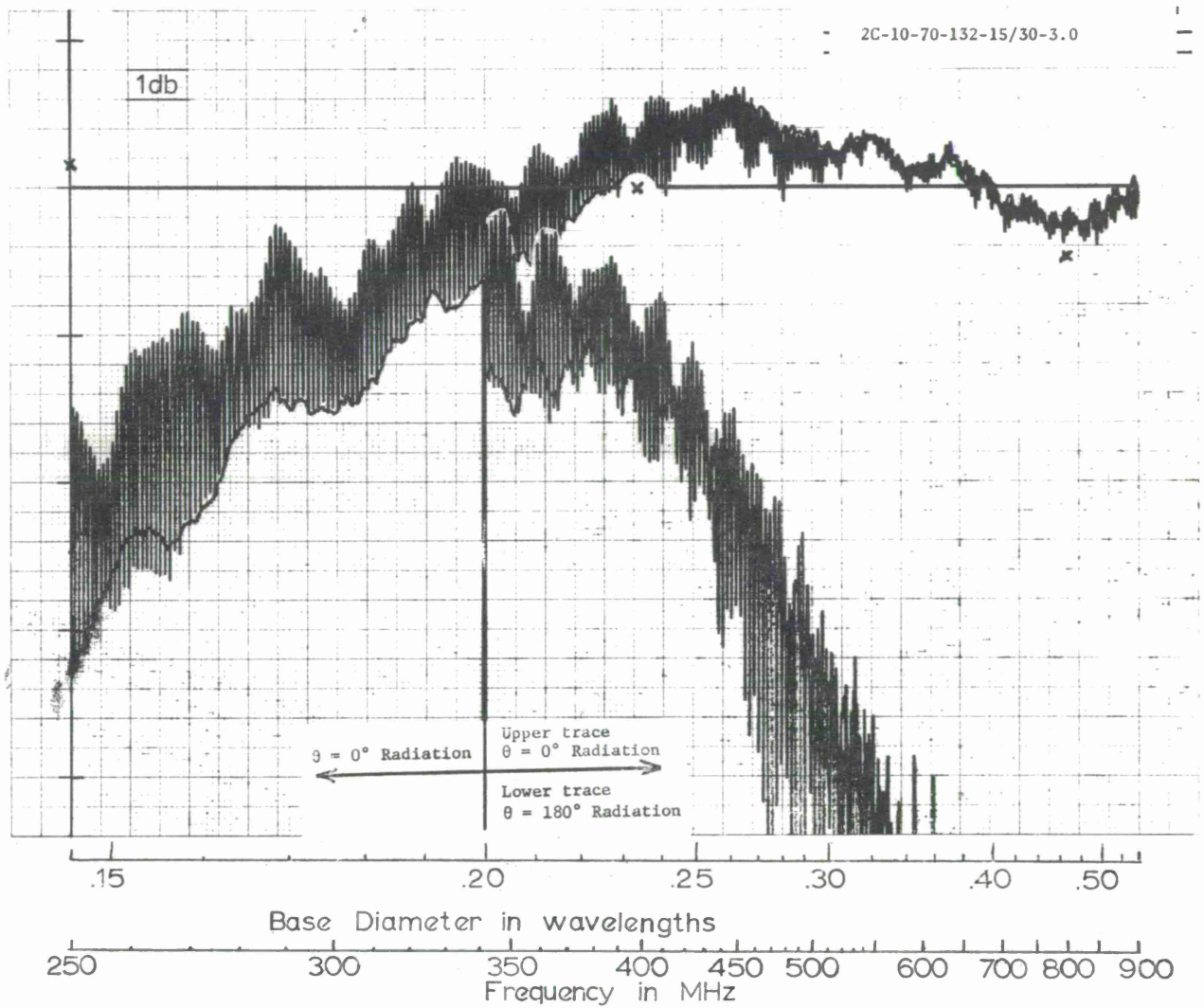

Figure E-10 Relative amplitude of axial radiation from slow-wave conical spiral antenna, α = 70°, arm width (15/30) slowing factor 3.0. Data points (x) are isotropic levels.

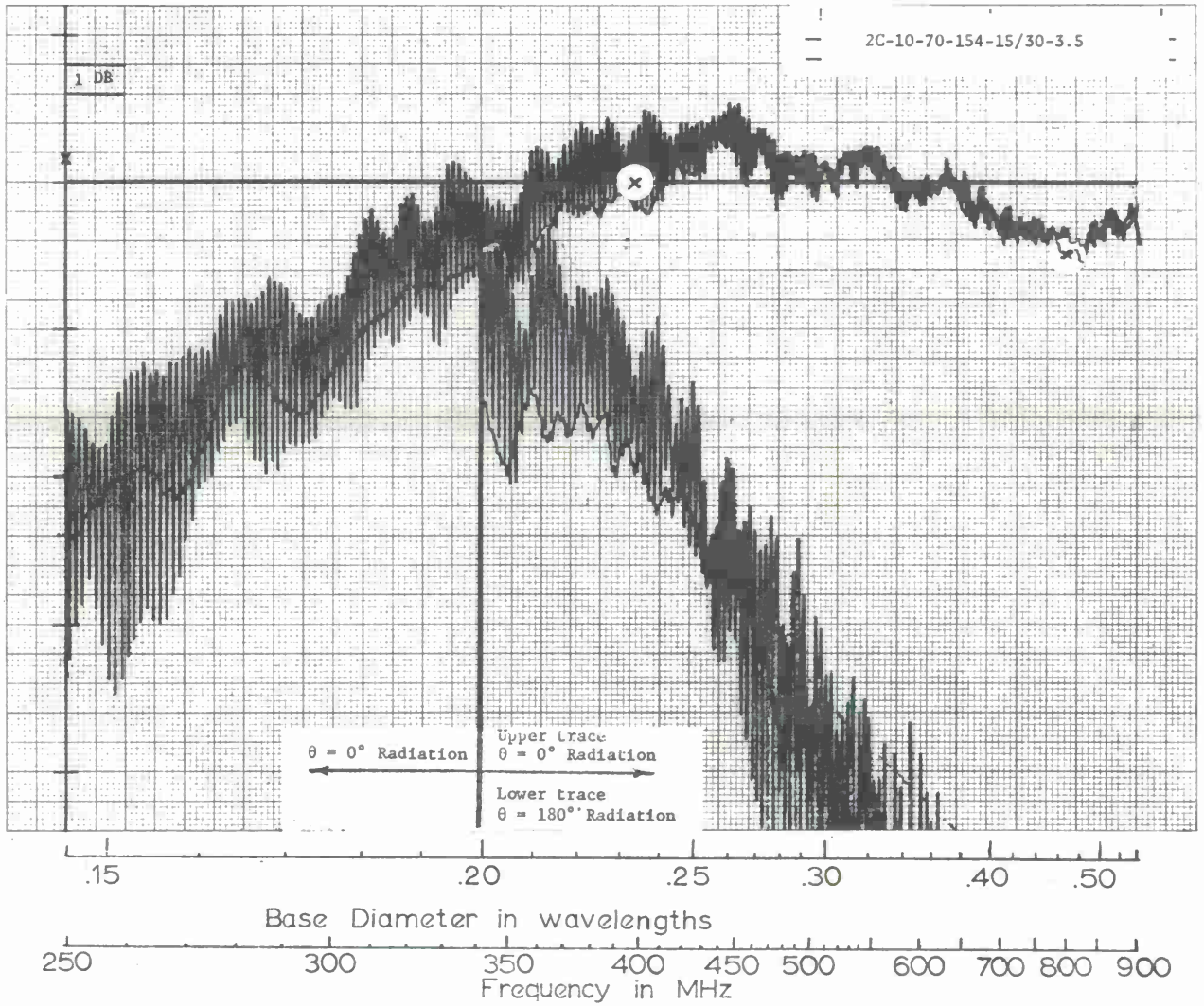

Figure E-11 Relative amplitude of axial radiation from slow-wave conical spiral antenna, $\alpha = 70°$, arm width (15/30) slowing factor 3.5. Data points (x) are isotropic levels.

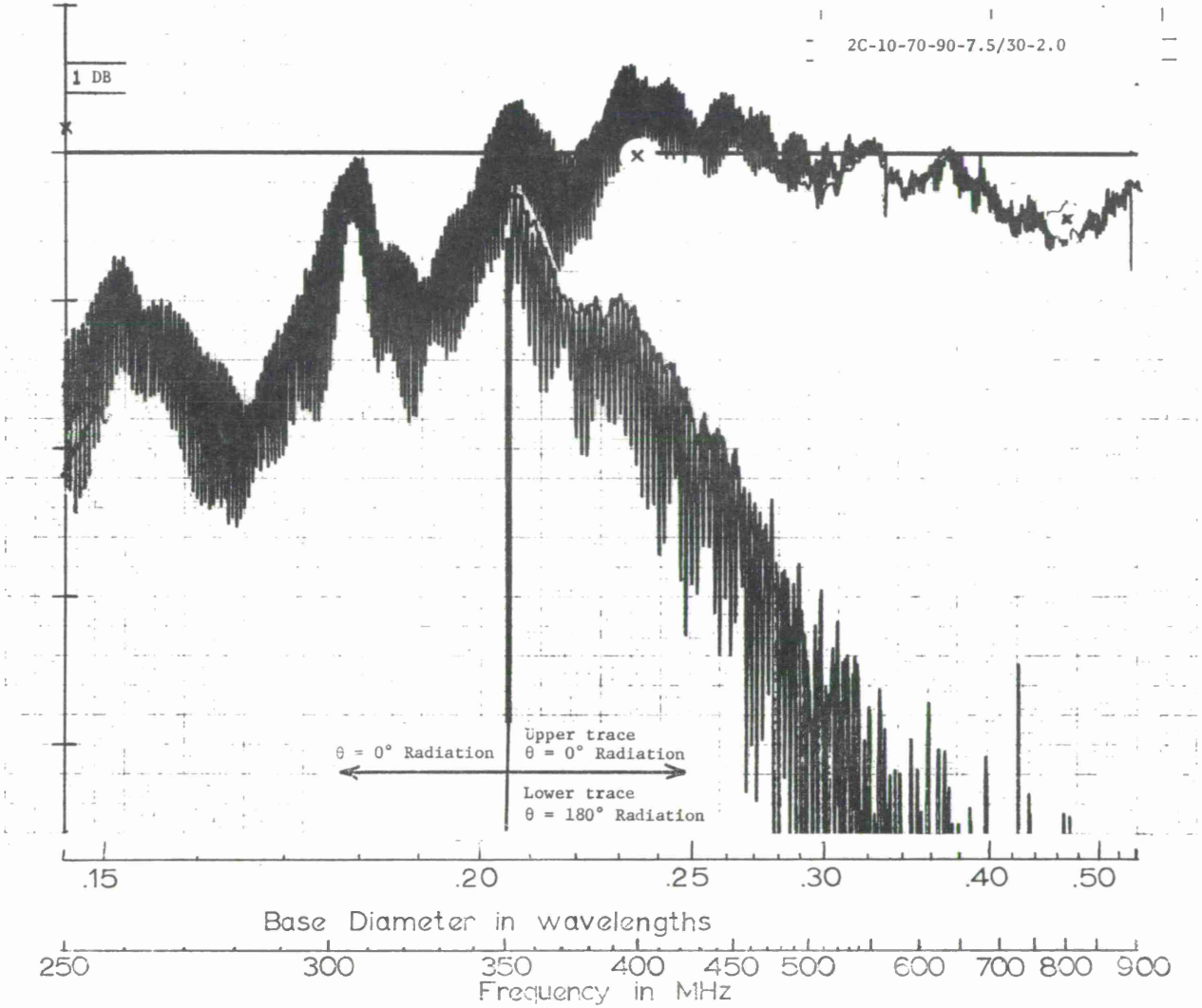

Figure E-12 Relative amplitude of axial radiation from slow-wave conical spiral antenna, $\alpha = 70°$, arm width (7.5/30), slowing factor 2.0. Data points (x) are isotropic levels.

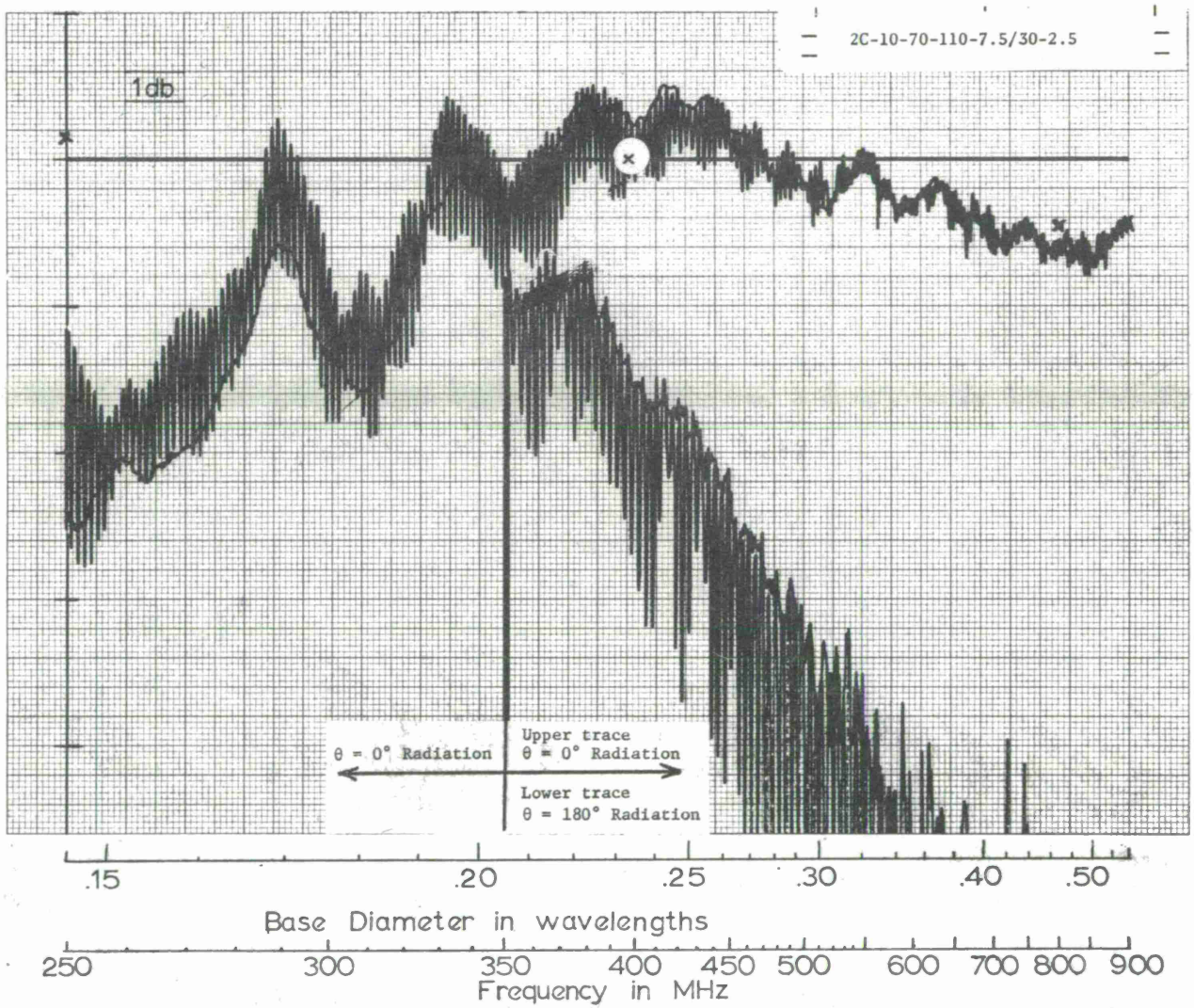

Figure E-13 Relative amplitude of axial radiation from slow-wave conical spiral antenna, α = 70°, arm width (7.5/30), slowing factor 2.5. Data points (x) are isotropic levels.

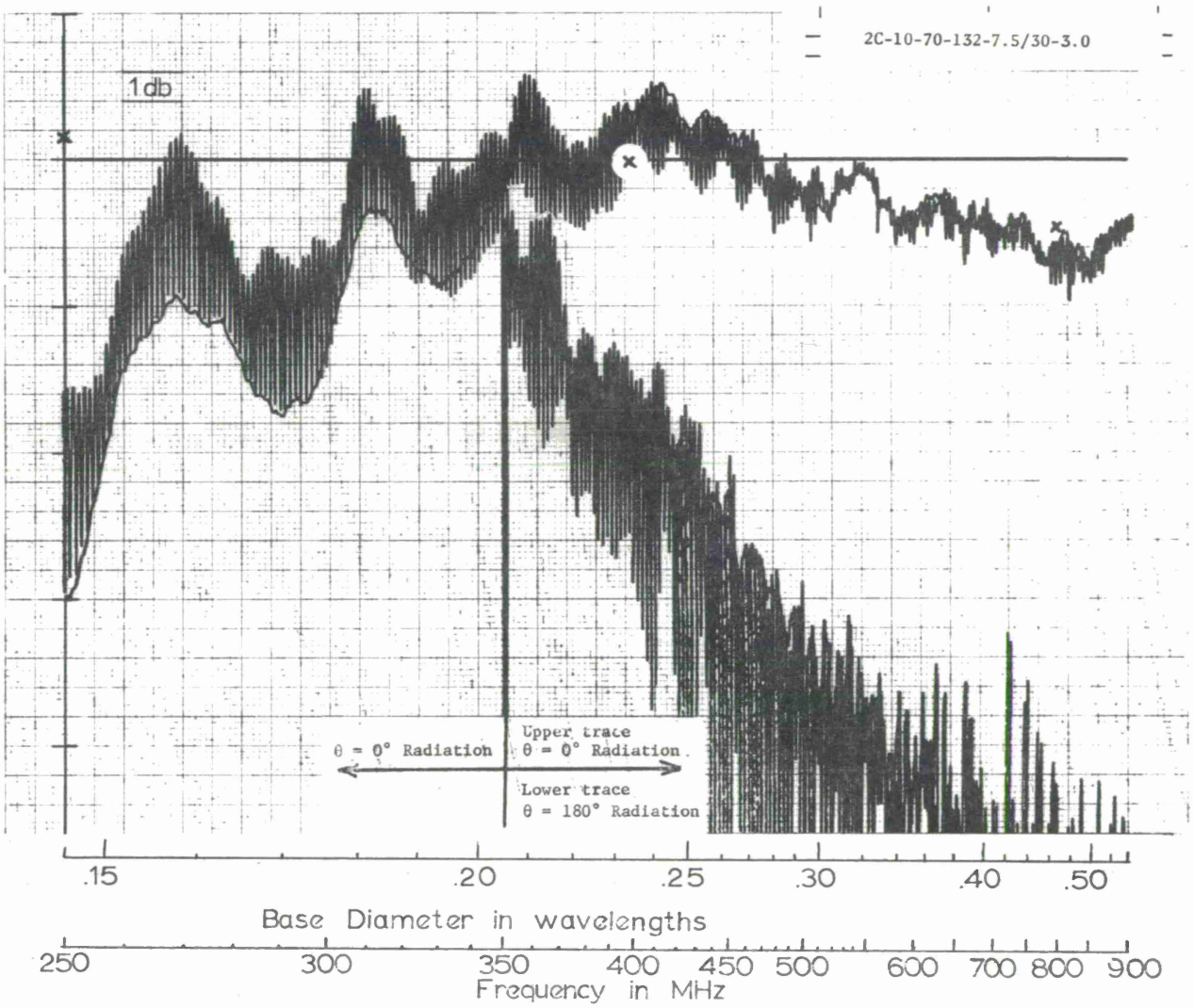

Figure E-14 Relative amplitude of axial radiation from slow-wave conical spiral antenna, $\alpha = 70°$, arm width (7.5/30), slowing factor 3.0. Data points (x) are isotropic levels.

UNCLASSIFIED
Security Classification

DOCUMENT CONTROL DATA - R&D

(Security classification of title, body of abstract and indexing annotation must be entered when the overall report is classified)

1. ORIGINATING ACTIVITY *(Corporate author)*
University of Illinois, Electromagnetics Laboratory (Formerly Antenna Laboratory) under Purchase Order CC-401 to M.I.T. Lincoln Laboratory

2a. REPORT SECURITY CLASSIFICATION
Unclassified

2b. GROUP
None

3. REPORT TITLE
An Investigation of Some Slow-Wave Conical Log-Spiral and Helical Antennas

4. DESCRIPTIVE NOTES *(Type of report and inclusive dates)*
Final Report for period 1 September 1971 - 31 August 1972

5. AUTHOR(S) *(Last name, first name, initial)*
Dyson, John D.

6. REPORT DATE	7a. TOTAL NO. OF PAGES	7b. NO. OF REFS
30 November 1972	139	6

8a. CONTRACT OR GRANT NO.
F19628-70-C-0230

b. PROJECT NO.
627A

c. Purchase Order CC-401

d.

9a. ORIGINATOR'S REPORT NUMBER(S)
UIAL-73-1

9b. OTHER REPORT NO(S) *(Any other numbers that may be assigned this report)*
ESD-TR-72-365

10. AVAILABILITY/LIMITATION NOTICES
Approved for public release; distribution unlimited.

11. SUPPLEMENTARY NOTES
None

12. SPONSORING MILITARY ACTIVITY
Air Force Systems Command, USAF

13. ABSTRACT

This is a two part report.

The first part is concerned with the characteristics of conical spiral antennas constructed with zig-zag, i.e., slow-wave geometry, arms. This construction permits a reduction in size of approximately 15 percent below that required for the conventional antenna. It also increases the pattern beamwidth and lowers the characteristic impedance.

In part 2, a 2 1/4-turn monofilar conical helix, fed at the base of the cone against an inner metal core, was investigated. This small circumference (approximately 1/4 wavelength) antenna can be made to be an axial radiating structure, while the conventional helix of this size radiates a maximum of energy broadside to the antenna axis.

14. KEY WORDS

spiral antenna
helix antenna
slow-wave antenna
unbalanced spiral antenna

UNCLASSIFIED
Security Classification